POLITECNICO DI TORINO

I Facoltà di Ingegneria

Master of Science in Biomedical Engineering

M.Sc. Thesis

NON-INVASIVE BLOOD PRESSURE ESTIMATION BASED ON ELECTRO/PHONOCARDIOGRAM

Supervisor

Prof. Marco KNAFLITZ

Assistant Supervisor

E**ng. Andrea VITALI**

Candidate

Paula TRUJILLO DIAZ

Academic Year 2010-2011

ACKNOWLEDGMENTS

I would like to express my gratitude to the whole Remote Health Monitoring division of the Advanced System Technology Team of STMicroelectronics for the opportunity of doing this thesis, for the supervision, help and advice during the research activity. My deepest gratitude to Andrea Vitali for the patient guidance and all the intuitions provided. I'm indebted to him for his encouragement throughout the whole process. I would also like to thank Professor Marco Knaflitz for providing this thesis opportunity and guidance.

Many thanks to all my friends who have been around all these years, who have been helping me at different occasions and in one way or another have influenced this thesis.

I must acknowledge my boyfriend and best friend, Juan, without his love, patience and encouragement, I would not have finished this thesis.

Lately, and most importantly I wish to thanks my family, Emiliano, Liliana, Natalia and Daniela. They have always supported and encourage me to do my best in all matters of life. To them I dedicate this thesis.

ABSTRACT

This thesis describes the theory, investigation, and development of a non-invasive continuous blood pressure measurement system for integration in a remote monitoring device.

Remote non-invasive continuous monitoring of physiological parameters, such as the heart rate, respiratory rate, oxygen saturation, blood pressure, represents one of the key aims of modern biomedical technologies. Remote monitoring of patients presents huge advantages either from patients' point of view or hospitals and general practitioners corporations.

STMicroelectronics is developing a miniaturized device, the Body Gateway, which allows this kind of monitoring. A prototype of the device is shown in Figure 0.1. The Body Gateway is currently used to compute the heart rate and detect heart beats from the acquired ECG signal, perform an estimation of body physical activity by acquiring accelerometer signals, and measure the thoracic bioimpedance, which allows the estimation of volume changes related to breathing and the estimation of density changes related to the accumulation of fluids. Moreover the device can compare different signals to enhance outputs and generate additional information: for example, it can detect if the heart rate matches the physical activity of the patient. The goal of this device is to integrate other sensors to perform non-invasive measurements of a range of different parameters on the body and transmit the data over a large distance for clinical evaluation.

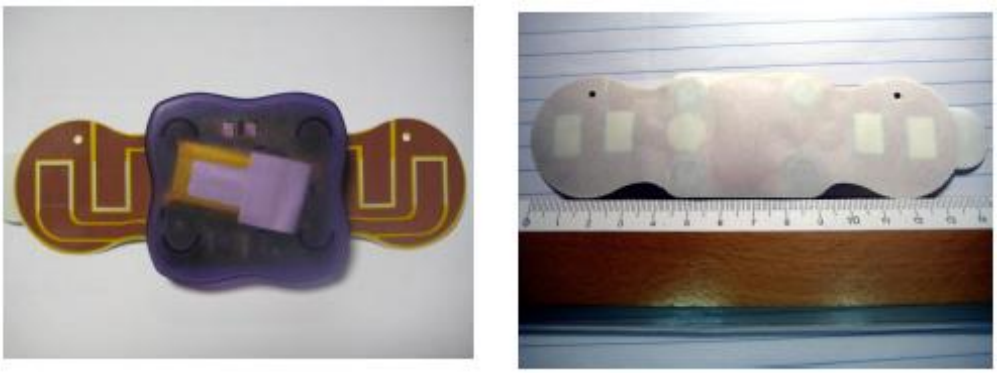

Figure 0.1. Body Gateway

A fundamental part of the device is the digital signal processing. As far as a wearable device is concern, all algorithms must be embedded and im-

plemented on a microcontroller, which has a computational power lower than standard Personal Computers. A Bluetooth RF system is used to transmit data from the device to the patient's mobile phone and subsequently it is transmitted via Internet to the medical staff, who will be able to observe the acquired signal and the estimation of the related parameters on a PC. A general diagram of the transmission system is shown in Figure 0.2.

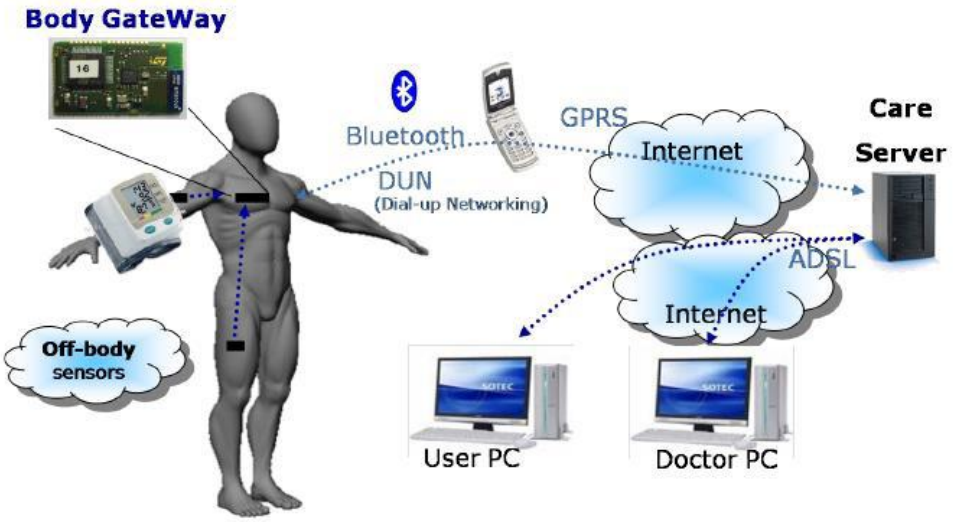

Figure 0.2. Diagram of the transmission system of the Body GateWay.

The blood pressure is an important physiological parameter and often there is a need for continuous or periodical monitoring. The aim of this thesis is to estimate blood pressure based on electrocardiographic (ECG) and phonocardiographic (PCG) signals. For this purpose, a prototype of an electronic device has been developed in order to acquire the ECG and PCG signals and send them via Bluetooth to a PC for offline analysis. This activity has been performed in collaboration with the Remote Health monitoring group of the Advance System Technology division of STMicroelectronics.

The logical progression of the covered topics is explained below.

The first chapter provides an introduction on the principles of blood pressure and a historical overview of the different blood pressure measurement methods. A short description of the anatomy and physiology of the heart and blood vessels and their contribution to the blood pressure are given in Section 1.1. Section 1.2 gives a brief description of the traditional blood pressure measurement methods.

The second chapter introduces some novel techniques to measure blood pressure in a non-invasive continuous way. Alternative techniques involving the measuring of the transit time of the pulse pressure wave through the arterial tree are described. The definition of Pulse Transit Timer (PTT) and RS2 (defined as the time interval measured from the R wave of electrocardiographic (ECG) signal to the peak of second heart sound of phonocardiographic (PCG) signal) are given in Section 2.1. Novel methods to calculate arterial blood pressure by using PTT and RS2 are introduced in Section 2.2. Section 2.3 gives a description of some techniques based on the analysis of the PCG signal. Section 2.4 describes novel non-invasive methods to estimate the pulmonary artery pressure based on the analysis of the PCG signal. Section 2.5, describes the solution implemented in this thesis, which involves the design and implementation of an electronic device able to acquire the ECG and PCG signals and send them via Blue tooth to the computer for off-line analysis. The acquisition of ECG and PCG signals offers different possibilities to estimate BP, such as:

- Relationship between RS2 and BP
- Relationship between amplitude of S2 and BP
- Double integration of the PCG to estimate BP
- Time and frequency analysis of S2 to estimate PAP

Section 2.5 also describes other possibilities that were considered to be implemented in this thesis (such as the acquisition and analysis of PPG signal), and explains the advantages of the chosen solution.

Chapter three provides the description of the implemented hardware. In Section 3.1 an introduction to the implemented solution is given. Section 3.2 describes the analog circuit used to acquire the ECG signal. Section 3.3 provides a description of the implemented circuit used to acquire the PCG signal; the different options considered to acquired and demodulate the PCG signal are also described in this section. The power management if the circuit is described in Section 3.4. The microcontroller and Bluetooth module, used to convert the ECG and PCG analog signals into digital and transmit them to a PC, is described in Section 3.5. Section 3.6 provides a description of the prototype design, including the PCB (Printed Circuit Board) layout design and the design of the case that contains the PCB and the battery.

Chapter four provides a description of the software. Section 4.1 briefly describes the used STM32 microcontroller. Section 4.2 and Section 4.3 describe the implemented firmware used to convert into digital the ECG and

PCG signals and transmit them via Bluetooth to a PC for offline analysis. Section 4.4 provides the flowcharts of the processes described the in previous sections.

Chapter 5 provides a description of the different signal processing techniques used in this project. They include traditional filtering, peak detector, and spectral estimators. The main concepts of analysis and design of digital filters are presented in section 5.3, and some examples are illustrated in the processing of the ECG and the PCG signals. Section 5.4 shows the test results of an experiment conducted on 5 healthy subjects to analyze the capabilities of RS2 on SBP estimation.

The last chapter reports the conclusions and future developments.

TABLE OF CONTENTS

FIGURES AND TABLES

LIST OF ABBREVIATIONS

A_2	Aortic component of the second heart sound (S2)
AAMI	American Association for the Advancement of Medical Instrumentation
ABS	Acrylonitrile Butadine Styrene
AC	Alternating Current
ADC	Analog to Digital Conversion
BHS	British Hypertension Society
BP	Blood Pressure
BT	Bluetooth
CCF	Cross Correlation Function
CO	Cardiac Output
DBP	Diastolic Blood Pressure
DC	Direct Current
ECG	Electrocardiogram
FIR	Finite Impulse Response Filter
HHT	Hilbert-Huang Transform
HPF	High Pass Filter
HSE	High Speed External Clock
INA	Instrumentation Amplifier
KCL	Kirchhoff's Current Law
LPF	Low Pass Filter
LTI	Linear Time Invariant
MA	Motion Artifacts
MABP	Mean Arterial Blood Pressure (MABP = DBP + PP/3)
MEMS	Microelectromechanical System
NIBP	Non-invasive Blood Pressure

NN	Neural Network
OpAmp	Operational Amplifier
P_2	Pulmonary component of the second heart sound (S2)
PAP	Pulmonary Artery Pressure
PC	Personal Computer
PCB	Printed Circuit Board
PCG	Phonocardiogram
PDM	Pulse Density Modulation
PEP	Pre Ejection Period
PHT	Pulmonary Hypertension
PP	Pulse Pressure (PP = SBP – DBP)
PPG	Photoplethysmography
PR	Peripheral Resistance
PTT	Pulse Transit Time
PWM	Pulse Width Modulation
PWV	Pulse Wave Velocity
RC	Resistor-Capacitor Circuit
RF	Radio Frequency
RS1 signal	Time interval between the peak of the R wave of the ECG and the peak of the first heart sound of the PCG signal
RS2 signal signal	Time interval between the peak of the R wave of the ECG and the peak of the second heart sound of the PCG
S1	First Heart Sound
S2	Second Heart Sound
S1S2 the	Time interval between the peak of the first heart sound and peak of the second heart sound of the PCG signal
SBP	Systolic Blood Pressure

SI	Splitting Interval
SK	Sallen-Key analog filter topology
SNR	Signal to Noise Ratio
SPI	Serial Peripheral Interface
VCVS	Voltage-Controlled Voltage-Source
VTT	Vessel Transit Time

Chapter 1

INTRODUCTION TO BLOOD PRESSURE

The aim of this chapter is to provide an introduction on the principles of blood pressure and a historical overview of the different blood pressure measurement methods. A short description of the anatomy (structure) and physiology (function) of the heart and blood vessels and their contribution to the blood pressure will be given in section 1.1. The purpose of section 1.2 is to give a brief description of the blood pressure measurement methods.

1.1 PRINCIPLES OF BLOOD PRESSURE

Before describing what is the blood pressure (BP) and how it can be measure it seems logical to start with a brief account of the blood circulation [**1**] (Figure 1.1). In the average adult, the circulatory system contains approximately five liters of blood. At rest, the heart will pump almost this amount of blood around the body each minute. Assuming that a person is resting, the heart will beat approximately 70 times each minute (the heart rate), although the rate is variable and depends on many factors other than the level of physical activity. Therefore, each heartbeat propels around 70 ml of blood from the left side of the heart into the aorta. The amount of blood pumped into the aorta during each heartbeat is known as the stroke volume.

As Figure 1.1 indicates, there are effectively two separate circulations each fed by their own pump. Each pump corresponds to one side of the heart and has two chambers: the atria or receiving chambers and the ventricles or ejecting chambers. The right ventricle sends blood into the pulmonary circu-

lation via the pulmonary arteries. These vessels take the blood to the lungs where it releases carbon dioxide and soaks up oxygen. The blood returns though the pulmonary veins to the left atrium, flows through a valve to the left ventricle and is then pumped through the aorta to the arteries. After delivering oxygen and other nutrients to the tissues, blood returns through the veins to the right atrium.

The contraction of the ventricles is called systole and the interval between contractions when the ventricles are refilling with blood is called diastole. During systole, the aorta and the large arteries do stretch, but only to a limited extend. This requires a considerable amount of energy, which is store in the vessels walls. During the diastole, this energy is release in the form of elastic recoil. This squeezing effect helps to maintain the BP and the flow of the blood through the capillaries.

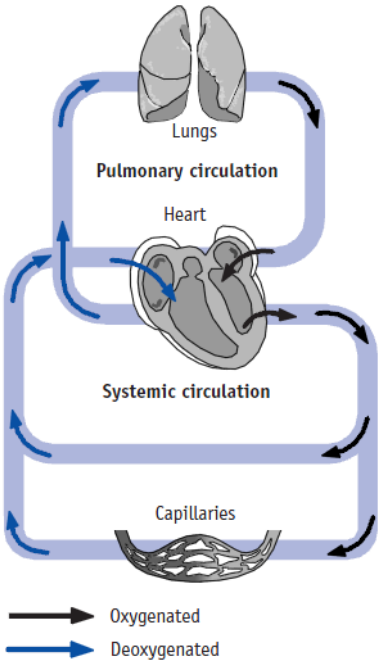

Figure 1.1. The circulation of the blood. Diagrammatic representation of the heart, lungs and circulation

Constriction or dilation of the arterioles, supplying a particular tissue, will determine what proportion of the cardiac output reaches the tissue capillaries. The total of all the resistance of the arterioles supplying the systemic circulation is the major constituent of the total **peripheral resistance**, which is the resistance to the passage of blood through the systemic system.

Blood pressure (BP) is the pressure exerted by circulating blood upon the walls of blood vessels, and is one of the principal vital signs. For each heartbeat, BP varies between systolic and diastolic pressures. Systolic pressure (SBP) is the peak pressure in the arteries, which occurs near the end of the cardiac cycle when the ventricles are contracting. Diastolic pressure (DBP) is minimum pressure in the arteries, which occurs near the beginning of the cardiac cycle when the ventricles are filled with blood. The reading is therefore the pressures during these two phases of the heart's action. The difference between the SBP and the DBP is the pulse pressure (PP) and the mean arterial blood pressure (MABP) is taken to be the DBP plus one-third of the pulse pressure (MABP = DBP + PP/3)

The BP depends upon two factors:

- The cardiac output (CO = stroke volume × heart rate)
- The peripheral resistance (PR)

For any given blood volume:

$$MABP = CO \times PR \qquad \textbf{Eq. 1.1}$$

The higher the cardiac output and peripheral resistance, the higher the BP. Increasing the peripheral resistance by constriction of the arterioles leads to a rise in BP; dilatation of the arterioles lowers the BP.

BP varies enormously, not just between individuals, but in the same individual from time to time. SBP and DBP are not static but undergo natural variations from one heartbeat to another and throughout the day. They also change in response to stress, nutritional factors, drugs, disease, exercise, and body position (for example, momentarily from standing up). Sometimes the variations are large. Older people have more collagen in their arterial walls than younger people and this makes the arteries stiffer and less elastic. It is very common to find that BP, especially SBP rises with age.

Due to the pulsatile nature of blood flow, arterial BP has a characteristic waveform. The contour of this pressure wave varies throughout the body, as well as with increasing age and cardiovascular disease states [**2**] (Figure 1.2). In normal individuals the pulse pressure is greater in the peripheral arteries than in the aorta (for example, PP is greater in the femoral artery than in the thoracic aorta, and it is greater in the brachial artery than in the aorta). However, this increase in pulse pressure between the aorta and peripheral arteries declines with age, as the elasticity of the arteries decreases (Nichols

et al 2005). Therefore, measurement of BP by standard sphygmomanometer is more useful for estimating central aortic BP in older subjects than in younger individuals.

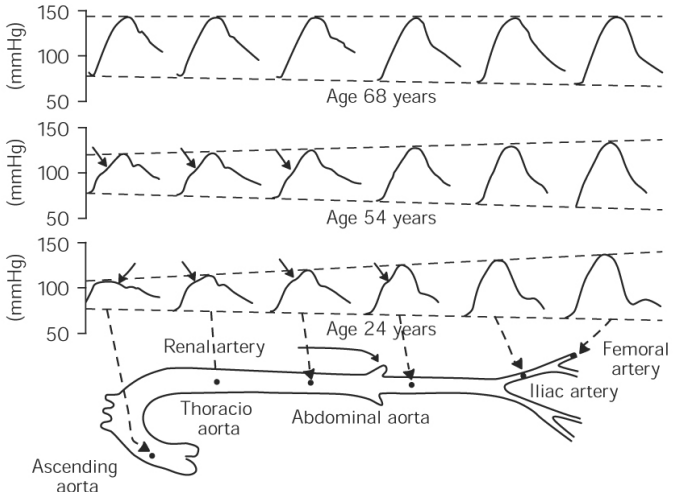

Figure 1.2. Typical arterial pressure waveforms according to age

Along with body temperature, respiratory rate, and pulse rate, BP is one of the four main vital signs routinely monitored by medical professionals and healthcare providers.

BP generally refers to the arterial pressure in the systemic circulation. However, measurement of pressures in the venous system and the pulmonary vessels plays an important role in intensive care medicine but requires an invasive central venous catheter. Table 1.1 reassumes the normal pressure range in different sites of the body.

Site		**Normal Pressure Range (in mmHg)**
Central venous pressure		3-8
Right ventricular pressure	Systolic	15-30
	Diastolic	3-8
Pulmonary artery pressure	Systolic	15-30
	diastolic	4-12
Pulmonary vein		2-15
Left ventricular pressure	Systolic	100-140
	Diastolic	3-12

Table 1.1. Normal Pressure Range in different sites of the body

1.2 BLOOD PRESSURE MEASUREMENT METHODS

Cardiovascular diseases are one of the leading causes of death. Blood pressure is an important physiological parameter and often there is a need for continuous or periodical monitoring, especially in patients that require intensive care.

This section gives an overview of the different BP measurement methods. The requirements for common international standards and accuracy are also shortly described.

In Chapter 2, novel techniques for non-invasive continuous BP measurement, based on phonocardiography (PCG), photoplethysmography (PPG) and electrocardiography (ECG) signals are introduced as an alternative to the methods presented in this section.

1.2.1 Standards and Accuracy Validation

In 1987, the American Association for the Advancement of Medical Instrumentation (AAMI) published a standard for sphygmomanometers, which included a protocol for evaluating the accuracy of devices. According to the AAMI standard [**3**]:

- The mean difference between different measurements must be less than 5 *mmHg*
- The standard deviation must be less than 8 *mmHg* with 85% of the measurements and the in the 20-250 *mmHg* range.
- Accuracy better than 10 *mmHg* must be achieved with 95% of the measurements.

In the protocol devised by the British Hypertension Society (BHS) in 1990, accuracy falls into four grades, A to D, where A denotes the greatest and D the least agreement. These grades represent the cumulative percentage of readings falling within 5, 10 and 15 *mmHg*. To fulfill the BHS protocol a device must achieve at least grade B.

	Absolute difference between standard and test device		
Grade	**≤5**	**≤10**	**≤15**
A	60%	85%	95%
B	50%	75%	90%
C	40%	65%	85%
D	Worse than C		

Table 1.2. Grading Criteria used by the BHS

1.2.2 Invasive Measurement

The most accurately arterial BP measurement is achieved invasively through an arterial line. Invasive arterial BP measurement with intravascular cannula involves direct measurement of arterial pressure by placing a cannula needle in an artery (usually radial, femoral, dorsalis pedis or branchial). The cannula must be connected to a sterile, fluid-filled system, which is connected to an electronic pressure transducer. The advantage of this system is that pressure is constantly monitored beat-by-beat, and a waveform (a graph of pressure against time) can be displayed. Invasive BP measurement methods are generally used in hospitals, especially in intensive care units since they are known to carry a risk (associated with complications such as thrombosis, infection, and bleeding). Patients with invasive arterial monitoring require very close supervision, as there is a danger of severe bleeding if the line becomes disconnected. Risks of these kinds could be avoid if there was a non-invasive method offering a high degree of accuracy and real time operation in a continuous, beat-to-beat mode. Further, the method should be insensitive to the patient's motion artifacts (due to voluntary or involuntary movements of patient while recording the data from the sensor) and respond rapidly to cardiovascular changes.

1.2.3 Auscultatory Method

The auscultatory method uses a stethoscope and a sphygmomanometer. This involves placing a cuff around the upper arm at roughly the same vertical height as the heart, attached to a mercury or aneroid manometer. A cuff of appropriate size is inflated it to a pressure greater than the SBP, which compresses the brachial artery. As the cuff is deflated, the blood flow

through the compressed artery resumes. The sounds associated with the changes in blood flow which occur as the pressure in the cuff is decreased, are known as the Korotkoff sounds. The physician determines BP by listening for the Korotkoff sounds with a stethoscope. The pressure at which this sound is first heard is the systolic BP. The cuff pressure is further released until no sound can be heard (fifth Korotkoff sound), at the diastolic arterial pressure. The appearance and disappearance of sound can be used to determine SBP and DBP, respectively, while the cuff deflates. However, establishing the point at which sound disappear is not always obvious, in fact, misleading readings are easy to record.

In ambulatory measurements, when the patient is able to move moderately, noise may become dominant, thereby spoiling the measurement. This may be avoided by using two identical microphones under the cuff, one located on the upper side and the other on the distal side. Ambient noise reaches both microphones at the same time, but the BP pulse propagating through the brachial artery arrives after a time delay. This phenomenon can be used for noise cancellation as described by Sebald et al (2002) [**4**].

Figure 1.3. Sphygmomanometer for auscultation

1.2.4 Oscillometric Method

The oscillometric method was first demonstrated in 1876 and involves the observation of oscillations in the sphygmomanometer cuff pressure which are caused by the oscillations of blood flow [**3**]. The electronic version of this method is sometimes used in long-term measurements and general practice. It uses a sphygmomanometer cuff like the auscultatory me-

thod, but with an electronic pressure sensor (transducer) to observe cuff pressure oscillations, electronics to automatically interpret them, and automatic inflation and deflation of the cuff. The size of the cuff must be correct for each patient: undersized cuffs may yield too high a pressure, whereas oversized cuffs yield too low a pressure. The pressure sensor should be calibrated periodically to maintain accuracy. Oscillometric measurement requires less skill than the auscultatory technique, and may be suitable for use by untrained staff and for automated patient home monitoring.

The values of SBP and DBP are computed, not actually measured from the raw data, using an algorithm; the computed results are displayed. The simplified measurement principle of the oscillometric method is a measurement of the amplitude of pressure change in the cuff as the cuff is inflated from above the systolic pressure. The amplitude suddenly grows larger as the pulse breaks through the occlusion. This is very close to systolic pressure. As the cuff pressure is further reduced, the pulsation increase in amplitude, reaches a maximum and then diminishes rapidly. The index of diastolic pressure is taken where this rapid transition begins. Therefore, the systolic blood pressure (SBP) and diastolic blood pressure (DBP) are obtained by identifying the region where there is a rapid increase then decrease in the amplitude of the pulses respectively. Mean arterial pressure (MAP) is located at the point of maximum oscillation.

An algorithm and experimentally obtained coefficients are used to adjust the oscillometric results to give readings which match the auscultatory results as well as possible. Some equipment uses computer-aided analysis of the instantaneous arterial pressure waveform to determine the systolic, mean, and diastolic points. Since many oscillometric devices have not been validated, caution must be given as most are not suitable for clinical and keen care settings.

1.2.5 Volume Clamp, or Vascular Unloading Method

In 1973, Penaz invented the continuous non-invasive BP measuring method based on a finger cuff, photoelectric plethysmogram (transmitter and detector), and the pressure controller unit. Boehmer (1987) from Ohmeda Monitoring Systems introduced a prototype device, later known as FinapresTM, based on the vascular unloading method, in which the cuff on the finger is pressurized to the same pressure as the artery. Cuff pressure was

controlled by electronic, automatic adjustments so that it equaled the intra-arterial pressure all times and pulsated with arterial pressure. These measurements consisted of photoplethysmographic measurements of finger volume; a light source and a detector located inside a transparent cuff measured blood volume alterations. Cuff pressure was controlled by a servo technique using a microprocessor to keep the blood flow stable; when the pressure inside the artery increased, external cuff pressure increased by the same amount at the same time. The system automatically corrected changes induces by smooth muscle contractions or relaxations.

Finapres devices are no longer available, since they have been replaced by another device, known as Finometer, a trademark of FMS, Finapres Medical Systems BV, Arnhem, Netherlands. The company also produces PortapresTM BP monitors, which measure two fingers alternately, enabling one finger to normalize while the other is being measured.

(a) (b)

Figure 1.4. (a) Finometer; (b) Portapres

The Finometer measures finger BP non-invasively on a beat-to-beat basis and gives a waveform measurements similar to intra-arterial recordings. The Finometer measures the brachial pressure and corrects for finger pressure accordingly. It also corrects for the hydrostatic height of the finger with respect to the heart level. In 2003 [**5**] the Finometer was validated according to the revised BHS protocol and the criteria of the AAMI. A validation test was carried out using a subject group of 102 black women, which was also divided into smaller groups, namely 24 hypertensive, 25 obese normotensive and 35 lean normotensive women. Finometer and mercury sphygmomanometer BP were taken. Within the whole group, the Finometer satisfied the AAMI criteria for accuracy and achieved and overall A/B grading according to BHS criteria. The average difference between the mercury

sphygmomanometer and Finometer readings for SBP and DBP were, respectively, -1.83±6.8 and 0.88±7.5.

1.2.6 Tonometric Method

The arterial tonometer is a pressure measurement method that can non-invasively and continuously record pressure alterations in a superficial artery with sufficient bony support, such as the radial artery [**6**]. It uses a miniature transducer or a rigid sensor array or a flexible diaphragm, which is attached on the skin above the pulsating artery. Skin and tissue located between the sensor and the array transfer pressure pulsations between them. When the pulsations reach their strongest level, the sensor is regarded as being correctly positioned. This can be facilitated by using a sensor array and selecting sensor elements with the strongest amplitude. This method requires that the sensors are closely alike in terms of sensitivity. Next the sensor or sensor array is pushed towards the vessel using, for example, air pressure. The vessel flattens when the pressure and, consequently, the force against the artery wall increases. Arterial pressure in the top of the flattened artery's center equals the supporting pressure, allowing the recording of an accurate BP profile. If the pressure increases too much, the artery will occlude totally and the measurement will be erroneous. Thus, the hold-down pressure must be continuously controlled using stress distribution information. Furthermore, the size of the sensor or sensor element must be small relative to the artery and the sensor material must be rigid, which has led to the use of piezoelectric or piezoresistive (made of silicon) materials. Moreover, sensor arrays enable the use of motion artifact cancellation methods to improve the signal-to-noise ratio.

In 1997, the tonometer monitor known as Colin Pilot 9200 was validated using intra-arterial BP as a reference, obtaining an accuracy of (2.24 ± 8.7) *mmHg* and (0.26 ± 8.88) *mmHg* which slightly exceeded the allowable standard deviation of error. Since then, the Colin tonometer has been used to estimate the waveform of central aortic BP using mathematical transformation. Nowadays, the Colin Pilot is represented by DRE Medical, Inc., USA. In recent years, new tonometric based devices have been developed. The SphygmoCor System is a non-invasive diagnostic technology that enables pulse wave analysis of the central, ascending aortic pressure wave. The SphygmoCor system obtains peripheral arterial pressure waveforms by applying an arterial applanation tonometer to the wrist. The tonometer partial-

ly compresses the radial artery and records a pressure wave over several cardiac cycles. This pressure wave is calibrated to brachial cuff BP measurements. The averaged peripheral waveform is then converted to an ascending aortic waveform using a generalized mathematical transfer function. Arterial tonometry has the possibility of monitoring BP continuously. However, due to wrist motion and high sensitivity to sensor position, the arterial tonometer is not convenient for use in rough environment.

Figure 1.5. Example of radial artery pressure waveform recorded with the SphygmoCor

1.2.7 Pulse Transit Time Methods

Pulse Wave Velocity (PWV) is a measure of the elasticity (or stiffness) of peripheral arterial blood vessels and its measurement is based on simultaneous measurement of two pulse waves at two different positions. By determining the pulse transit time (*PTT*) between these points and the distance measured between the two locations (*L*), PWV can be calculated:

$$PWV = \frac{L}{PTT}$$

PTT is the time it takes the pulse pressure waveform to travel between two arterial sites. An acute rise in BP causes vascular tone to increase and hence the arterial wall becomes stiffer causing the PTT to be shortened. Conversely, when BP falls, vascular tone decreases and PTT increases. It has been demonstrate than PTT is inversely proportional to BP.

The pressure pulse detection can be done with different kind of sensors, such as PPG sensors, microphones or piezoelectric sensors which generate a measurable voltage at the output contacts if they are mechanically deformed.

Next Chapter is dedicated to describe in detail the non-invasive BP measurement methods based on PTT.

Chapter 2

NON-INVASIVE CONTINUOUS BLOOD PRESSURE MEASUREMENT METHODS BASED ON ECG, PCG AND PPG SIGNALS

Traditional methods, described in chapter 1, such as the sphygmomanometry and the oscillometry are unable to monitor the short-term dynamic variability that occurs with BP, and the invasive nature of arterial cannulation limits its use to critically ill patients. A noninvasive beat-to-beat measurement of BP would be extremely valuable. A number of approaches have been developed, including finger blood-volume clamping and arterial tonometry. Although some studies have suggested that there is reasonable accuracy with these systems, the technology itself is generally expensive, cumbersome, and prone to motion artifacts (due to voluntary or involuntary movements of patient while recording the data from the sensor). An alternative technique involves measuring the transit time of the pulse pressure wave through the arterial tree. Recently a novel parameter RS2 (defined as the time interval measured from the R wave of electrocardiographic (ECG) signal to the peak of second heart sound of phonocardiographic (PCG) signal) was proposed for the same purpose.

Compared with apparatus based on oscillometry, tonometry and volume clamp, apparatus using pulse transit time (PTT) and RS2 to monitor BP are

more suitable in space because the sensors they use have simple structure and wear comfortably.

The definition of PTT is given in Section 2.1. Novel methods to calculate arterial BP by using PTT and RS2 are introduced in Section 2.2. Section 2.3 gives a description of some techniques based on the analysis of the PCG signal. Section 2.4 provides information about non invasive pulmonary artery pressure measurement methods based on PCG signals. Section 2.5 introduces the solution implemented in this thesis, which is explained in detail in Chapter 3.

2.1 PULSE TRANSIT TIME

Pulse Transit Time (PTT) refers to the time it takes a pulse wave to travel between two arterial sites. The speed at which this arterial pressure wave travels (Pulse Wave Velocity) is proportional to BP. An acute rise in BP causes vascular tone to increase and hence the arterial wall becomes stiffer causing the PTT to shorten. Conversely, when BP falls, vascular tone decreases and PTT increases.

Absolute values of PTT cannot be extrapolated as absolute values of BP at a given point in time, but PTT is capable of predicting changes in BP over a short period of time. Different expressions have been derived to characterize the relationship between the BP and the PTT. Most effective ones are Moens-Korteweg's and Bramwell-Hill's, which have been widely used. Essentially, the elasticity of an artery was recognized to be related to the velocity of the volume pulses propagating through it.

The pulse wave velocity (PWV) is defined by Moens and Korteweg as a function of such factors as the thickness of vessel wall (t), the elasticity of the arterial wall, the density of blood (ρ) and the interior diameter of the vessel (d). The equation is shown as follows:

$$PWV = \sqrt{\frac{tE}{\rho d}} \qquad \textbf{Eq. 2.1}$$

where E stands for the Young's modulus describing the elasticity of the arterial wall, and generally it is not a constant. Further, the Young's modulus E was described by Geddes as$E = E_0 e^{\alpha P}$, where E_0 is the modulus of

the zero pressure, α is a constant that depends on the vessel, varying from 0.016 $mmHg^{-1}$ to 0.018 $mmHg^{-1}$, and P is the BP. Then we have:

$$PWV = \sqrt{\frac{tE_0 e^{\alpha P}}{\rho d}} \qquad \textbf{Eq. 2.2}$$

Bramwell and Hill have found that the propagation velocity of the pulse wave in the artery filled with blood is related to the volume-pressure relationship of the artery, with the assumption that the artery is an elastic tube filled with an incompressible and invisible liquid, which can be written as:

$$PWV = \sqrt{\frac{V}{\rho}\frac{\Delta P}{\Delta V}} \qquad \textbf{Eq. 2.3}$$

where PWV is the velocity of pressure wave, V is the volume of the tube, ρ is the density of the blood, ΔV is the volume change, and ΔP is the change in the distending pressure.

The velocity of pressure wave can also be described as

$$PWV = \frac{L}{PTT} \qquad \textbf{Eq. 2.4}$$

where L is the length of the pulse wave propagation along the artery, and PTT is the pulse transit time. Therefore, the velocity of local pressure wave can be readily estimated by using this equation. It requires no knowledge of the thickness and diameter of the vessel, or of the elasticity of the arterial wall, but only the rate of increase of volume with pressure, which is simple and directly observable. The compliance, C, which represents how much the change in the volume is in response to a given change in the pressure:

$$C = \frac{\Delta V}{\Delta P} \qquad \textbf{Eq. 2.5}$$

Thus, PTT can be written in terms of compliance and volume:

$$\left(\frac{L}{PTT}\right)^2 = \frac{V}{\rho C} \qquad \textbf{Eq. 2.6}$$

According the above discussion, the BP is inversely proportional to pulse transit time, and the relationship between them is individual-dependent. Many authors apply the linear regression in estimating the BP [**7**]: first, the

coefficients of the model are identified based on the experimental data; second, the model is used for BP estimation.

Originally PTT was measured by recording the time interval between the passage of the arterial pulse wave at two consecutive sites. More recently, for ease of measurement, the electrocardiographic R wave has been used as the starting point as it corresponds approximately to the opening of the aortic valve. Advances in technology have allowed accurate estimation of the arrival of the pulse wave at a peripheral site such as the finger using photoplethysmography. Other sites where an arterial wave form can be detected such as the ear lobe can also be used, though they are less convenient. Therefore, PTT can be measured as the time interval between the peak of R wave of the electrocardiogram (ECG) and a characteristic point at predetermined thresholds of the photoplethysmogram (PPG) in the same cardiac cycle, which is the blood propagation period from the aortic valve to a peripheral site.

The starting point of PTT is the R wave peak of ECG, and mainly there are three different choices for the ending point [**8**]: (1) the foot of the PPG signal (Figure 2.1), (2) the peak of the PPG signal, and (3) the maximum inclination of the PPG signal. However, some authors define PTT in different ways and attention must be paid when reading about the topic. Together with the PTT, other time intervals can be defined as showed in Figure 2.1.

- PEP = Pre-Ejection Period: Time from R-peak (ECG) to the first heart sound (PCG). PEP represents the contraction time of the heart, which is the time it takes for the myocardium to raise enough pressure to open the aortic valve and start pushing blood out of the ventricle.
- VTT = Vessel Transit Time: time from first heart sound (PCG) to onset of peripheral pulse (PPG).

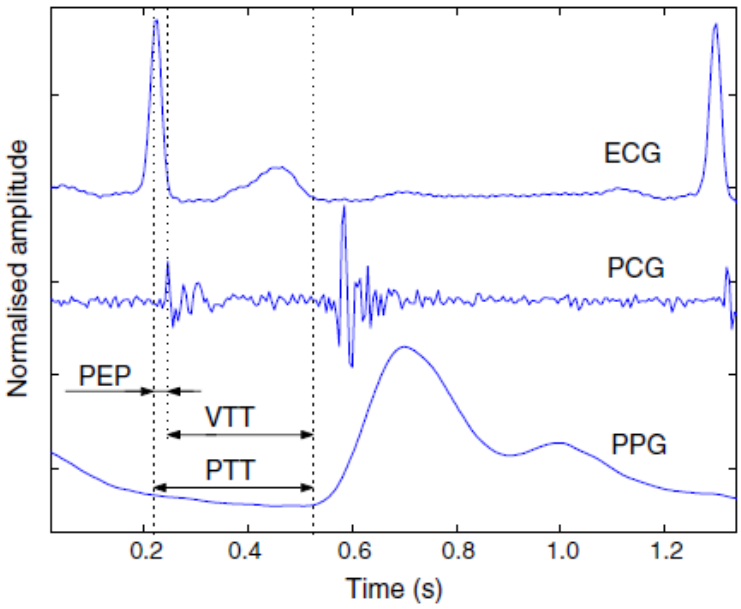

Figure 2.1. Definition of transit times; pre-ejection period (PEP), vessel transit time (VTT) and pulse wave transit time (PTT = PEP + VTT)

2.2 BLOOD PRESSURE MEASUREMENT METHODS BASED ON ECG, PPG AND PCG SIGNALS

Non-invasive and cuff-less measurement of arterial blood pressure (BP) is desirable for continuous patient monitoring. Among the possible techniques, pulse transit time (PTT) based approach for estimation of BP is one of the most promising. This section provides a brief description of different non-invasive methods to estimate BP based on PTT and other techniques based on the analysis of electrocardiographic (ECG), phonocardiographic (PCG) and photoplethysmographic (PPG) signals.

2.2.1 Blood Pressure Measurement Methods Based on PPG Signals

Pulse Wave Velocity (PWV) is a measure of the elasticity (or stiffness) of peripheral arterial blood vessels and its measurement is based on simultaneous measurement of two pulse waves at two different positions. By de-

termining the pulse transit time (PTT) between these points and the distance measured between the two locations, PWV can be calculated (Eq. 2.4)

$$PWV = \frac{L}{PTT}$$

The pressure pulse detection can be done with different kind of sensors, such as PPG sensors, microphones or piezoelectric sensors which generate a measurable voltage at the output contacts if they are mechanically deformed.

The research group led by Prof. Harry Asada at the Massachusetts Institute of Technology, USA, introduced a ring sensor in 1998. They proposed a method for cuff-less long-term BP monitoring using a state estimator. In this approach, only PPG sensors were placed around a patient's finger for continuous measurements 24 hours a day. In addition, the device contained a microcontroller required to control the pulsing of the LEDs, data acquisition, signal conditioning and filtering. It had also a MEMS accelerometer for artifact rejection and an RF transmitter and a button-type lithium battery. In the next generation of devices, this single ring sensor arrangement was replaced by a double, isolating, ring system, where the inertial mass of the battery and printed circuit board could not influence the inner ring, where the LEDs and the photo diode were placed (Figure 2.2).

This system was artifact-resistant and insensitive for ambient lighting, enabling its application to moving, continuous 24-hour heart rate monitoring for almost a month using a button cell battery. Later, they proposed artifact recovery method, based on a MEMS acceleration sensor. The method subtracts the signal produced by the MEMS sensor from the corrupted PPG.

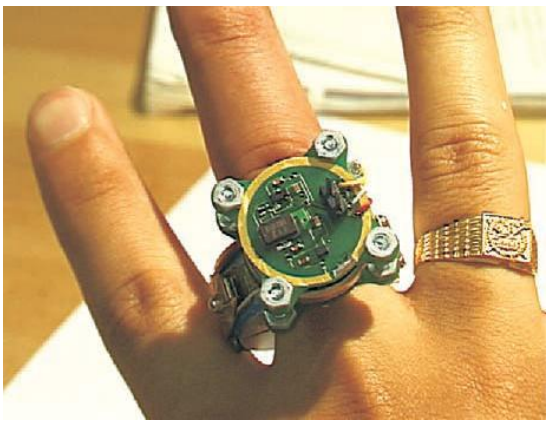

Figure 2.2. Prototype ring sensor with RF transmitter

In 2010, Asada's group has patented a wearable PWV BP sensor and methods of calibration [**9**]. PPG waveform data are simultaneously collected from leading sensor located along the lunar artery at the wrist and from the sensor located along the digital artery of a finger (Figure 2.3). Each PPG sensor provides a voltage output corresponding to the arterial circulatory waveform at that location. The pulse transit distance (Δx) between the two sensors is measured as the physical distance between the two sensors. The transit time (Δt) between the two sensors of the propagating pressure wave is determined from the circulatory waveforms captured by the two PPG sensors. The estimated peripheral PWV can be determined from:

$$PWV = (\Delta x) / (\Delta t) \quad \textbf{Eq. 2.7}$$

The ability to utilize PWV to estimate BP is based on the relationship that both the PWV and the BP shares with the arterial vessel elasticity E. Using the Moens-Korteweg equation (Eq. 2.2):

$$P = \frac{1}{\alpha}\left(ln\frac{d\rho c^2}{tE_0}\right) \quad \textbf{Eq. 2.8}$$

or,

$$P = k_1(\ln(c^2) + k_2) \quad \textbf{Eq. 2.9}$$

where k_1 and k_2 are constant. The value of k_1 can be estimated by measuring the effect that a change in peripheral arterial pressure (ΔP) has on the measured peripheral wave speed. A change in the peripheral arterial pressure may be achieved by altering the height (h_s) of the sensor relative to the height of the heart (h_0). By altering the height of the two sensors relative to the heart a measurable change in arterial pressure is produced which is equal to the hydrostatic pressure difference created by the difference in height between the heart and the sensors:

$$\Delta P = \rho g(h_s - h_0) \quad \textbf{Eq. 2.10}$$

Measurement of PWV taken at two heights along with the difference in height between the two locations provides a solution for the constant k_1:

$$P_1 = P + \rho g(h_{s1} - h_0) = k_1(\ln({c_1}^2) + k_2) \quad \textbf{Eq. 2.11}$$

$$P_2 = P + \rho g(h_{s2} - h_0) = k_1(\ln({c_2}^2) + k_2) \quad \textbf{Eq. 2.12}$$

$$P_1 - P_2 = \rho g(h_{s1} - h_{s2}) = k_1[\ln({c_1}^2) - \ln({c_2}^2)] \quad \textbf{Eq. 2.13}$$

The constant k_1 can be calculated for any individual as:

$$k_1 = \left(\frac{\rho g(h_{s1} - h_{s2})}{2\ln\left(\frac{c_1}{c_2}\right)} \right) \quad \textbf{Eq. 2.14}$$

Determination of k_2 depends on its variability across the population and/or for a given individual:

If k_2 shows a little variation across specific population subsets, which may be grouped according to age, sex, etc, then using a set of empirically predetermined k_2 terms may be suffice for accurate pressure estimation.

If large individual variation in k_2 does exist, the individual calibration will be required.

If k_2 is relatively constant for an individual in different cardiovascular states, then a single calibration for each state will be required.

Initial calibration can be achieved using a DPB reading (P_{cuff}) from an oscillometric cuff along with the corresponding estimates of wave speed from the onset times of the two circulatory waveforms and knowledge of k_1:

$$k_2 = \frac{1}{k_1} P_{cuff} - \ln(c^2) \quad \textbf{Eq. 2.15}$$

Once the initial calibration of the various states is achieved determination of k_1 alone should allow to determine which previously identified k_2 is appropriated for the current pressure estimation. If the individual variability of k_2 is very large, then k_2 requires estimation each time the two sensors are attached to the patient.

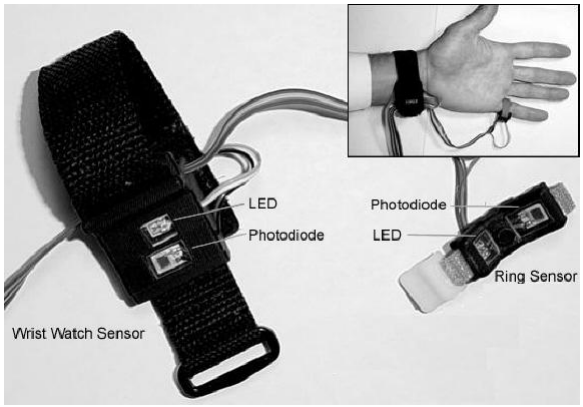

Figure 2.3. Wearable BP measurement system proposed by Asada's research group

The 2010 device combines not only a unique dual in-line PPG device architecture with the adaptive hydrostatic calibration but also novel system identification techniques to accurately estimate the calibration parameters (Figure 2.4).

In the last decade, different research groups have developed PPG based measurement systems. In 2004, a research group of the Southern Taiwan University of Technology proposed a dual channel PWV measurement system consisting in two parts: a portable non-invasive signal interception device and a pulse wave analytic software. The device measured the pulse wave signals (PPG) of finger and toe and calculated the PWV ad the ratio of pulse wave transmission distance and the transmission time (Figure 2.5).

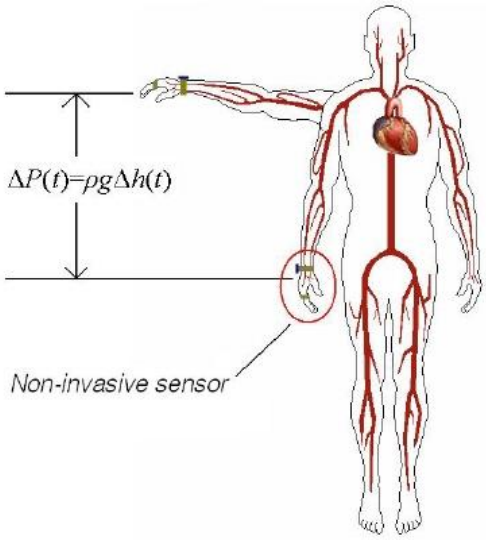

Figure 2.4. Wearable BP estimation using adaptive hydrostatic calibration of peripheral PPT measurements

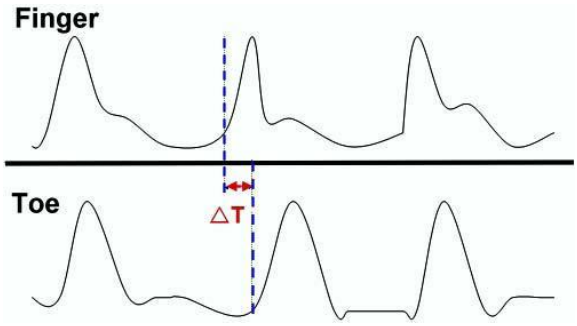

Figure 2.5. Time difference of pulse wave pace point of finger and toe

In the USA, the company Intelesens patented a method which uses a high speed transducers to provide an accurate measurement even over a short distance of the lower arm without the need of the ECG measurement for synchronization [**10**]. The Pulsesens system is based on two fast response piezoelectric sensors, which can be used on various parts of the body, such as the lower arm (Figure 2.6). This system is wireless and is capable of transmit the information to a standard PC. The system is easy to place and reliable readings can be obtained without skilled staff, meaning it could be a home based monitoring system.

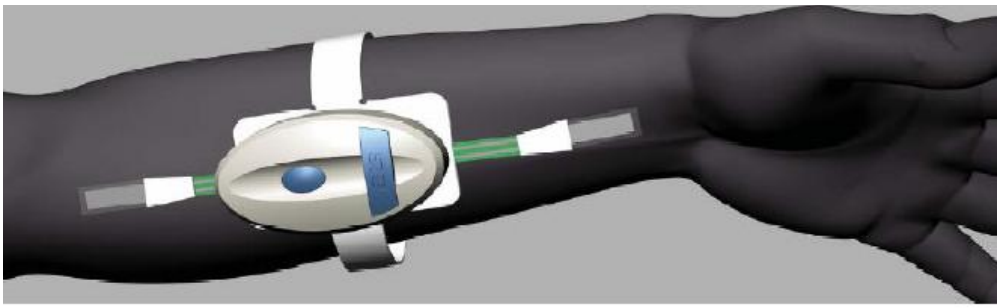

Figure 2.6. Pulsesens system from Intelesens in radial/brachial form

2.2.2 Measurement Methods Based on PPG and ECG Signals

Since the discovery of the volume clamp method and experience gained of the Finapres BP measurement method, optical photoplethysmographic (PPG) finger pulse detection has been the principal pulse detection method for many researchers.

In 2000, the research group led by Prof. Wenxi Chen at the Soka University in Japan, proposed a continuous non-invasive method of systolic BP estimation based on measuring the beat-to-beat time interval between R peak

in the ECG signal and the onset of the PPG in an oximeter sensor placed on a fingertip [**11**]. The SBP was estimated by combining two separately obtained components: a higher frequency component obtained by extracting a specific frequency band of PTT and a lower frequency component obtained from the intermittently acquired SBP measurements with an auscultatory or oscillometric system. Figure 2.7 illustrates the estimation of SBP from PTT and intermittent calibration points. The PTT is filtered through a narrow band-pass filter ($F_L = 0.00053$ *Hz*, $F_H = 0.004$ *Hz*) and multiplied by a coefficient to create the higher frequency component. The lower frequency component is the result of a linear interpolation from the discrete points (marked as 'O') of calibration measurement at a regular interval of 5 minutes. The estimated SBP is obtained by combining the HFC and the LFC.

The method was examined in 20 patients during cardiovascular surgery using an invasive method as reference. The obtained accuracy for SBP was 0.97 ± 0.02 *mmHg* and the error remained within ±10% in 97.8% of the monitoring period. They found that reliable information on SBP change can be extracted from the variation in PTT even if this was not enough to estimate the absolute level of SBP. This means that variation in the SBP can be estimated from the PTT in a defined frequency band. The problem was that the lower frequency component of PTT was not as well correlated to SBP as well as to its absolute level (DC component); thus, a slow change in BP cannot be determined from the PTT. To solve this difficulty, they proposed a method of combined the PTT and intermittent calibration measurement to estimate SBP continuously.

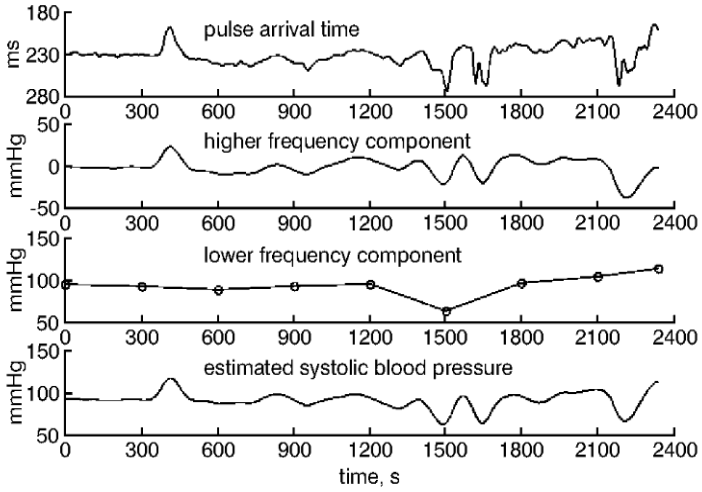

Figure 2.7. Illustration showing the estimation of SBP from pulse arrival time and intermittent calibration points

The principle used by Chen's group was the analytical expression described by the Moens-Korteweg formula (Eq. 2.2):

$$PWV = \sqrt{\frac{tE_0 e^{\alpha P}}{\rho d}}$$

where t is the thickness of vessel wall, ρ is the density of blood, d is the interior diameter of the vessel, E_0 is the modulus of the zero pressure, α is a constant that depends on the vessel, varying from 0.016 $mmHg^{-1}$ to 0.018 $mmHg^{-1}$, and P is the BP. Responding to BP variation, the change in the elastic modulus overshadows that of the wall thickness and vessel diameter. This is the reason why an increase in BP accompanies an increase in the PWV. The PTT is inversely proportional to PWV and it can be written as (Eq. 2.4):

$$PWV = \frac{L}{PTT}$$

Therefore:

$$\frac{tE_0 e^{\alpha P}}{\rho d} = \frac{L^2}{PTT^2} \qquad \textbf{Eq. 2.16}$$

taking the logarithm:

$$P = \frac{1}{\alpha}\left[ln\left(\frac{\rho d L^2}{tE_0}\right) - 2\,ln(PTT)\right] \qquad \textbf{Eq. 2.17}$$

if the changes in t and d with respect to the change in BP are negligible , and if the change in the arterial wall tonus (E_0) is slow enough, the first term of the right-hand side can be regarded as a constant during a short period, so that:

$$\Delta P = -\frac{2}{\alpha T}\Delta T \qquad \textbf{Eq. 2.18}$$

From the last equation, it can be seen that, during a short period, if the change in vessel elasticity E_0 is negligible, the change in the PTT can be linearly related to the change in BP. If the estimated BP, P_e, is written as:

$$P_e = P_b + \Delta P \qquad \textbf{Eq. 2.19}$$

where P_b is the base BP level, while ΔP is the change over the base level P_b, then:

$$P_e = P_b - \frac{2}{\alpha T_b}\Delta T \qquad \textbf{Eq. 2.20}$$

where ΔT is the change in the PTT and T_b is the value of the PTT corresponding to the pressure P_b. It is clear that an estimated BP value consists of two terms: a base BP level P_b, and a changing component ΔP, which can be estimated from the change in the PTT (ΔT).

The results of their work showed that combining separately obtained higher frequency and lower frequency components can give an estimation of SBP. The slower change component and DC level of systolic BP can be estimated from the lower frequency component, which is obtained by using an auscultatory system with automatic cuff inflation and deflation.

In the last decade, the research group led by Prof. Yuan Ting Zhang in Hong Kong, has explored the topic. Zhang's group, presented in 2001 a method for non-invasive and cuffless BP measurements for telemedicine purposes. In this method, ECG was used as a timing base and start signal, and PPG from a finger as a stop signal. They defined two stop signals: PTTp and PTTf, which are the time intervals measured from the R-wave of electrocardiographic signal to the peak and the foot of PPG respectively (Figure 2.8). They studied, the relationship between SBP and PTTs and the results showed that SBP was correlated with PTTp and PTTf, with $r=-0.77$ and $r=-0.92$ respectively. The results supported that PTTf was a potential parameter which could be implemented in a personalized wearable device for continuous SBP monitoring at home.

They proposed a device including a WAP-based Internet connection. In 2003, Zheng and Zhang published a paper describing measurements with three different types of PPG ring: convex, flat and concave. A convex-type sensor, in which the LED and the detector are 1 cm apart on the palm side, proved best in compensating for motion artifacts. Lee and Zhang also proposed mathematical methods to compensate for motion artifacts, referred to as stationary wavelet transform and wavelet transform modulus maxima, achieving a remarkable improvement.

Teng and Zhang used this PPG ring for BP measurements on 15 young, healthy subjects. To provide reference measurements, they used oscillometric measurements, taken at three different stages: rest, step-climbing exercise and recovery from the exercise, indicated an accuracy of (0.2 ± 7.3) *mmHg* for systolic and (0.0 ± 4.4) *mmHg* for diastolic BP. A year later,

Hung reported a wireless measurement concept using Bluetooth for telecommunication from a PPG ring to a mobile phone, PC or PDA device. The achieved accuracy was (1.8 ± 7.6) *mmHg* for systolic and (0.5 ± 5.3) *mmHg* for diastolic BP. Poon and Zhang extended the measurements to include 85 subjects reaching an accuracy of (0.6 ± 9.8) *mmHg* for systolic and (0.9 ± 5.6) *mmHg* for diastolic BP.

The results of Zhang's research group studies have shown that beat-to-beat PTT and SBP were highly correlated within a short period but the correlation coefficient decreased when the number of beats increased. A common solution to the calibration of PTT-based is to use readings of conventional cuff-based BP devices [**12**]. Nevertheless, the results of their studies found that this approach may not be suitable for estimating beat-to-beat BP. In recent papers, they have considered the inherent nature of the nonlinear and non-stationary properties of the measured ECG and PPG signals applying different kinds of signal processing techniques, such as the Hilbert-Huang Transform (HHT) which can effectively process the nonlinear and non-stationary signals [**13**].

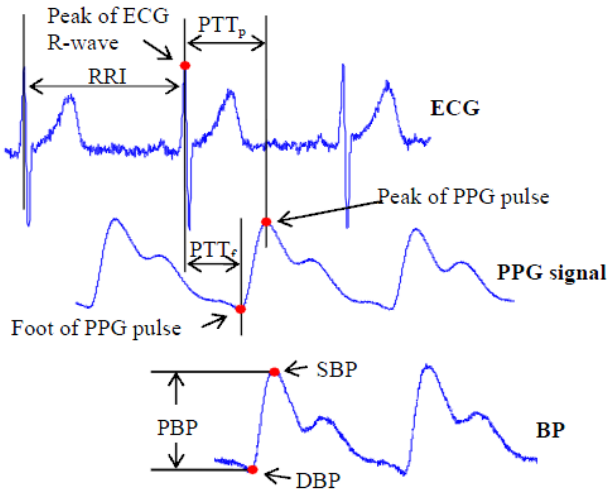

Figure 2.8. Definitions of PTTp and PTTf

In summary, different research groups have shown that beat-to-beat PTT and SBP are highly correlated, but in order to obtain absolute values of BP calibration must be performed. By integration the estimation algorithm into an automatic system of cuff control with oscillometric or Korotkoff sound detection, a convenient non-invasive BP monitoring system can be realized.

2.2.3 Measurement Methods Based on PCG and ECG Signals

To achieve continuous and cuffless BP monitoring, PTT has been reported as a potential parameter. Recently a novel parameter RS2 (defined as the time interval measured from the R wave of electrocardiographic (ECG) signal to the peak of second heart sound of phonocardiographic (PCG) signal) was proposed for the same purpose.

Zhang's research group has studied the relationship between SBP and PTT as well as the relationship between SBP and RS2. The results have shown that SBP is correlated with both PTT and RS2, where the mean individual correlations are r=-0.95 and r=-0.85 respectively, showing that RS2 is possible to be used for continuous and non-invasive monitoring of SBP [**14**]. In order to compare the capabilities of PTT and RS2 on SBP estimation, the relationship between SBP and PTT as well as the relationship between SBP and RS2 were studied after exercise.

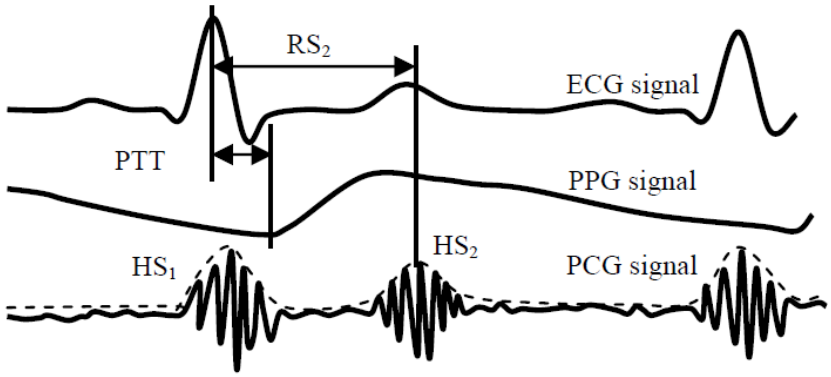

Figure 2.9. An illustration shows the definitions of PTT and RS2 (HS1 and HS2 refer to the first and second heart sound respectively)

The study compared the capabilities of PTT and RS2 on SBP estimation and found that predicting SBP from RS2 have larger deviation than that from PTT after exercises. The large deviations resulted from the RS2 approach is possibly associated with the deep breath after exercises. Compared with PPG signal, deep breath immediately after exercises may affect PCG signal more pronouncedly than it does on PPG signal. Moreover, the noise induced from deep breath may override the heart sound and result in noisy PCG signal. As a result, the effects of deep breath may induce unavoidable error on the peak detection of PCG signal when it is acquired immediately after exercises.

Zhang's group proposed a modified mathematical model of heart-arterial interaction to give insight into the connection between SBP and RS2 [**15**]. The onset of second heart sound is triggered by the closure of aortic valve due to the interaction of left ventricle and arterial system. Non-invasive experiments found that RS2 had a close inverse correlation with arterial SBP. To investigate the underline connections between them, a modified model of heart-arterial system was proposed, where the heart is described as a pressure source depending on time, ventricular volume, outflow, and heart rate, and the arterial system as a nonlinear system incorporating a pressure-dependent compliance. The electrical analog of this model is presented in Figure 2.10. The left ventricle is described as a pressure source depending on time *t*, ventricular volume *Vv*, outflow *Qv* and heart rate *H*. In the modified model, the left ventricular model is coupled to a nonlinear model of arterial system which consists of three elements: characteristic impedance of the proximal aorta R_0, total peripheral resistance R_s, and a pressure-dependent compliance *C(p)*.

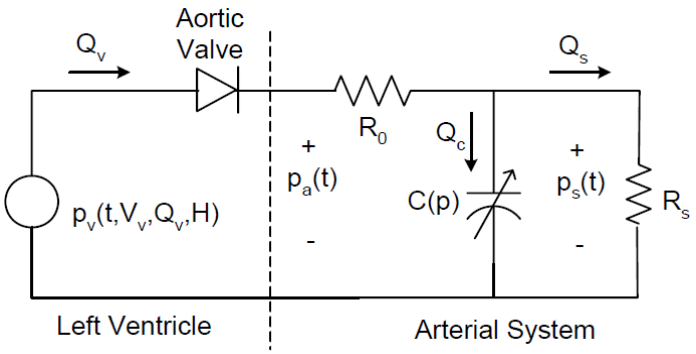

Figure 2.10. Modified model of heart-arterial system

Simulation results show that the modified model is able to reflect the cardiovascular function qualitatively. The results also demonstrate that RS2 is inversely correlated with aortic BP under the effect of changing peripheral resistance, heart rate and contractility. Further studies have also shown that that the increasing aortic pressure results in an increase in frequency and amplitude of produced sound.

2.3 HEART SOUNDS ANALYSIS

The primary task of the heart is to serve as a pump propelling blood around the circulatory system. When the heart contracts, blood is forced

through the valves. First from the atria to the ventricles and then from the ventricles out through the body. Four valves prevent the blood from flowing backwards; the atrioventricular valves (the mitral and tricuspid valve) prevent blood from flowing back from the ventricles to the atria and the semilunar valves (aortic and pulmonary valves) prevent blood from flowing back towards the ventricles once being pumped into the aorta and the pulmonary artery, respectively.

Cardiac muscle cells can possess at least four properties: automaticity (the ability to initiate an electrical impulse), conductivity (the ability to conduct electrical impulses), contractility (the ability to shorten and do work) and lusitropy (the ability to relax). An action potential generated in the sinoatrial node (which normally controls the heart rate) will spread through the atria and initiate atrial contraction. The atria are electrically isolated from the ventricles, connected only via the atrioventricular node which briefly delays the signal. The delay in the transmission allows the atria to empty before the ventricles contract. Cardiac action potentials are conducted to the body surface, where they can be measured as an electrical potential that varies with the current flow through the heart. The ECG can be seen as a projection of a dominant vector (represented by the summation in time and space of the action potentials from each muscle cell) onto a lead vector, whose direction is defined by the position of the measurement electrodes in relation to the heart. The ECG describes the different electrical phases of the heart, where depolarization of the atria gives rise to the P-wave, depolarization of the ventricles combined with repolarization of the atria results in the QRS-complex and repolarization of the ventricles results in the T-wave[**16**].

The electrical R-wave, representing ventricular depolarization, precedes the beginning of ventricular contraction. The ventricular contraction causes a rapid rise in the left ventricular pressure. As soon as the ventricular pressure exceeds the atrial pressure, the mitral valve closes. This is when S1 is heard. When the ventricular pressure exceeds the aortic pressure, the aortic valve opens, and the blood flows from the ventricle to the aorta. At the end of blood ejection, the pressure in the ventricle falls below the aortic pressure, and the aortic valve closes, giving rise to S2. The pressure in the ventricle drops steeply, and when it falls below the atrial pressure, the mitral valve opens, and the rapid filling phase begins. The rapid filling phase might cause an impact sound, the third heart sound (S3), when blood collides with the ventricular wall. Similarly, atrial systole may also produce an audible forth heart sound (S4).

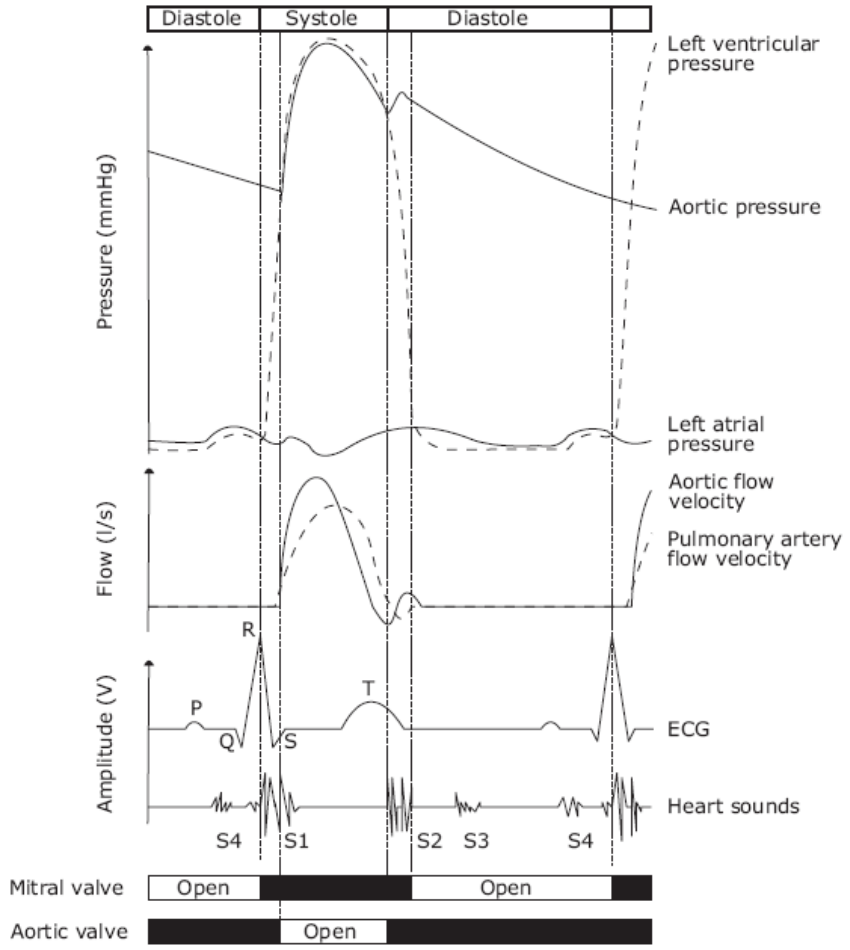

Figure 2.11. Wiggers diagram, showing pressures and flows in the left side of the heart over one heart cycle and how they relate to electrical (ECG) and mechanical (PCG) activity.

The technique of deciphering the sounds from the body based on their intensity, frequency, duration, number and quality is called auscultation. The acoustical signal is affected by a chain of transfer functions before the physician's actual decision-making process starts. The signal transmitted from the sound source is propagated through the human body, where the sound waves are both reflected and absorbed. The most compressible tissues such as lung tissue and fat contribute most to the absorption. Low frequencies are less attenuated compared to high frequencies, but the high frequencies are easier to perceive. Auscultation is usually performed with a stethoscope, which constitutes the second transfer function affecting the sound signal. A basic stethoscope consists of three components: the earpieces, the tubing and the chest piece. It is important that the chest piece fits tightly against the

body because air leakage heavily distorts and weakens the signal. The bell is used to pick up low frequency sounds such as S3 and S4, whereas the diaphragm is used to pick up high frequency sounds such as lung sounds and certain murmurs. From the chest piece the sound is propagated through the tubing to the ear pieces.

The third and last transfer function which affects the sound is the physicians' auditory system. Human hearing is nonlinear and frequency dependent. Further, sound reception deteriorates with age. Fortunately this age discrepancy mainly affects high frequencies above the bioacoustical range.

A graphical representation of the waveform of cardiac sounds (Figure 2.12) is called a phonocardiogram, and the technique used to capture the sound signal is referred to as phonocardiography. This technique allows a visual interpretation of the cardiac sounds, thus allowing thorough investigation of temporal dependencies between mechanical processes of the heart and the sounds produced.

The relationship between blood volumes, pressures and flows within the heart determines the opening and closing of the heart valves. Normal heart sounds occur during the closure of the valves, but how they are actually generated is still debated. S1 is heard in relation to the closing of the atrioventricular valves, and is believed to include four major components.

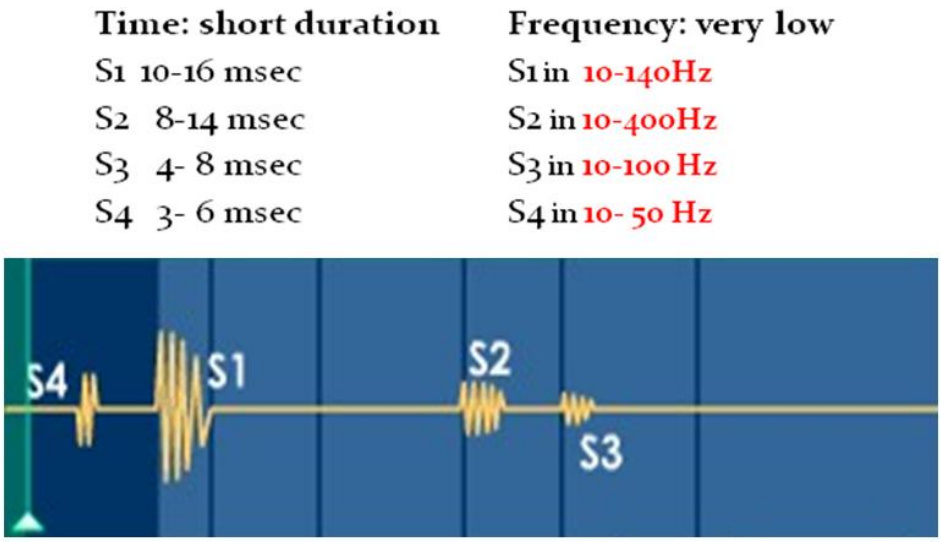

Figure 2.12. Representation of heart sounds. S1: onset of the ventricular contraction; S2: closure of the semilunar valves; S3: ventricular gallop; S4: atrial gallop

The initial vibrations occur when the first contraction of the ventricles accelerate blood towards the atria, just before closure of the atrioventricular valves. The second component is caused by the momentum of the moving blood as it overstretches the atrioventricular valves and recoils back towards the ventricles. The third component involves oscillation of blood between the root of the aorta (and the pulmonary artery) and the ventricular walls, and the fourth component represents the vibrations caused by turbulence in the ejected blood flowing out through aorta.

S2 signals the end of systole and the beginning of diastole, and is heard at the time of the closing of the aortic and pulmonary valves. S2 contains two components, one originating from aortic valve closure and the other from pulmonary valve closure. These two coincide with the ending of left and right ventricular ejection. Since right ventricular ejection ends after left ventricular ejection, the pulmonary sound component occurs slightly after the aortic sound component. The splitting between the two components increases during inspiration because blood-return to the right heart increases, vascular capacitance of the pulmonary bed increases and blood return to the left side of the heart decreases. The opposite occurs during expiration, placing the two components tightly together.

There are also a third and a fourth heart sound (S3 and S4), both connected to the diastolic filling period. The rapid filling phase starts with the opening of the atrioventricular valves. Most investigators attribute S3 to the energy released with the sudden deceleration of blood that enters the left ventricle throughout this period. A fourth heart sound may occur during atrial systole when a final volume of blood is forced into the ventricles.

In last century, several research groups studied the possible relationship between BP and specific characteristics of S1 and S2. There is wide agreement that normal heart sounds (S1 and S2) as heard by cardiac auscultation are not caused directly by the closing of the valves, but by vibrations set up in cardiac blood vessels by the sudden pressure change caused by the closing of the heart valves. That is, PCG and pressure tracing are different manifestations of the same cardiac energy.

2.3.1 Blood Pressure Dependency on First Heart Sound

Sakamoto et al., Circulation Research, 1965, studied whether the amplitude of S1 could be quantitatively related to a force function of ventricular

pressure rise. The function tested were the first and second derivates (rate of change, and rate of rate of change) of ventricular pressure [**17**]. Their results showed that the amplitude of the first sound is not directly related to stroke output, P-R interval, heart rate, diastolic, or systolic ventricular or aortic pressures. Only the peak rate of rise of left ventricular systolic pressure (first derivative maximum) had a consistent relationship to first sound amplitude, suggesting left ventricular pressure (LVP) may be estimated via analysis of S1. Figure 2.13 shows the relationship of S1 amplitude to the maximal rate of left ventricular pressure rise.

Other researchers have shown there is a certain correspondence between the left ventricular PCG and the left ventricular pressure second derivative as well as between the aortic phonocardiogram and the aortic pressure second derivative. This result has led to consider that double integration of the PCG might be used to estimate pressure, or at least to provide some useful information for estimating the pressure using statistical methods [**18**] (Figure 2.14).

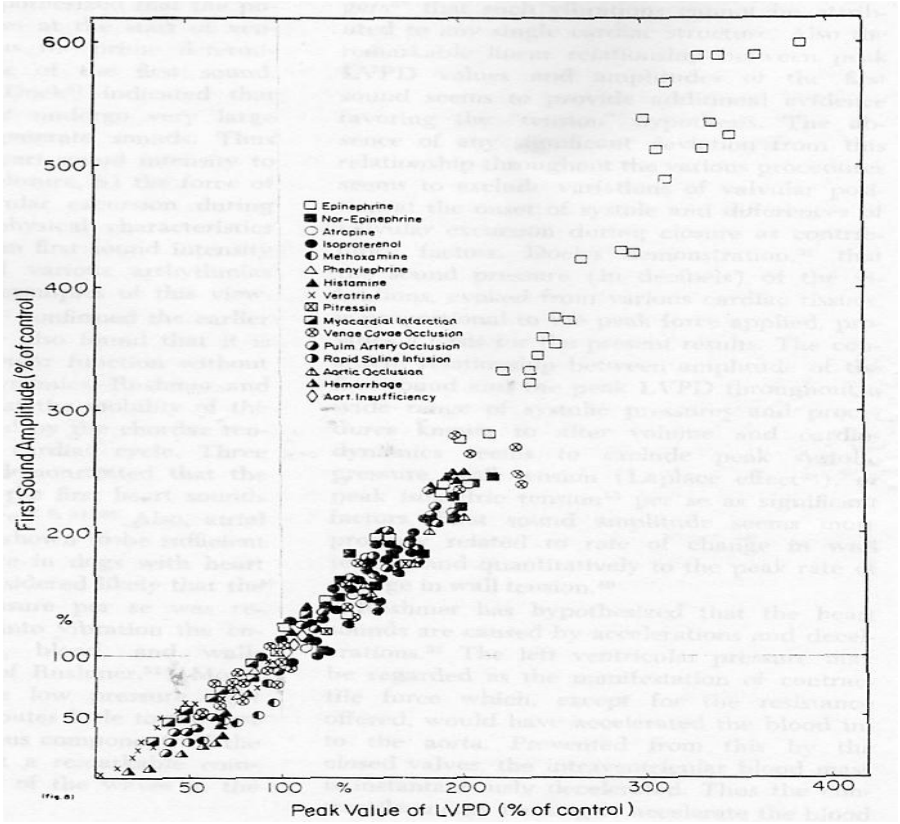

Figure 2.13. Relationship of first heart sound amplitude to the maximal rate of left ventricular pressure rise

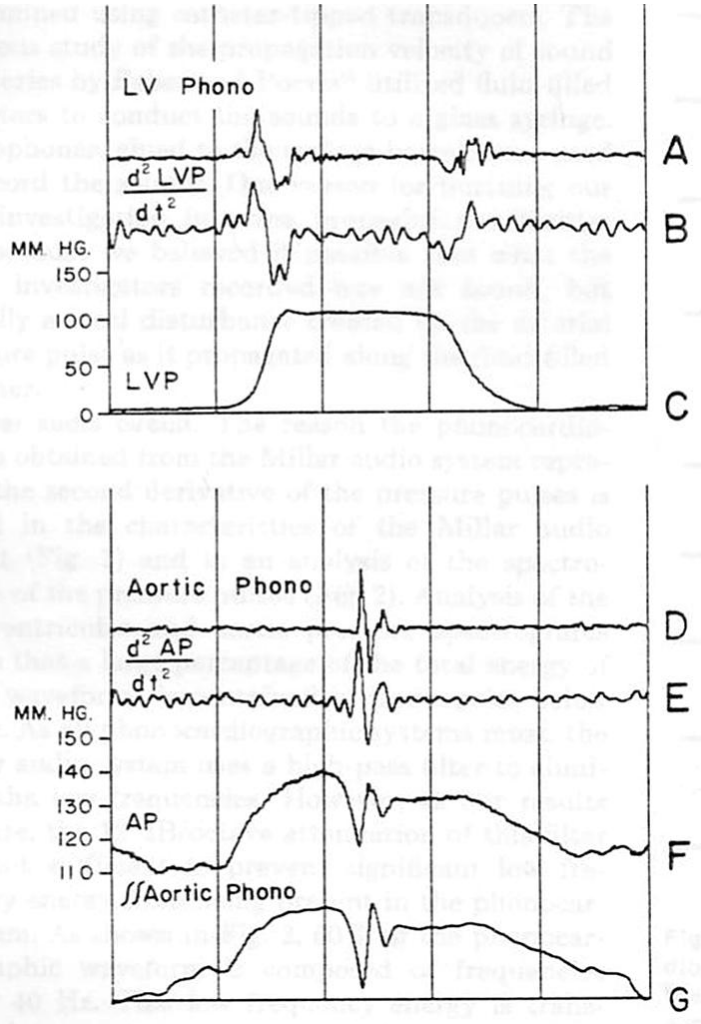

Figure 2.14. Relation between the second derivative of left ventricular and aortic pressure and left ventricular and aortic phonocardiogram.

2.3.2 Blood Pressure Dependency on Second Heart Sound

For many years it has been known in medical diagnostics that the second heart sound of a hypertensive patient shows a characteristic accentuation. This qualitative knowledge yielded to the idea that the acoustic features of S2 correlate with BP. The second heart sound originates at the end of the systole, triggered by the closure of the pulmonary and aortic valves, which occurs shortly after the BP maximum in the aorta. The mechanical oscillation is caused by the elasticity of the vessel walls and the inertia of the blood column. The acoustic spectrum of the second heart sound is expected to depend upon SBP.

The method of pattern recognition has been used in some investigations [**19**]. In the learning phase heart sound features from the individual patient are stored with their dependence upon the measured BP. In the phase of measurement a computer program associates the measured acoustical pattern with the most similar stored pattern, and BP is determined by this association. However, it requires a learning phase with the individual patient, which requires a large quantity of BP values.

Bombardini et al. [**20**], showed that BP (systolic, diastolic and mean) correlated closely with S2 amplitude. This may be explained by the fact that amplitude is primarily determined by one factor, the force of valve closure. Previous studies have shown that it is possible to estimate systemic BP using the spectral information of S2. A mathematical model for the vibration of the closed aortic valve was proposed by Zhang et al. [**21**], showing that the increasing aortic pressure results in an increase both in frequency and amplitude of produced sound. The studies have shown that hemodynamic variables, such as heart rate and BP, correlated more closely with amplitude than with frequency. This may be explained by the fact that amplitude is primarily determined by one factor, force of valve closure, whereas frequency depends on the force of closure, heart volume, and the resonance frequencies of the heart and great vessels. Thus, differences in heart size and intravascular volume status could explain the greater variability (and, thus, weaker statistical correlation) in frequency than amplitude characteristics.

2.4 PULMONARY ARTERY PRESSURE MEASUREMENT

The pulmonary artery pressure (PAP) is a measure found in the pulmonary artery. Pulmonary hypertension (PHT) is an increase in BP in the pulmonary artery and is serious cardiovascular dysfunction that is difficult to assess non-invasively. As the options for treatment of pulmonary hypertension have expanded, the requirement for accurate and non-invasive methods to allow regular and safe estimation of PAP has increased. Consequently, it would be useful to develop other non-invasive methods to allow frequent and accurate measurement of PAP. Different acoustic techniques based on PCG have been proposed by different research groups.

The second heart tone is caused by the closure of semilunar valves and thus by the vibrations that are generated in the heart by the sudden blood

deceleration, at the end of the ventricular systole. Two components can be distinguished: (1) A_2, the aortic component; (2) P_2, the pulmonary one. Both tones have a duration lower than 50 ms and the same frequency content, but they are characterized by a different intensity due to the difference between the closure pressure of the respective valves.

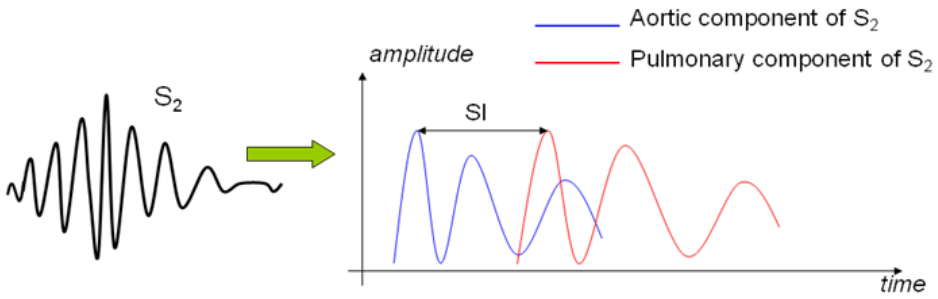

Figure 2.15. Aortic and pulmonary components of S2

Xu et al. [**22**], proposed a method relating systolic, diastolic, and mean pulmonary artery pressure (PAP) to the splitting interval (SI) between the aortic and pulmonary valve closure sounds. The time interval between the aortic (A_2) and the pulmonary (P_2) components of S2, as well as the dominant frequency of P_2, are increased in the presence of pulmonary hypertension. It has therefore been suggested that the A_2- P_2 splitting interval may be useful to estimate the PAP. This technique is based on the modeling of aortic (A_2) and pulmonary (P_2) components using nonlinear transient chirp signals and visual design of a 2-D mask of the Wigner-Ville distribution.

Figure 2.16 represents the principle of the method:

A. The original S2 signal in the time domain.
B. A_2 and P_2 components detected and reconstructed using a spectral dechirping approach.
C. Measurement of SI on the cross correlation function (CCF) between A_2 and P_2.

In panels A and B, time zero is a relative temporal reference corresponding to the beginning of the 100 *ms* temporal window containing S2; in panel C, time zero corresponds to the onset of A_2, as shown in panel B.

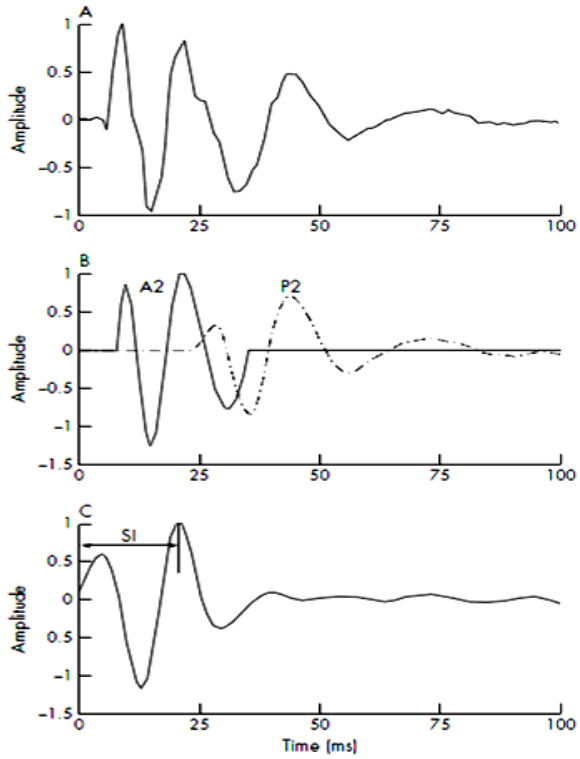

Figure 2.16. Method for the estimation of the splitting interval (SI) between the aortic (A_2) and pulmonary (P_2) components of the second heart sound (S2).

Mohler et at. [**23**] proposed a passive non-invasive method for measurement systemic and/or pulmonic BP. The method accomplishes the measurement through detection, identification and characterization of S2 acoustic signature associated with heart valve closure. The method states that the closure of the aortic and pulmonary semilunar heart valves generate a sound component that is in the audio range. As the systemic or pulmonic BP increases, the frequency components of the related heart valve also increases.

Longhini et al. [**24**] attempted a different approach to the non-invasive estimation of PAP devising a method based on the modifications induced by an increased PAP on the power spectrum of the pulmonary component of S2. They used fast-Fourier analysis to examine the acoustics characteristics of this heart sound to define its frequency distribution in patients with normal and increased PAP to search a relationship between the PAP level and the spectral characteristics of the pulmonary component of S2. In the Longhini method the PCG, ECG were acquired along with the carotid pulse. S2 was extracted from the PCG and the pulmonary component P_2 was extracted from S2 by checking the dicrotic notch of the simultaneous carotid pulse.

The discrete Fourier Transform was applied to P_2 and the maximum amplitude frequency component f_0 was checked. The PAP was then calculated with the equation:

$$PAP = 18.9 * Q + 0.5 * f_0 + 0.3 \quad \textbf{Eq. 2.21}$$

where the Q factor is equal to: $Q = f_0 / B$

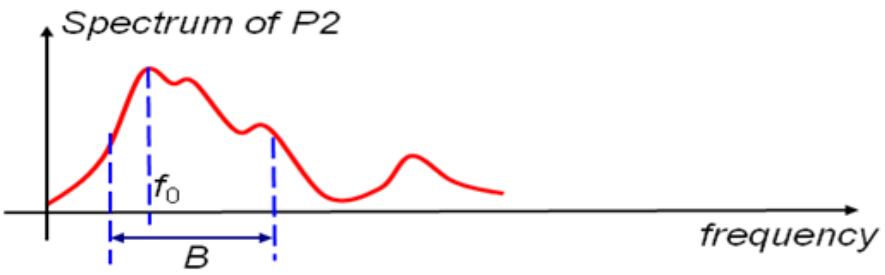

Figure 2.17. Representation of f_0 and B in the spectrum of P_2

The studies performed by Longhini were based only on spectral features extracted from S2, even if it was well known that the splitting interval was an important indicator of pulmonary hypertension. In addition, the relationships between the mean and systolic PAP and the spectral features were modeled with linear regression functions.

Tranulis et al. [**25**] proposed a method for the estimation of PAP by a neural network (NN) analysis using features based on time-frequency representations of S2. To obtain the information required to train and test the NN, an animal model of pulmonary hypertension (PHT) was developed and 9 pigs were investigated. During the test PCG, ECG and PAP were recorded. Different time-frequency techniques (Coiflet wavelet decomposition, Wigner-Ville distribution) were used to extract features from S2 and train the NN. One of the main advantages of the NN was that it could integrate the non linear relationship between the time and frequency features of S2 and the PAP. Consequently, the NN method should provide a more robust PAP estimator, especially for the detection of PHT vs. normal PAP. However, a large number of data is required in order to train the NN.

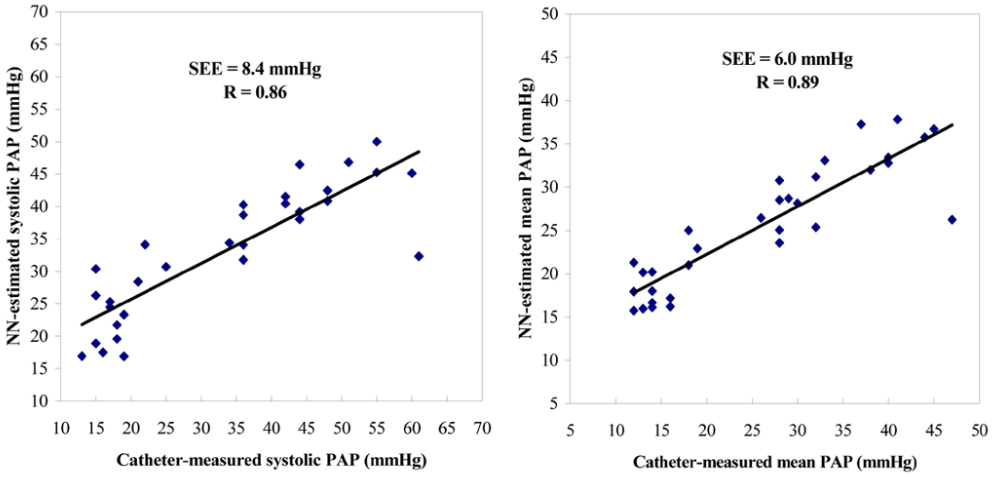

Figure 2.18. Correlation between the systolic (A) or mean (B) PAPs estimated using the NN method and directly measured by catheter. The solid line represents the regression line.

L. Longhini and L. Peretto, from the Unitersità di Ferrara, Italy, developed a method based on the time domain analysis of S2 [**26**]. In the method, the pulmonary component P_2 is extracted from S2 and it is analyzed to obtain its number of oscillations (k) in a given time interval (T), evaluating the number of times the first derivative inverts its sign. The method is based on the vibration-modes analysis, analyzing in the time domain the vibrations produced by the pulmonary valve closure. They applied the following relationship to generate an indirect estimation of PAP:

$$Systolic\ PAP = 22 \times (2^{\frac{k}{6}} - 2) \qquad \textbf{Eq. 2.22}$$

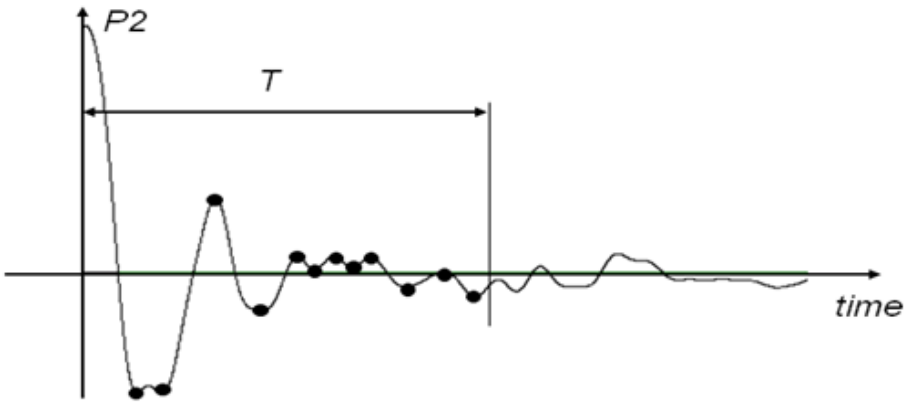

Figure 2.19. Time-domain analysis if P_2 to obtain the number of oscillations (k) in a given time interval (T)

2.5 IMPLEMENTED SOLUTION

As it was described in the previous sections, non-invasive techniques based on the acquisition and analysis of the ECG, PPG and PCG signals can be used to estimate systemic BP. PTT (defined as the time interval between the R wave of ECG signal to the foot of the PPG signal) has been reported as a potential parameter, and recently RS2 (defined as the time interval measured from the R wave of ECG signal to the peak of S2 of the PCG signal), was proposed for the same purpose.

In this thesis work, a device for the acquisition of the ECG and PCG signals was implemented. It was decided to acquire the ECG and PCG signals, rather than the ECG and PPG signal, because the PCG offers different possibilities to estimate BP, such as:

- Relationship between RS2 and BP
- Relationship between amplitude of S2 and BP
- Double integration of the PCG to estimate BP
- Time and frequency analysis of S2 to estimate PAP

One of the purposes of this thesis work was to implement a prototype, including the sensors to acquire the ECG and PCG signals, and a microcontroller and Bluetooth module to transmit the data to a PC for offline analysis. The future goal is to integrate this system to the Body Gateway device, in development by Remote Health monitoring group of the Advanced System Technology division of STMicroelectronics.

The Body Gateway is a remote monitoring device, currently used to compute the heart rate and detect heart beats from the acquired ECG signal. Furthermore it is able to perform an estimation of body physical activity by acquiring accelerometer signals. The goal of this device is to integrate other sensors to perform non-invasive measurements of a range of different parameters of the body.

The Body Gateway is a miniaturized device that goes on the chest. For the sake of the device's size and the comfort of the patient all the sensors should go on the Body Gateway. One of the important reason why the PCG signal was chosen instead of the PPG is that the PPG (generally acquired in the wrist or finger) would have needed satellite sensors distant from the Body Gateway, and this could have compromised the portability, size and comfort of the device.

Since 2008 several prototypes of the Body Gateway device has been developed in different materials as shown in Figure 2.20 and Figure 2.21.

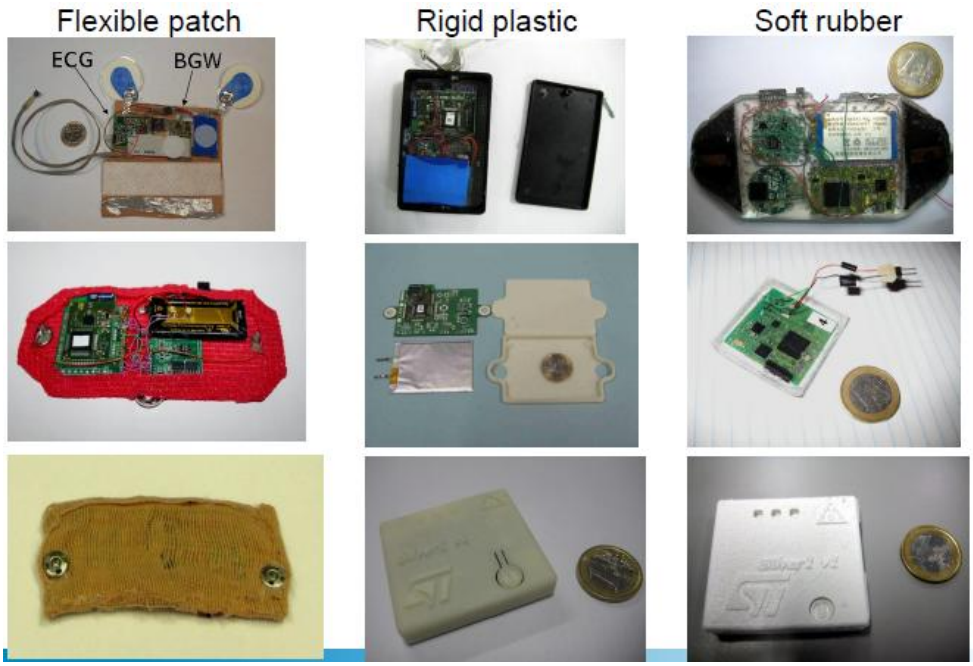

Figure 2.20. Body Gateway prototypes 2008-2009

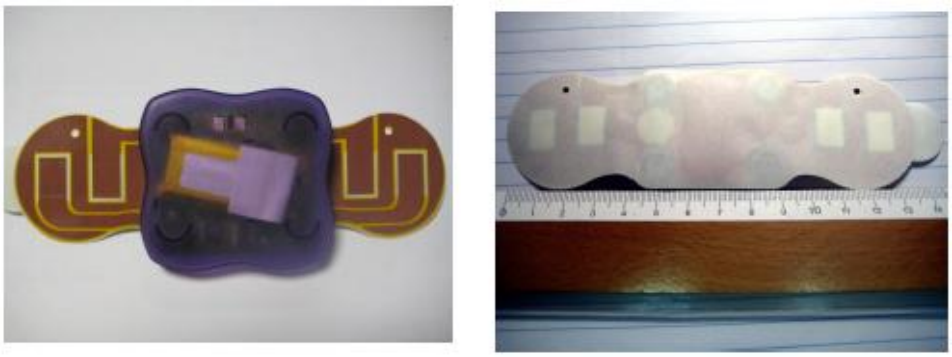

Figure 2.21. Body Gateway prototype 2010

In next chapter the implemented electronic prototype based in the techniques described in this chapter is presented. The circuits used to acquires the ECG and PCG analog signals are described in detail. The different electronic design considerations are also described. Finally, the PCB layout design and case design are also described.

Chapter 3

HARDWARE

As it was described in Chapter 2, non-invasive techniques based on the acquisition and analysis of the ECG, PPG and PCG signals can be used to estimate systemic BP. In this thesis work, a device for the acquisition of the ECG and PCG signals was implemented. Section 2.5 provides an introduction to the implemented solution.

In this chapter the ECG and PCG measurement setup is presented. Section 3.1 gives a general introduction to the implemented prototype. Section 3.2 and Section 3.3 provide a detail description of the designed circuits that are used to acquired the analog ECG and PCG signals, respectively. Section 3.3 describes the power management of the circuit. In section 3.4 the microcontroller and Bluetooth module used to transmit the acquired signals to a PC for offline analysis is described. Section 3.5 describes the design of the PCB layout and the design of the case that contains the device which is used as a mechanical interface between the circuit and the patient's chest.

3.1 GENERAL DESCRIPTION OF THE IMPLEMENTED PROTOTYPE

As it was described in Chapter 2, non-invasive techniques based on the acquisition and analysis of the ECG and PCG signals can be used to estimate systemic BP. RS2, defined as the time interval measured from the R wave of ECG signal to the peak of S2 of the PCG signal, has been reported as a potential parameter to estimate BP. In this thesis work, a device for the acquisition of the ECG and PCG signals was implemented. An introduction to the implemented solution is given in Section 2.5.

The acquisition of ECG and PCG signals offer different possibilities to estimate BP, such as:

- Relationship between RS2 and BP
- Relationship between amplitude of S2 and BP
- Double integration of the PCG to estimate BP
- Time and frequency analysis of S2 to estimate PAP

The main purpose of this thesis work was to implement an electronic prototype able to acquire the ECG and PCG signals and send them via Bluetooth to a PC per offline analysis. Since the future goal of this thesis is to integrate the implemented prototype into the Body Gateway, all the design considerations were made taking into account the fact that the device should be small, portable and comfortable to use.

A general block scheme of the Body Gateway hardware is shown in Figure 3.1.

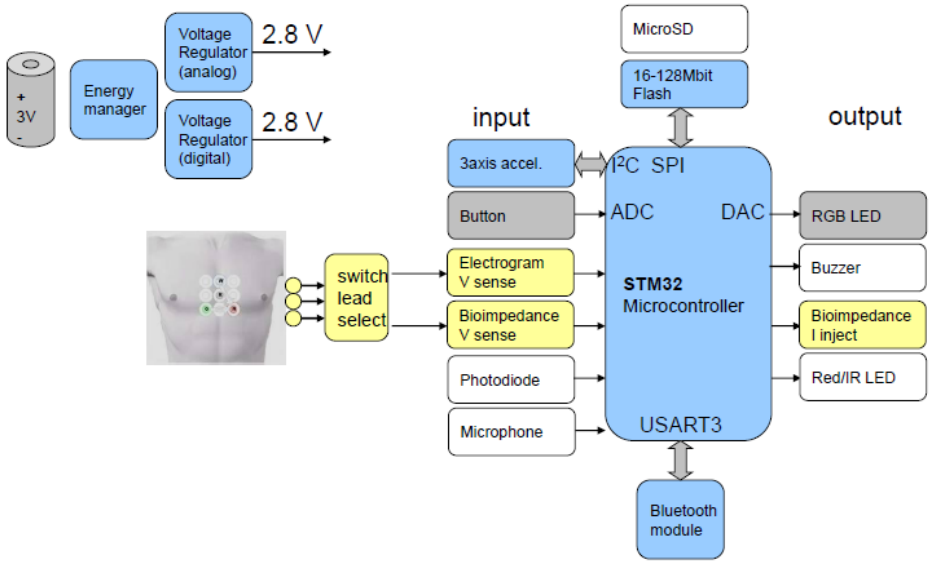

Figure 3.1. Body Gateway hardware block scheme

The general hardware block scheme of the system implemented in this thesis work is shown in Figure 3.2. The hardware has four main components:

- ECG circuit
- PCG circuit
- Power management
- Microcontroller and Bluetooth module

Each part of the device will be described in the following sections.

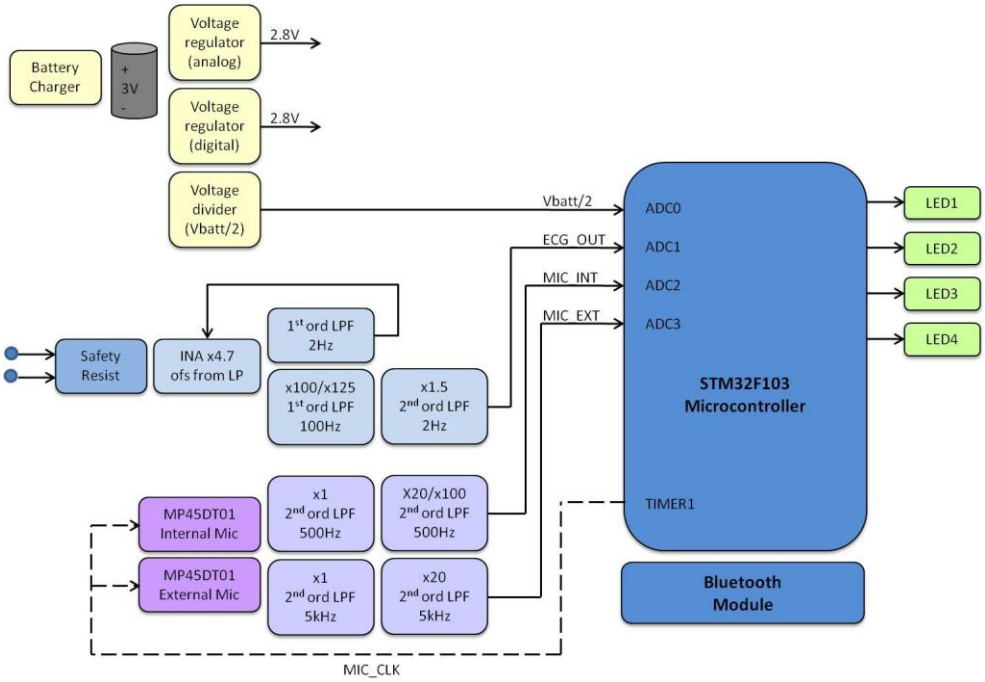

Figure 3.2. Hardware Block Scheme

3.2 ECG CIRCUIT

The ECG is an interpretation of the electrical activity of the heart over time captured and externally recorded by skin electrodes. The ECG works mostly by detecting and amplifying the tiny electrical changes on the skin that are caused when the heart muscle depolarizes during each heart beat. This is detected as tiny rises and falls in the voltage between two electrodes placed on either side of the heart.

Usually more than two electrodes are used and the can be combined into a number of pairs. The output from each pair is known as a lead. Each lead is said to look at the heart from a different angle. For the purpose of this thesis, only two electrodes are used and therefore only one lead is considered. The position of the electrodes has a notably influence on the ECG waveform. The word lead may refer to the tracing of the voltage difference between two of the electrodes.

In the implemented prototype, the electrodes are placed directly on the chest, separated between each other by 8.6 *cm*. Since the purpose of acquir-

ing the ECG signal is to identify the R peak of the signal as the starting point of the RS2 time interval, it is enough to use only two electrodes. However, the electrodes should be placed on the chest in a position where the ECG obtained has a waveform in which is easy to identify the R peak.

A typical ECG tracing of the cardiac cycle (heartbeat) consists of a P wave, a QRS complex, a T wave, and a U wave which is normally visible in 50 to 75% of ECGs. The baseline voltage of the electrocardiogram is known as the isoelectric line. Typically the isoelectric line is measured as the portion of the tracing following the T wave and preceding the next P wave. Table 3.1 describes some of the features of the ECG signal and Figure 3.3 shows a schematic representation of a normal ECG [**27**].

Feature	Description	Duration
RR interval	The interval between an R wave and the next R wave. Normal resting heart rate is between 60 and 100 *bpm*	0.6 to 1.2 *s*
P wave	During normal atrial depolarization, the main electrical vector is directed from the SA node towards the AV node, and spreads from the right atrium to the left atrium. This turns into the P wave on the ECG.	80 *ms*
PR interval	The PR interval is measured from the beginning of the P wave to the beginning of the QRS complex. The PR interval reflects the time the electrical impulse takes to travel from the sinus node through the AV node and entering the ventricles. The PR interval is therefore a good estimate of AV node function.	120 to 200 *ms*
PR segment	The PR segment connects the P wave and the QRS complex. This coincides with the electrical conduction from the AV node to the bundle of His to the bundle branches and then to the Purkinje Fibers. This electrical activity does not produce a contraction directly and is merely traveling down towards the ventricles and this shows up flat on the ECG. The PR interval is more clinically relevant.	50 to 120 *ms*
QRS complex	The QRS complex reflects the rapid depolarization of the right and left ventricles. They have a large muscle mass compared to the atria and so the QRS complex usually has a much larger amplitude than the P-wave.	80 to 120 *ms*
J-point	The point at which the QRS complex finishes and the ST segment begins. Used to measure the degree of ST elevation or depression present.	N/A
ST segment	The ST segment connects the QRS complex and the T wave. The ST segment represents the period when the ventricles are depolarized. It is isoelectric.	80 to 120 *ms*
T wave	The T wave represents the repolarization (or recovery) of the ventricles. The interval from the beginning of the QRS complex to the apex of the T wave is referred to as the absolute refractory period. The last half of the T wave is referred to as the relative refrac-	160 *ms*

	tory period (or vulnerable period).	
ST interval	The ST interval is measured from the J point to the end of the T wave.	320 *ms*
QT interval	The QT interval is measured from the beginning of the QRS complex to the end of the T wave. A prolonged QT interval is a risk factor for ventricular tachyarrhythmias and sudden death. It varies with heart rate and for clinical relevance requires a correction for this, giving the QTc.	300 to 430 *ms*
U wave	The U wave is hypothesized to be caused by the repolarization of the interventricular septum. They normally have a low amplitude, and even more often completely absent. They always follow the T wave and also follow the same direction in amplitude. If they are too prominent we suspect hypokalemia, hypercalcemia or hyperthyroidism usually.	
J wave	The J wave, elevated J-Point or Osborn Wave appears as a late delta wave following the QRS or as a small secondary R wave . It is considered pathognomonic of hypothermia or hypocalcemia.	

Table 3.1. Features of an ECG Signal

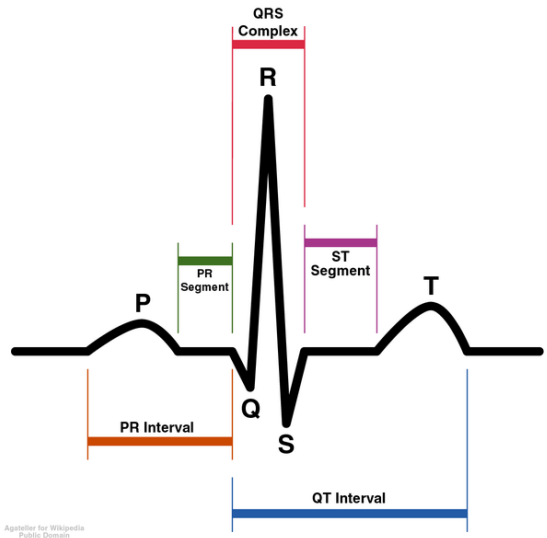

Figure 3.3. Schematic representation of normal ECG

The ECG signal has the following characteristics:

- AC signal with bandwidth of 0.05 to 100 *Hz*, sometimes up to 400 *kHz*
- About 1 mV peak-to-peak amplitude, but it depends on the distance between the electrodes

- External noise at higher frequencies
- Common-mode voltages (common to all electrodes)

The common-mode voltage is comprised of two parts:

1) 50- or 60-*Hz* interferences
2) DC electrode offset potential

Other noise or higher frequencies within the biophysical bandwidth come from:

- Movement artifacts that change the skin-electrode interface
- Muscle contraction or electromyographic spikes
- Respiration
- Electromagnetic interferences
- Noise from other electronic devices that couple into the input

Some noise can be cancelled with a high-input-impedance instrumentation amplifier (INA), which removes the AC line noise common to both inputs and amplifies the remaining unequal signals present on the inputs

The ECG circuit used in this thesis, previously designed by the Remote Monitoring Division of STMicroelectronics, has the following components (Figure 3.4):

- Two skin electrodes
- Input bias resistors and protection resistors on the input wires, that come before the INA
- A single supply instrumentation amplifier (LT1789)
- A first order low pass filter (cutoff frequency=2 *Hz*) to obtain the DC of the output signal of the INA and use it in feedback as its reference value
- A first order low pass filter and a second order low pass filter in order to amplify and filter the signal.
- The analog output of the ECG would be an input to the microcontroller ADC, which will perform the analog/digital conversion.

The circuit has also a digital switch in order to choose (by software) the gain of circuit.

The first part of the circuit consist of the skin electrodes and the single supply instrumentation amplifier (INA) LT1789. The block diagram of the

INA is shown in Figure 3.5. The gain of the LT1789 is set by the value of resistor R_G, applied across pins 1 and 8. The gain G_1 is:

$$G_1 = 1 + 200k\Omega/R_G, \qquad \textbf{Eq. 3.1}$$

In this case:

$$G_1 = 1 + \frac{200k\Omega}{54k\Omega} = 4.7$$

On the output of the INA there is a first order low pass filter with a cutoff frequency of 2 *Hz.*

$$F_{cutoff} = \frac{1}{2 * \pi * 1\mu F * 80k\Omega} \approx 2\ Hz$$

This filter is used to obtain the DC of the output signal of the INA and it is used in feedback as its reference value.

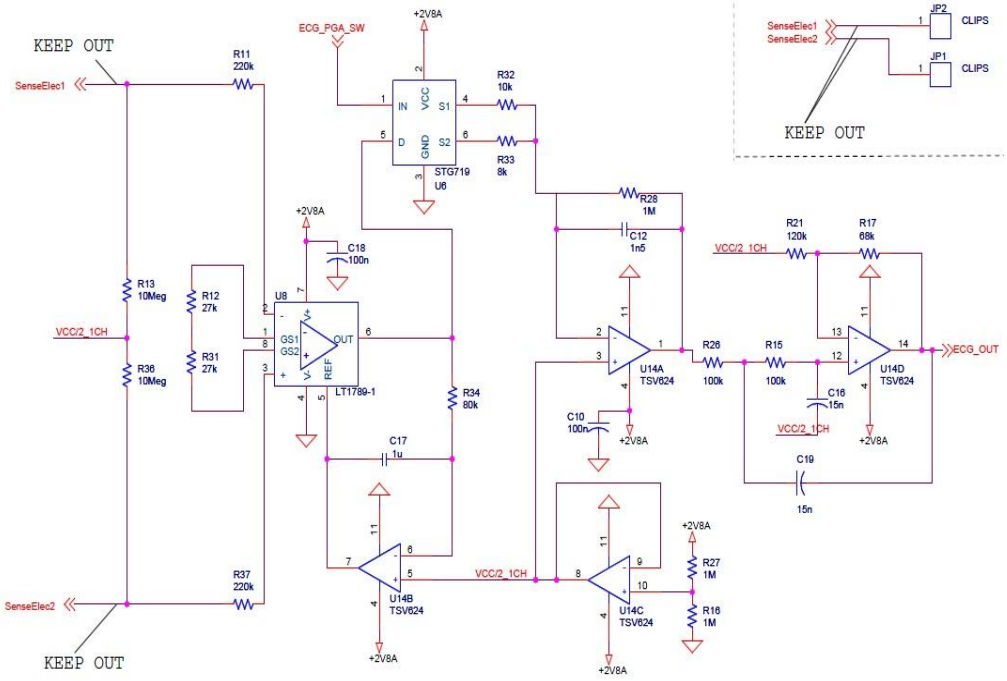

Figure 3.4. ECG Schematic

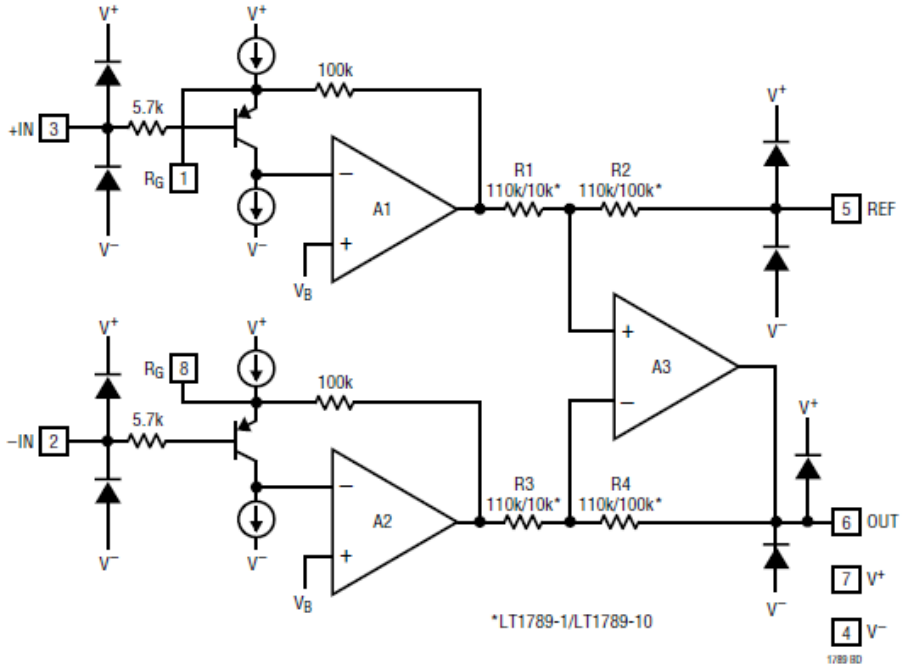

Figure 3.5. LT1789 Block Diagram

The next filter is a first order low pass filter with a cutoff frequency and gain equal to:

$$F_{cutoff} = \frac{1}{2 * \pi * 1.5nF * 1M\Omega} \approx 100\ Hz$$

$$G_2 = \frac{1}{1M\Omega * R}$$

The value of *R* is selected using the switch. For $R=8k\Omega$, the value of the gain is $G_2=125$, and for $R=10k\Omega$, the gain would be $G_2=100$.

The input of the STG719 switch (Pin 1) is connected to the microcontroller, in order to choose via software the value of R and, therefore, the gain of the filter. The truth table of the switch is shown in Table 3.2.

IN	SWITCH S1	SWITCH S2
L	ON	OFF
H	OFF	ON

Table 3.2. STG719 Switch Truth Table

The last filter is a second order low pass has a cutoff frequency and gain equal to:

$$F_{cutoff} = \frac{1}{2 * \pi * 15nF * 100k\Omega} \approx 106\ Hz$$

$$G_3 = \frac{120k\Omega}{68k\Omega} \approx 1.8$$

Both the first order and the second order low pass filters have the function of amplify and filter the signal.

The total gain of the circuit is given by the multiplication of G_1, G_2 and G_3.

The analog output of the ECG circuit would be an input to the microcontroller ADC, which will perform the analog/digital conversion with a sampling frequency of 800 *Hz*, and a 12-bit resolution.

3.3 **PCG CIRCUIT**

The classical way to acquire heart sounds is using a microphone. A microphone is an acoustic-to-electric transducer or sensor that converts sound into an electrical signal. There are different kinds of microphones, such as the condenser microphones and the MEMS microphone, shown in Figure 3.6.

The sensor chosen to acquire the PCG signal was the MP45DT01 MEMS digital microphone. This new product, produced by the STMicroelectronics, is an ultra-compact low power stereo microphone, operates with a single supply voltage (1.64V–3.6V), has omni-directional sensitivity, and provides a digital signal in PDM format. Two microphones were used: one to acquire the heart sounds (internal microphone) and one to detect the external noise for noise cancellation.

The characteristics of the chosen microphone are: signal to noise ratio (SNR) of 60.5 *dB*, frequency range from 20 *Hz* to 20 *kHz*, and small dimensions (3x4 mm), making it ideal to acquire the PCG signal and integrate it in the Body Gateway device.

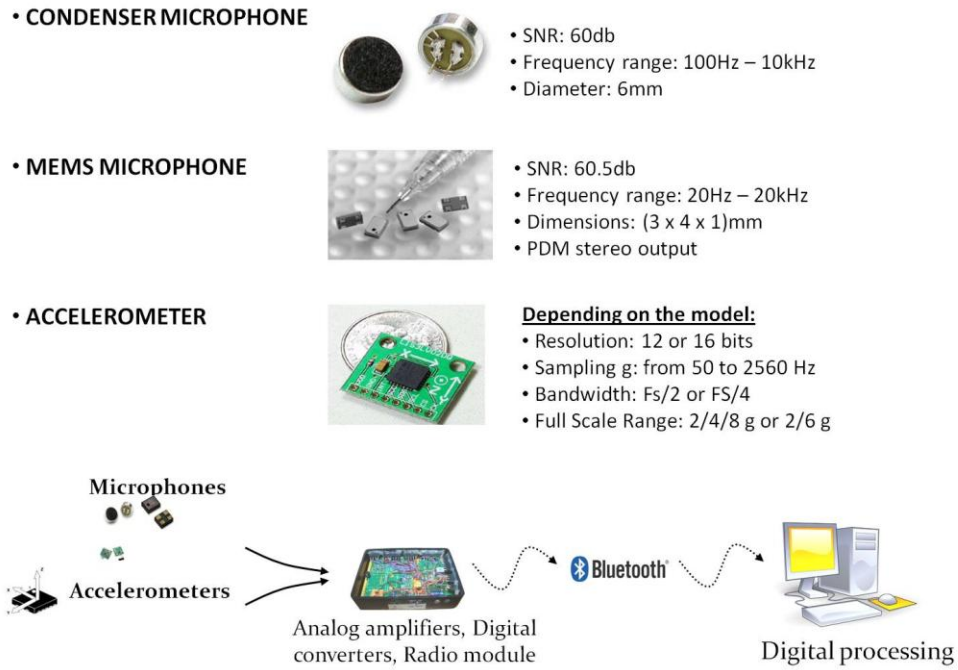

Figure 3.6. Hear sound recording techniques

Since the output of the MEMS microphones is a digital PDM signal, we have considered two possibilities, which are explain in detail in section 3.3.1 and section 3.3.2:

1. Work with the PDM digital output of the microphones.
2. Filter the signals with a low pass filter (demodulate the PDM signals into an analog signal), amplified them and convert them into digital with the microcontroller ADC.

3.3.1 PDM Digital Signal: Decoding and Audio Signal Reconstruction

The MP45DT01 MEMS microphone outputs a PDM signal (Figure 3.7), which is a high frequency (1 to 3.25 *MHz*) stream of 1-bit digital samples. The microphone's PDM output is synchronous with its input clock, which is generated by an STM32 timer. The clock frequency used for both microphones was 2.4 *MHz*.

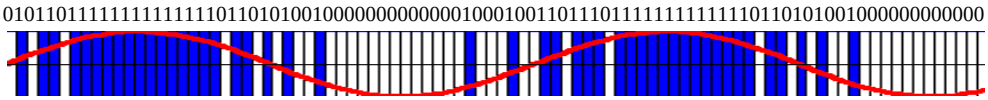

Figure 3.7. An example of PDM a sine wave. 1s represented by blue, 0s represented by white, overlaid with the sine wave

Even though the output of the microphones is a PDM signal, when the pulses are very close between each other they blend together and it is not possible to distinguish the rising edge or the falling edge. In practice, the PDM signal becomes a PWM signal (Pulse Width Modulation), and it makes it difficult to count the pulses correctly.

The PWM uses a rectangular pulse wave whose pulse width is modulated, resulting in the variation of the average value of the waveform. The PWM signal is a rectangular signal with variable duty cycle.

In the PDM signal the relative density of the pulses corresponds to the analog signal's amplitude. A run consisting of all 1s would correspond to the maximum (positive) amplitude value, all 0s would correspond to the minimum (negative) amplitude value, and alternating 1s and 0s would correspond to a zero amplitude value. The continuous amplitude waveform is recovered by low-pass filtering the bipolar PDM bitstream. The PWM is the special case of PDM where all the pulses corresponding to one sample are contiguous in the digital signal. Figure 3.8 shows an example of a PWM signal and a PDM signal.

When the microphone PDM output signal has the pulses very close between each other (high density of pulses), the pulses are not longer separate, they blend together and the waveform becomes a PWM. In this case, using a timer to count the number of pulses will not give a correct result.

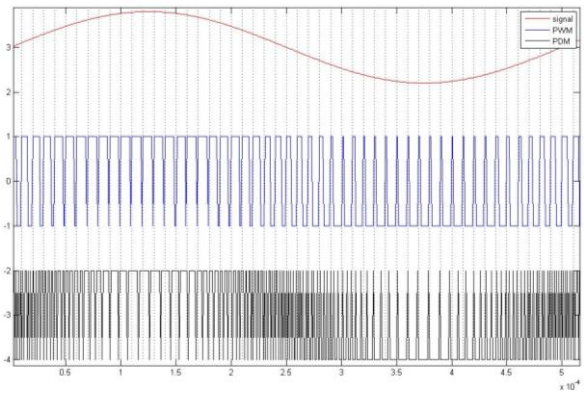

Figure 3.8. PDM and PWM signals

If the output of the microphone was a PWM signal it would be possible to use one of the microcontroller timer, programmed to obtain the duty cycle PWM in one period. On the other hand, if the microphone output was a PDM signal, with the pulses well defined, it would be possible to count the number of impulses with the microcontroller timer.

One possible solution is to use an AND gate between the microphone output and the microphone clock. The output of the AND gate will be connected to one of the microcontroller timer, programmed as counter with the output of the AND gate used as an external clock signal. This way, we can be sure that the it would be possible to identify the rising edge or the falling edge of every impulse.

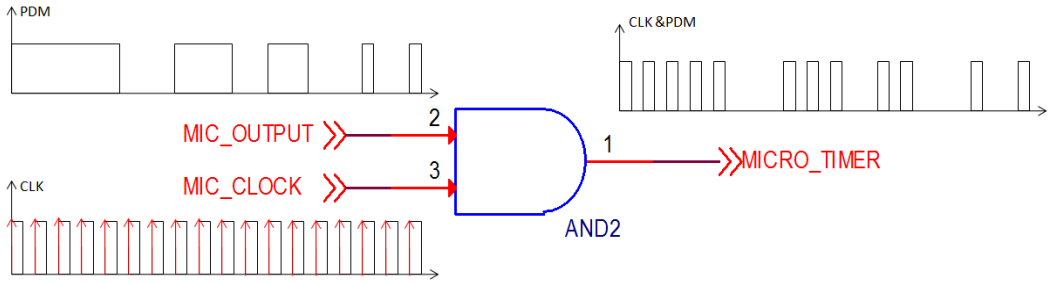

Figure 3.9. AND between the microphone output and the MIC_CLOCK.

However, to implement this solution four timers would have be needed: one timer to generate the microphones clock, two timers to count the number of pulses (one for each microphone) and one timer to restart the counting every millisecond in order to obtain the number of pulses per millisecond. Additionally, it would be necessary to filter and decimate the digital signal in order to obtain the sound signal at the required frequency and resolution.

Another possible solution to the acquisition of the PDM output signal is to use the microcontroller SPI (Serial Peripheral Interface). The output is acquired in blocks of 8 samples by using a synchronous serial port (SPI) of the STM32 microcontroller. The microphone's PDM output is synchronous with its input clock; therefore an STM32 timer generates a single clock signal for both the microphones and the serial-to-parallel converter of the STM32's SPI (Figure 3.10).

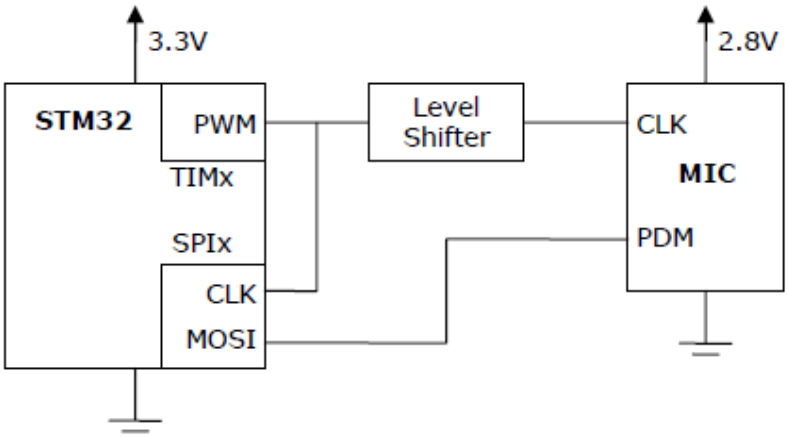

Figure 3.10. Microphone connection to the STM32's SPI

The PDM signal from the microphone has to be filtered and decimated in order to obtain a sound signal at the required frequency and resolution (Figure 3.11)

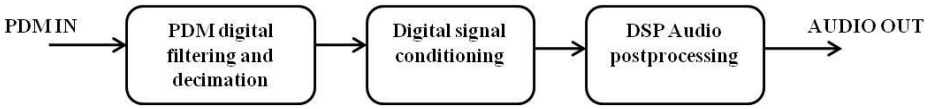

Figure 3.11. PDM Digital signal processing

Assuming an input frequency of 2.4 *MHz* and a desired output frequency of 30 *kHz*, the filter stages could be configured as follows:

1. The first stage is a FIR filter with decimation factor 8. A useful feature of the decimation factor 8 is that a byte contains exactly 8 input signal values (because input signal values have only 1-bit resolution). The resulting sampling frequency of the output signal is 300 *kHz*. Since the input signal has 1-bit resolution, this filter can output only 256 possible distinct output values. This fact can be exploited to optimize this stage by using three 8-bit look-up tables. Thus, the output signal could be amplified.
2. The second stage is a FIR filter with decimation factor 10. The resulting output signal sampling frequency is 30 *kHz*.

The digital audio signal resulting from the previous filter pipeline has to be further processed for proper signal conditioning, in order to have 16 bit signed resolution.

1. The first stage is a high pass filter designed mainly to remove the signal DC offset.
2. The second stage is a low pass filter at 500 *Hz* (range of frequencies of our interest).
3. Gain can be controlled by an external integer variable.
4. Saturation stage sets the range for output audio samples to 16 bit signed.

This solution is an optimized software implementation for the PDM signal decoding and audio signal reconstruction. However, for the purpose of this thesis, this solution was not implemented because it would have needed two SPI ports (one for each microphone). As it would be explain in detail in section 3.5, only one SPI port was available since not all the pins of the STM32 microcontroller were available for use.

3.3.2 PDM Analog Demodulation

The other possibility that was considered and the one chosen to be implemented, is to decode the PDM signal into an analog signal using an analog low pass filter. The function of a low pass filter is essentially to average the signal. The average amplitude of pulses is measured by the density of those pulses over time, thus a low pass filter is the only step required in the decoding process. Then, the analog signal can be amplified and converted into digital with the microcontroller ADC. These digitalized signals are finally sent to a PC via blue tooth for off-line analysis.

The general block scheme of the acquisition chain is shown in Figure 3.12.

Figure 3.12. PCG acquisition chain block scheme

3.3.2.1 *Analog Low Pass Filters*

The first low pass filters in the acquisition chain are second order active filters with a cutoff frequency of 500 *Hz*. The Sallen-Key (SK) topology was used to implement these filters. The SK is a degenerate form of a voltage-controlled voltage-source (VCVS) filter topology. A VCVS filter uses a super-unity-gain voltage amplifier with practically infinite input impedance and zero output impedance to implement a 2-pole low pass filter. The super-unity-gain amplifier allows very high Q factor and passband gain without the use of inductors. A filter is a variation on a VCVS filter that uses a unity-gain amplifier. Implementations of SK filters often use an operational amplifier. The generic unity-gain SK filter topology implemented with a unity-gain operational amplifier is shown in Figure 3.13.

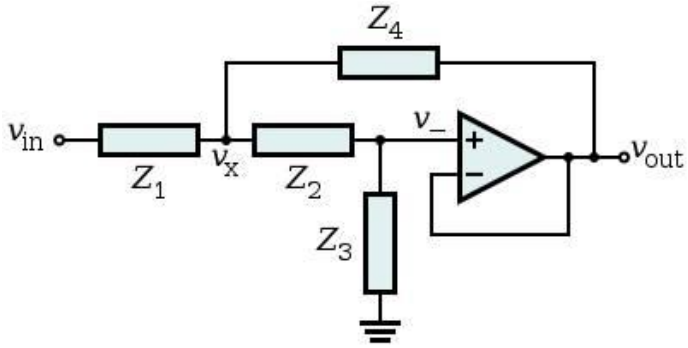

Figure 3.13. The generic Sallen–Key filter topology.

The following analysis is based on the assumption that the operational amplifier is ideal. Because the operational amplifier (OpAmp) is in a negative-feedback configuration, its v_+ and v_- inputs must match (i.e., $v_+ = v_-$). However, the inverting input v_- is connected directly to the output v_{out}, and so

$$v_+ = v_- = v_{out} \qquad \textbf{Eq. 3.2}$$

By Kirchhoff's current law (KCL) applied at the v_x node,

$$\frac{v_{in} - v_x}{Z_1} = \frac{v_x - v_{out}}{Z_4} + \frac{v_x - v_-}{Z_2} \qquad \textbf{Eq. 3.3}$$

By combining Eq. 3.2 and Eq. 3.3,

$$\frac{v_{in} - v_x}{Z_1} = \frac{v_x - v_{out}}{Z_4} + \frac{v_x - v_{out}}{Z_2} \qquad \textbf{Eq. 3.4}$$

Applying KCL again at the OpAmp's non-inverting input v_+ (= v_- = v_{out}) gives

$$\frac{v_x - v_{out}}{Z_2} = \frac{v_{out}}{Z_3} \quad \textbf{Eq. 3.5}$$

which means that

$$v_x = v_{out}\left(\frac{Z_2}{Z_3} + 1\right) \quad \textbf{Eq. 3.6}$$

Combining Eq. 3.3 and Eq. 3.6 gives

$$\frac{v_{in} - v_{out}\left(\frac{Z_2}{Z_3} + 1\right)}{Z_1} = \frac{v_{out}\left(\frac{Z_2}{Z_3} + 1\right) - v_{out}}{Z_4} + \frac{v_{out}\left(\frac{Z_2}{Z_3} + 1\right) - v_{out}}{Z_2} \quad \textbf{Eq. 3.7}$$

Rearranging Eq. 3.7 gives the transfer function

$$\frac{v_{out}}{v_{in}} = \frac{Z_3 Z_4}{Z_1 Z_2 + Z_4(Z_1 + Z_2) + Z_3 Z_4} \quad \textbf{Eq. 3.8}$$

which typically describes a second-order LTI system.

By choosing different passive components (e.g., resistors and capacitors) for Z_1, Z_2, Z_3 and Z_4, the filter can be made with low-pass, bandpass, and high-pass characteristics.

A unity-gain low pass configuration was used for the implementation and is shown in Figure 3.14.

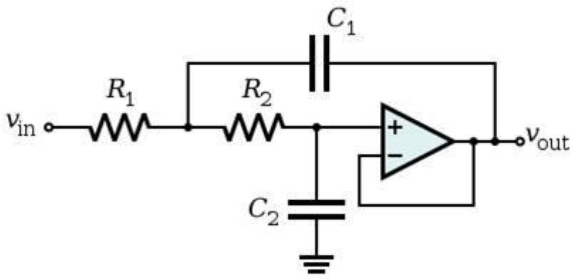

Figure 3.14. A unity-gain low-pass filter implemented with a Sallen–Key topology

A TSV635 operational amplifier was used. This circuit is equivalent to the generic case above with

$$Z_1 = R_1, \qquad Z_2 = R_2, \qquad Z_3 = \frac{1}{sC_2}, \qquad and \quad Z_4 = \frac{1}{sC_1}$$

Where $s = j\omega = \left(\sqrt{-1}\right)2\pi f$, and f is a frequency of a pure sine wave input. The capacitor's impedance is frequency dependent and the resistor's impedance is not.

The transfer function for this second-order unity-gain low-pass filter is:

$$H(s) = \frac{(2\pi f_c)^2}{s^2 + 2\pi\frac{f_c}{Q} + (2\pi f_c)} \qquad \textbf{Eq. 3.9}$$

where the cutoff frequency *f* and the *Q* factor are given by:

$$f_c = \frac{1}{2\pi\sqrt{R_1 R_2 C_1 C_2}} \qquad \textbf{Eq. 3.10}$$

and

$$2\zeta = \frac{1}{Q} = \frac{\sqrt{R_1 R_2 C_1 C_2}}{\mathrm{C_1}}\left(\frac{1}{\mathrm{R_1}} + \frac{1}{\mathrm{R_2}}\right) \qquad \textbf{Eq. 3.11}$$

So,

$$Q = \frac{\sqrt{R_1 R_2 C_1 C_2}}{\mathrm{C_1(R_1 + R_2)}} \qquad \textbf{Eq. 3.12}$$

The *Q* factor determines the height and width of the peak of the frequency response of the filter. As this parameter increases, the filter will tend to "ring" at a single resonant frequency near f_c. A second-order Butterworth filter, which has maximally flat passband frequency response, has a *Q* of $1/\sqrt{2}$.

The circuit implemented has the following values:

$$R_1 = 33k\Omega, \qquad R_2 = 33k\Omega, \qquad C_1 = 10nF, \qquad and \quad C_2 = 10nF$$

Therefore, the *fc* and *Q* expressions are:

$$f_c = \frac{1}{2\pi\sqrt{33k\Omega * 33k\Omega * 10nF * 10nF}} = 482.3Hz$$

$$Q = \frac{\sqrt{33k\Omega * 33k\Omega * 10nF * 10nF}}{10\text{nF}(33k\Omega + 33k\Omega)} = 0.5$$

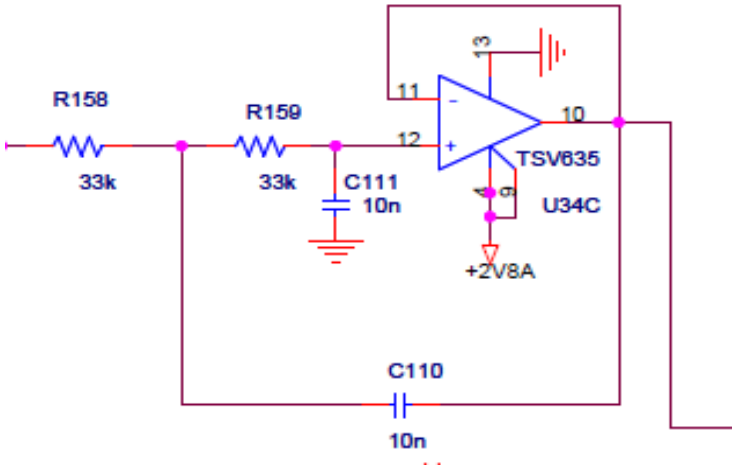

Figure 3.15. Low-pass filter implemented with a Sallen–Key topology, with fc=482 *Hz* and Q=0.5

In this thesis, the SK filter was implemented using a TSV635 operational amplifier. The implemented filter has the behavior similar to the Butterworth filter, which has a flat frequency response in the passband. However, the TSV635 operational amplifier has not the ideal behavior (*Zout≠0*) and the frequency response is different to the one expected with an ideal OpAmp.

The simulation of the frequency response of SK filters implemented using a real OpAmp are shown in Figure 3.16, Figure 3.17, and Figure 3.18. The simulations were done using Matlab R2009b. In the three simulations, the SK filter was implemented using a TSV635 OpAmp (700 *kHz* band, gain 90 *dB*).

Figure 3.16 shows the frequency response of a SK filter with a cutoff frequency of 500 *Hz* and *Zo=R=180* Ω. It can be seen that in the pass band the ideal SK and the SK with *Zo=R* have approximately the same behavior, but in the case of *Zo≠0*, the SK filter has a high frequency leak.

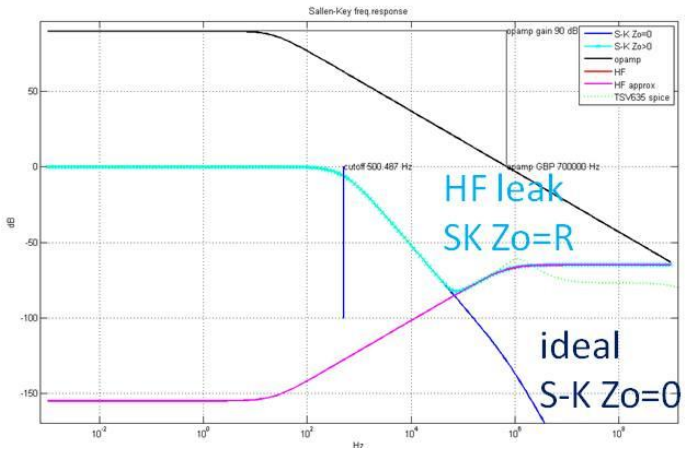

Figure 3.16. SK frequency response with Zo=R

Figure 3.17 shows the frequency response of the SK filter with $Zo=RLC=Z_1//Z_2$, where $Z_1 = 180\Omega + s\ 30\mu H$, and $Z_2 = 60\Omega + 1/(s\ 0.5nF)$. This would be the real frequency behavior of a SK filter implemented with a TSV635 OpAmp. It can be seen that the high frequency leak is also evident.

Figure 3.18 shows the frequency response with a SK filter with $Zo=RLC=Z_1//Z_2$ (with the same values as in Figure 3.17) and a passive RC filter on the output ($R=100\Omega$, $C=0.047\mu F$). It can be seen that the high frequency leak has been attenuated. This suggests that an passive RC filter on the SK output can be useful to prevent the high frequency leak that is evident when using real OpAmps.

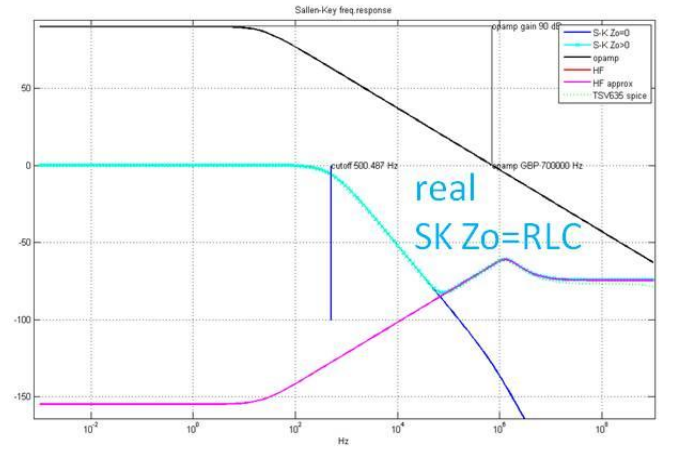

Figure 3.17. SK frequency response with Zo=RLC

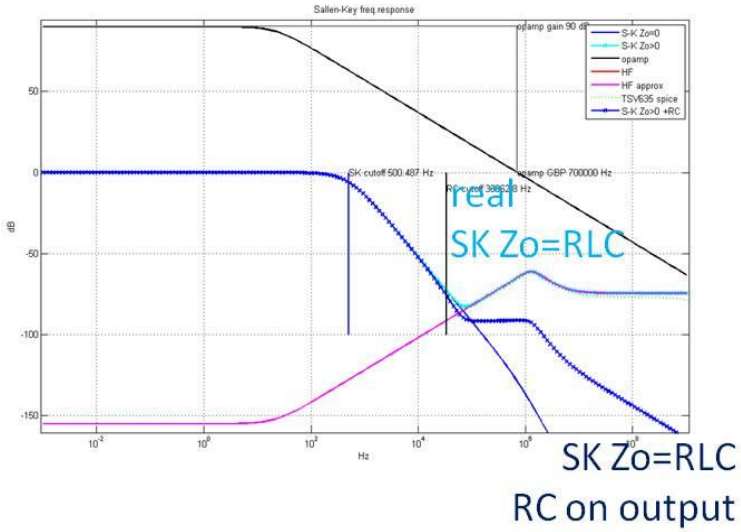

Figure 3.18. SK frequency response with Zo=RLC and RC on output

The following figures show the simulation results of the PDM demodulation using a RC filter (Figure 3.19), a SK filter (Figure 3.20) and a SK with a RC filter on output (Figure 3.21). In all three simulations, the PDM signals had a duty cycle of 50% and a frequency of 2.4 *MHz* (which is the microphone's clock frequency). Figure 3.22 shows the frequency response of the SK filters with and without the RC on the output

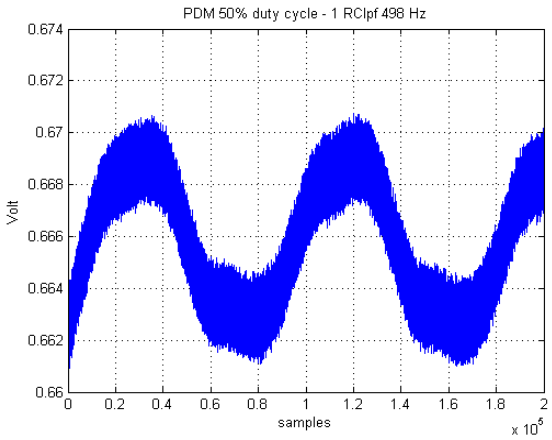

Figure 3.19. RC filter with a cutoff frequency of 500 *Hz*

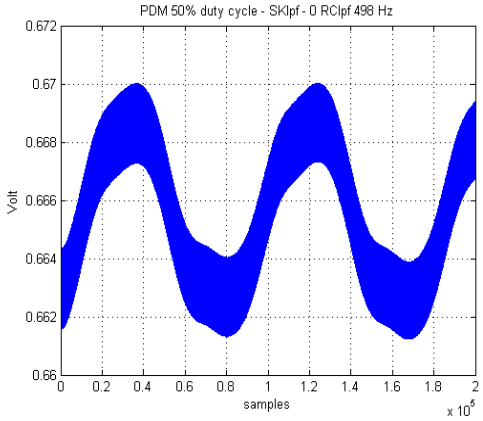

Figure 3.20. SK filter with a cutoff frequency of 500 *Hz*

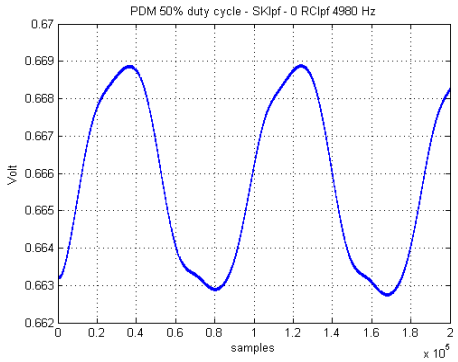

Figure 3.21. SK filter with a fcutoff=500 *Hz* and a RC filter on output

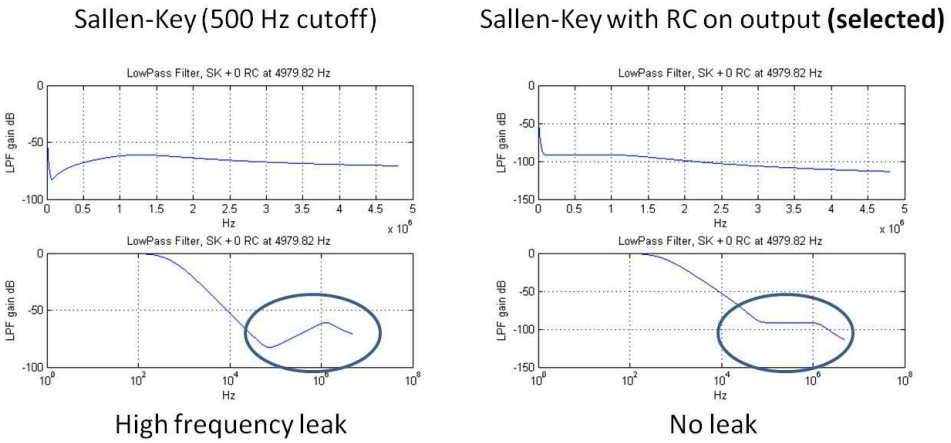

Figure 3.22. Frequency response of SK filter with and without the RC on the output (cutoff frequency = 500 *Hz*)

The SK filter with a passive RC filter on the output was selected. After the RC filter, a buffer was used to isolate this first filtering stage of the next one.

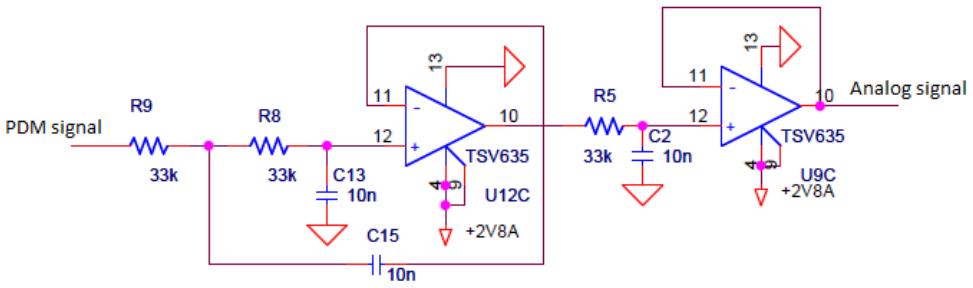

Figure 3.23. Analog low pass filter implemented to demodulate the PDM signal

3.3.2.2 *Offset Subtraction and Gain Stage*

The analog signal obtained in the previous stage has an offset value (DC constant value) that needs to be subtracted before the amplification of the signal. Since the OpAmp TSV635 are single supply, a virtual ground must be created and isolated with coupling C. The coupling *C* on input avoid shortening virtual ground (*Vcc/2*) to ground, but also act as high pass filter removing DC component.

The virtual ground, also known as *Vref=Vcc/2*, may be generated by a DAC or a voltage divider and should be buffered with low-noise voltage feedback OpAmp, as shown in Figure 3.24.

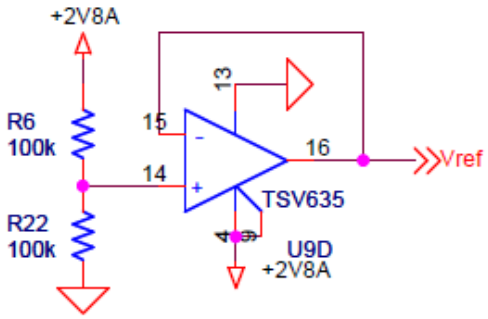

Figure 3.24. Virtual ground

The stage of amplification and offset subtraction is shown in Figure 3.25.

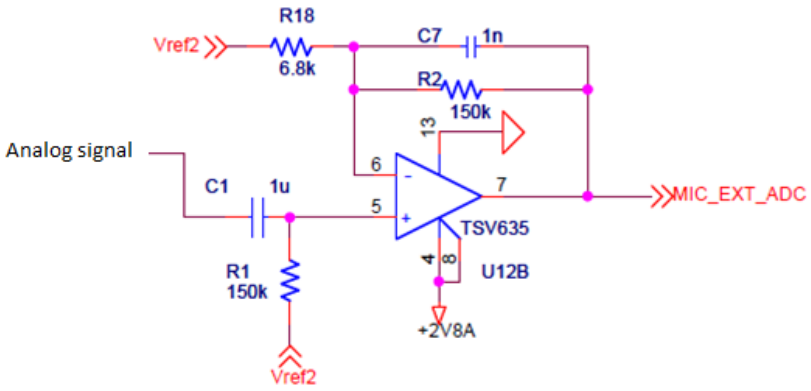

Figure 3.25. Filter implemented to subtract the DC offset and amplify the analog signal

This filter has a transfer function equal to:

$$\frac{v_{in}}{v_{out}} = \frac{sR_1C_1}{1+sR_1C_1}\left(1+\frac{R_2}{R_{18}}\frac{1}{sR_2C_7+1}\right) \qquad \textbf{Eq. 3.13}$$

This is a pass band filter with two poles and two zeros. The poles are located at

$$f_{p1} = \frac{1}{2\pi C_1 R_1} = 1Hz, \text{ and } f_{p2} = \frac{1}{2\pi C_7 R_2} = 1kHz,$$

and the poles are located at:

$$f_{z1} = 0Hz \text{ and } f_{z2} = \frac{R_1+R_2}{2\pi C_1 R_1 R_2} = 24.5kHz.$$

The frequency response shown in Figure 3.26. The passband is in the range of frequencies between 1 *Hz* and 1 *kHz*.

The filter's gain is equal to:

$$Gain = \frac{R_2}{R_{18}} = \frac{150k\Omega}{6.8k\Omega} \approx 20$$

which can be changed by varying the value of R_{18}.

After this stage, the analog signal is ready to feed the microcontroller ADC.

The complete PCG circuit is shown in Figure 3.27.

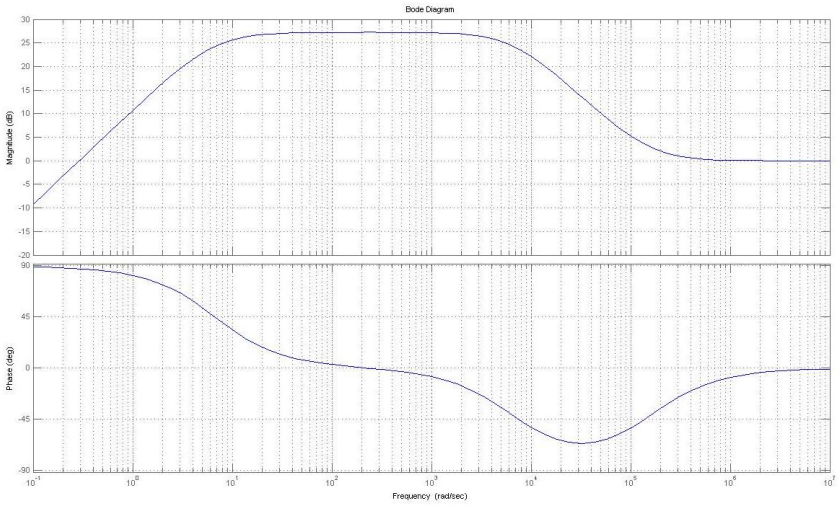

Figure 3.26. Frequency response of the pass band filter

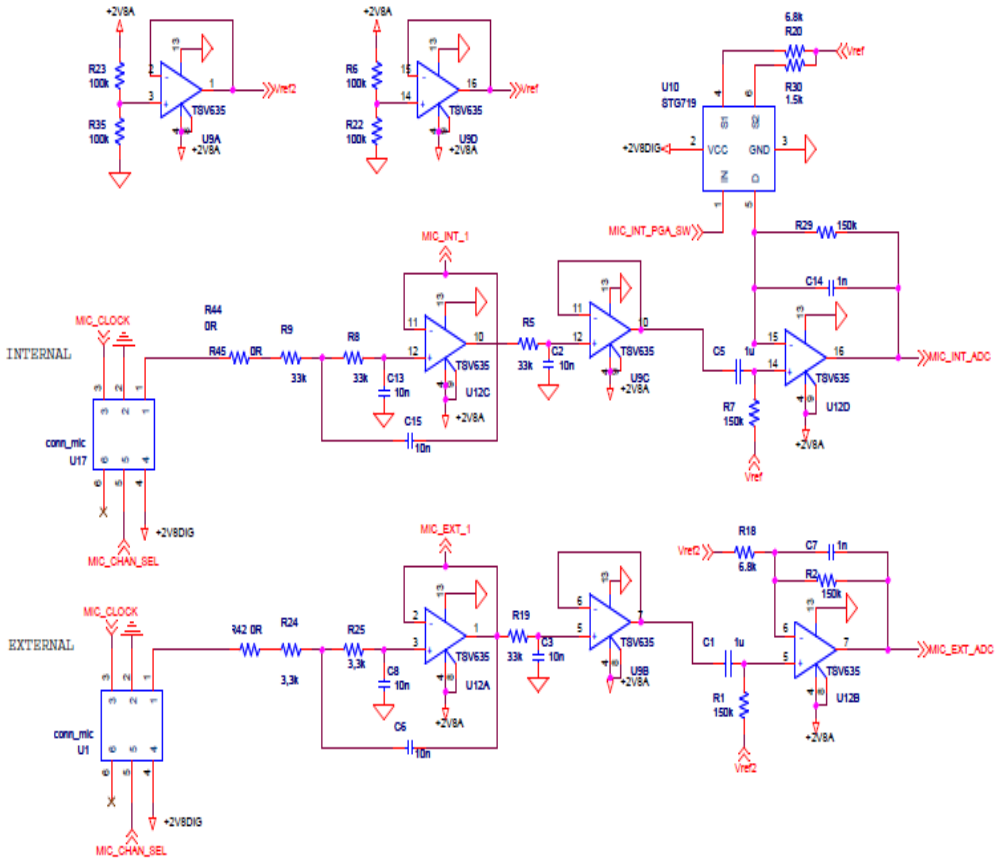

Figure 3.27. PCG schematic

3.3.2.3 *Circuit Simulation*

The circuit time response was simulated using PSpice. The input signal used was the PDM signal corresponding of a sinusoidal signal of 400 *Hz*. The low pass filters (SK and RC) cutoff frequency was 500 *Hz*, and the gain of the circuit was 33. For the purpose of the simulation, the range of frequencies of the pass band filter was between 160 *Hz* and 1 *kHz*, but in the real circuit this range goes from 1 *Hz* to 1 *kHz* (otherwise, the simulation would have taken much longer). The results of the simulation are shown in Figure 3.28.

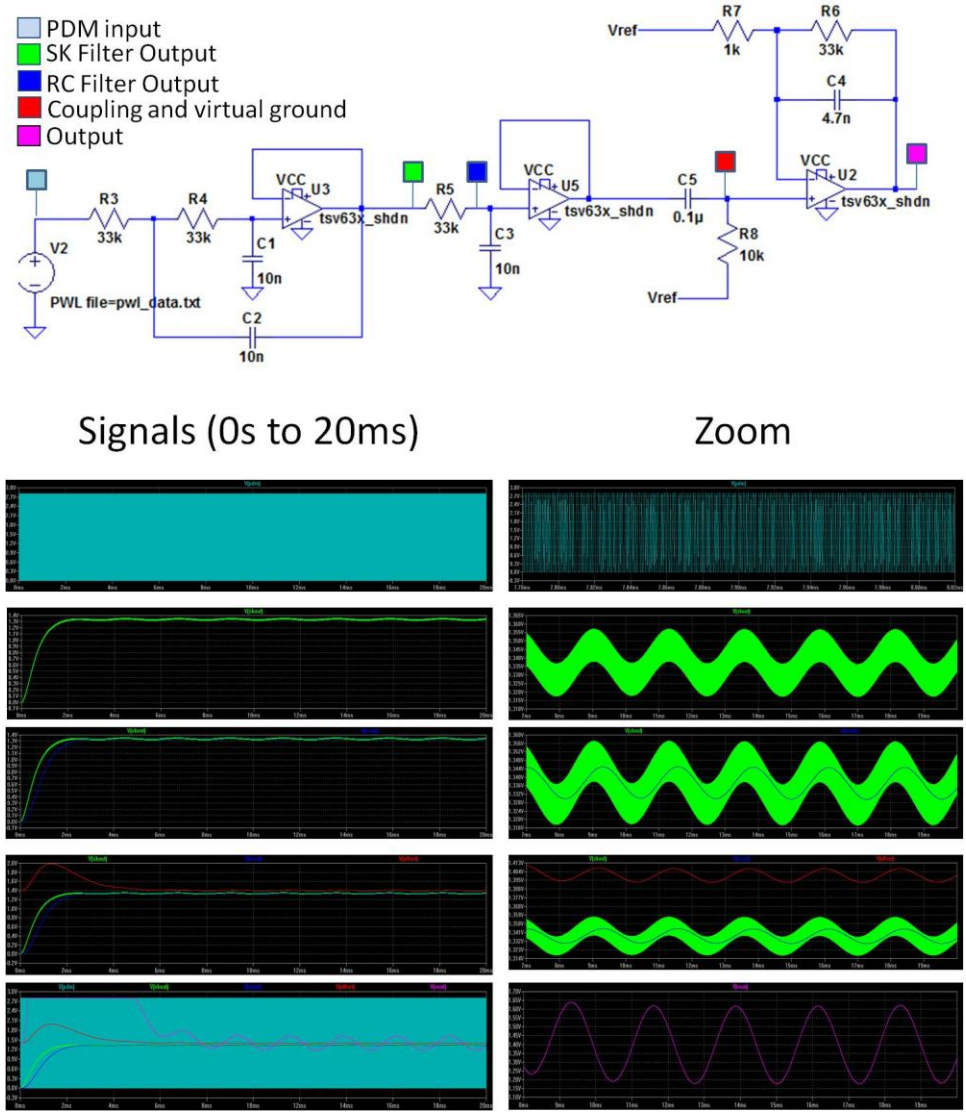

Figure 3.28. Time response of the PCG circuit

3.4 POWER MANAGEMENT

The battery used to feed the circuit was a rechargeable Lithium-ion (3.7VDC, 600mAh and 2.22Wh). A STC4054 battery charger was used to charge the battery and a LED was used to visually notice when the battery was charging. A mechanic switch was used to turn on and off the circuit. Two LD3985M28R voltage regulators were used to obtain a regulated DC value of 2.8V, used to feed the rest of the circuit. The DC output of one of the regulators was used to feed to analog components (2V8A), while the output of the other regulator was used to feed the digital components. The power management circuit is shown in Figure 3.29.

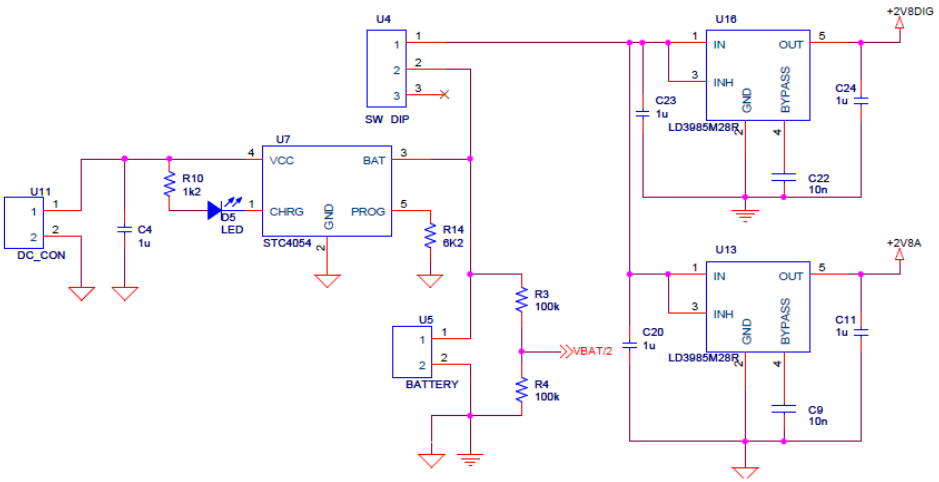

Figure 3.29. Power Management Schematic

The value of the voltage of the battery divided by two (*Vbat/2*) feeds the microcontroller ADC in order to control the battery voltage value. A LED will indicate if *Vbat/2 < 1.45V*.

3.5 MICROCONTROLLER AND BLUETOOTH MODULE

The SPBT2532C2A module (Figure 3.30), containing the STM32 microcontroller and the Bluetooth transmission module, was used to convert the analog signals (ECG signal and PCG signals) into digital and to transmit them via Bluetooth to a PC for offline analysis. It was also used to generate the digital clock signal (MIC_CLOCK) necessary to activate the microphones.

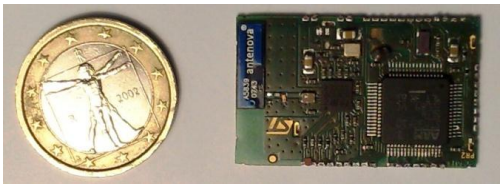

Figure 3.30. SPBT2532C2A module

This module contains the microcontroller STM32F103RCT6, characterized by low power consumption and high efficiency. It uses 32 bits RISC ARM Cortex-M3 core, working at a maximum frequency of 72 *MHz*. It has several embedded high speed memories I\O and peripherals connected through two APB bus (Advanced Peripheral Bus). The microcontroller is provided with three 12 bit ADCs, four general purposes 16 bit timers, two PWM timers as well as standard and advanced communication interfaces (I^2C, SPI, I^2S, SDIO, USART, USB and CAN). The module also contains two oscillators (ASD2-13*MHz* and OV-7604-C7-32.768 *kHz*), a Bluetooth 3.0 module (STLC2500DB), a multilayer chip band pass filter for Bluetooth (DEA212450BT) and the Bluetooth antenna. The complete schematic of the module is shown in Figure 3.31. As it can be seen in the schematic, the module has 40 pins, of which 5 pins correspond to the JTAG connector, and 19 pins correspond to the microcontroller I/O pins available for use. Table 3.3 shows the microcontroller I/O pins available for use and their alternate functions.

Module PIN number	PIN NAME	ALTERNATE FUNCTIONS
6	PA0	WKUP/USART2_CTS/ADC123_IN0/TIM2_CH1_ETR/TIM5_CH1/TIM8_ETR
7	PA1	USART2_RTS/ADC123_IN1/TIM5_CH2/TIM2_CH2
8	PA2	USART2_TX/TIM5_CH3/ADC123_IN2/TIM2_CH3
9	PA3	USART2_RX/TIM5_CH4/ADC123_IN3/TIM2_CH4
10	PA4	SPI1_NSS/USART2_CK/DAC_OUT1/ADC12_IN4
11	PA5	SPI1_SCK/DAC_OUT2 ADC12_IN5
12	PA6	SPI1_MISO/TIM8_BKIN/ADC12_IN6/TIM3_CH1
13	PA7	SPI1_MOSI/TIM8_CH1N/ADC12_IN7/TIM3_CH2
14	PA9	USART1_TX/TIM1_CH2
15	PA10	USART1_RX/TIM1_CH3
16	PA11	USART1_CTS/USBDM/CAN_RX/TIM1_CH4
22	PA12	USART1_RTS/USBDP/CAN_TX/TIM1_ETR
23	PB1	ADC12_IN9/TIM3_CH4/TIM8_CH3N
24	PB5	I2C1_SMBA/ SPI3_MOSI/I2S3_SD
32	PB6	I2C1_SCL/ TIM4_CH1
33	PB7	I2C1_SDA/FSMC_NADV/TIM4_CH2
34	PB12	SPI2_NSS/I2S2_WS/I2C2_SMBA/USART3_CK/TIM1_BKIN
35	PB15	SPI2_MOSI/I2S2_SD/TIM1_CH3N
36	PC7	I2S3_MCK/TIM8_CH2/SDIO_D7

Table 3.3. Available microcontroller pins for use and their function

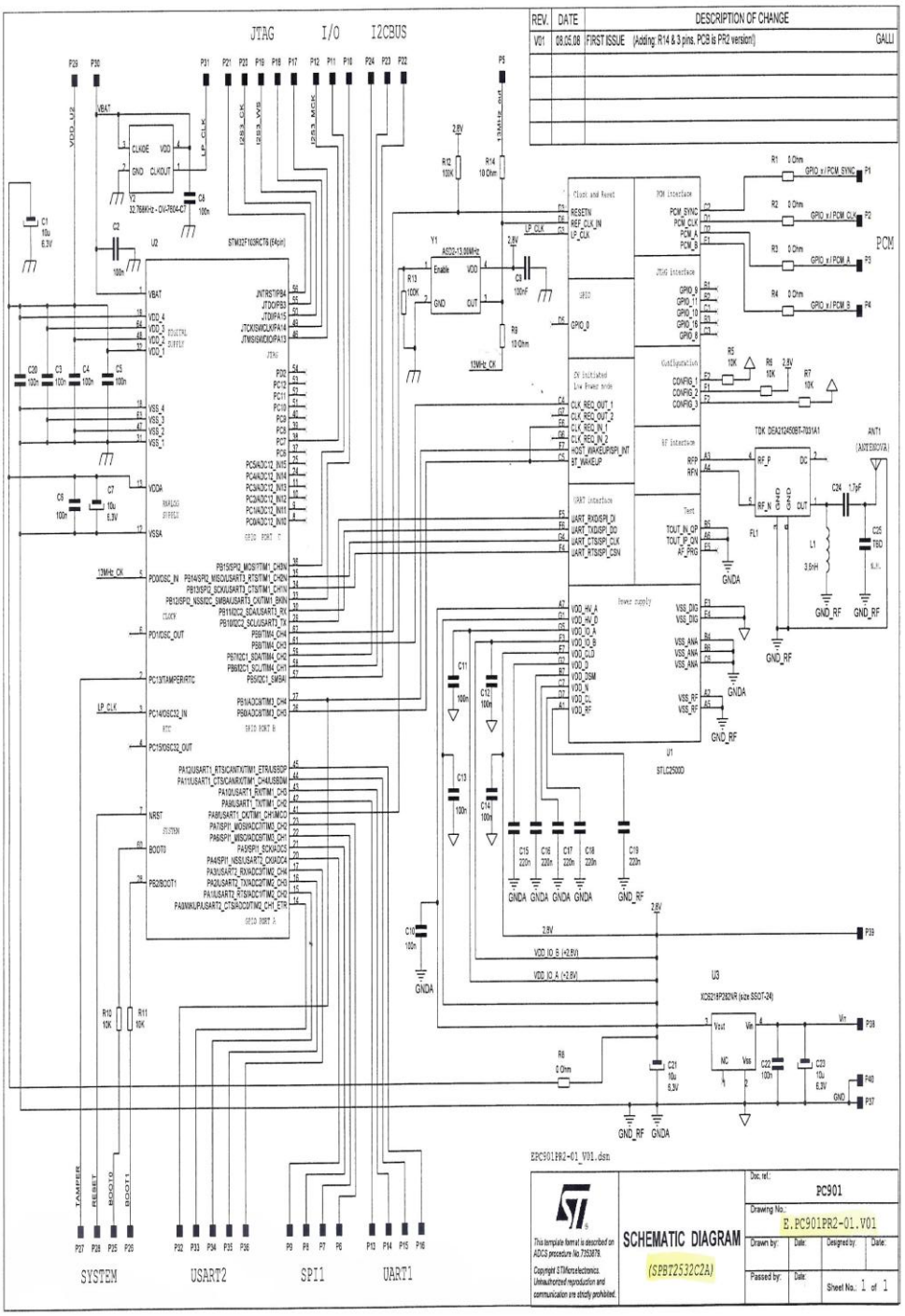

Figure 3.31. MCU and BT module schematic

Figure 3.32 shows the connections between the SPG module and the rest of the circuit.

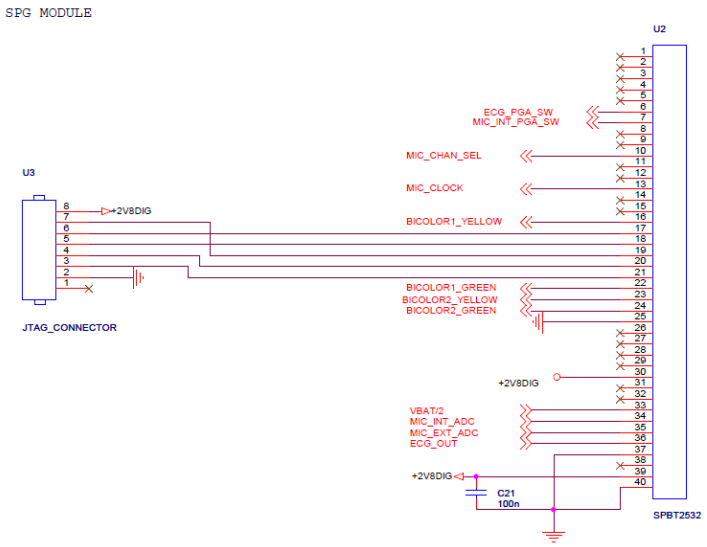

Figure 3.32. Connections between the SPG module and the rest of the circuit

The Vbat/2, ECG and PCG analog signals are connected to the microcontroller ADC. The A/D conversion of the various channels can be performed in single, continuous, scan or discontinuous mode, making it possible to convert into digital almost simultaneously the Vbat/2, ECG and PCG analog signals. All the signals have been sampled with a frequency of 800 *Hz*. The result of the ADC is stored in a left-aligned or right-aligned 16-bit data register and with a DMA request the data was transfer to the memory location selected. Deeper details about the firmware are given in chapter 4. The ECG and PCG acquired signals are finally transmitted via Bluetooth to a PC for offline processing.

3.6 PROTOTYPE DESIGN

The design of the prototype for the BP measurement system is consisted of three main stages:

- Circuit design (described in sections 3.2, 3.3, 3.4 and 3.5)
- Layout design for PCB (Printed Circuit Board)
- Design of the case that contains the PCB and the battery.

Next sections describe the layout and the case design.

3.6.1 Layout Design

The Printed Circuit Board (PCB) is used to mechanically support and electrically connect the electronic components using conductive pathways, track or signal traces etched from copper sheets laminated onto a non-conductive substrate. The board is typically coated with a solder mask that is green in color. The PCB made in thesis work is a double-sided rigid printed circuit board with two layers. The components can be mounted on a printed circuit board are of two types:

- SMD (surface mounted device): components are mechanically design to have small metal tabs or ends caps that could be soldered directly to the PCB surface. Components are small and can be placed on both sides of the board, allowing much higher circuit densities.
- PTH (pin through hole): the components cross the circuit board that hosts them through plated holes..

The holes drilled into the board can be of two types: holes for the terminal of PTH components and holes to allow the electrical and thermal connection of conductors on opposite sides of the PCB, named vias.

As for SMD components, their terminals are welded to the special areas (pads) which are electrically connected (thanks to the pathways on the two layers of copper) to other components within the circuit. The pathways (electrical connections between components) are obtained by selective chemical removal of excess copper. The outer parts of the copper layers are protected from oxidation and unwanted electrical contacts with an insulating solder mask. Off course, the deposition of the solder mask does not cover areas of the PCB dedicated to the SMD components, the holes for the PTH components and, sometimes, vias holes.

The design the layout for the PCB was done using the OrCAD Capture and the Allegro PCB Editor software. The design consisted of the following steps:

1. Verify that all the necessary component's footprints are in the Allegro library and create the ones that are missing (creating the padstacks and components symbols).
2. Create a new board design file and define the board outline.
3. Set the design constrains.
4. Import logic from the schematic made with OrCAD Capture CIS.

5. Component placement
6. Routing and glossing
7. Create the copper areas and positive or negative planes (GND planes)
8. Preparation for post processing (rename the components and export the new names to the OrCAD schematic)
9. Preparation of the board design for manufacturing (create silkscreens, artwork, Gerber files, drill legend and drill file).

The layout designed is shown in Figure 3.33.

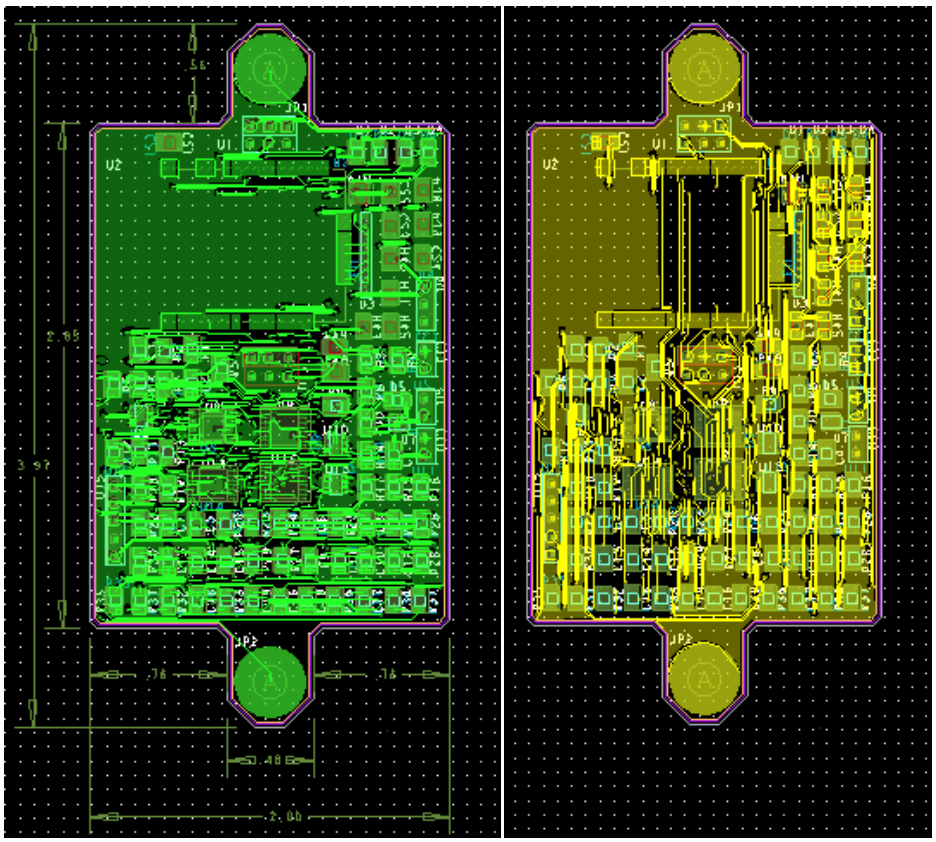

(a) Top View **(b) Bottom View**

Figure 3.33. Layout: top and bottom view (dimensions in mills)

It was decided to place the ECG electrodes on each side of the board, the internal microphone on the center and the external microphone close to one of the ECG electrodes. The analog components were placed on the upper side of the PCB and the digital components on the bottom side.

Figure 3.34 shows the resulted PCB, and Figure 3.35 shows the functional printed circuit assembly with all the components attached. All the components were soldered by hand under a microscope.

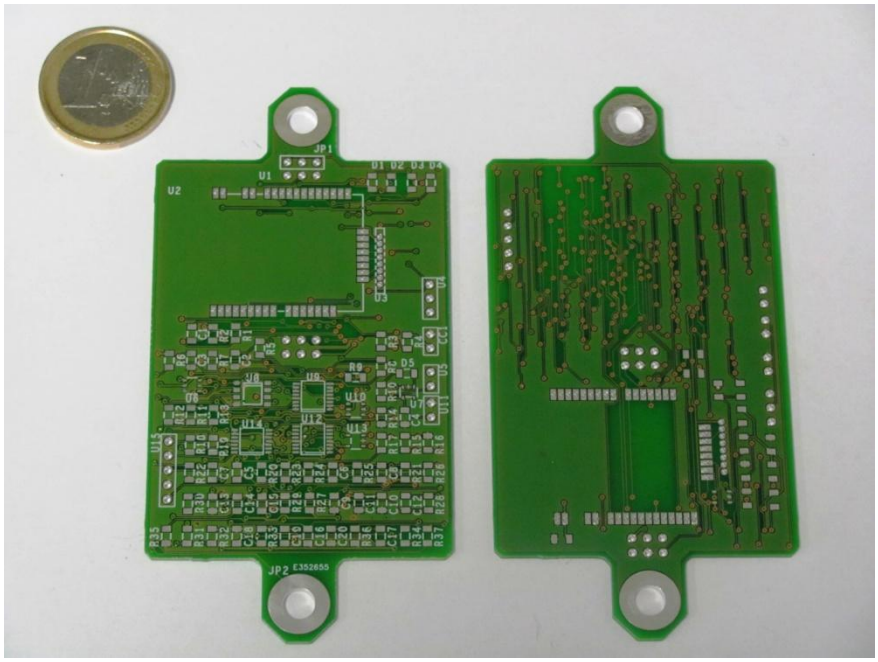

Figure 3.34. Printed Circuit Board (PCB)

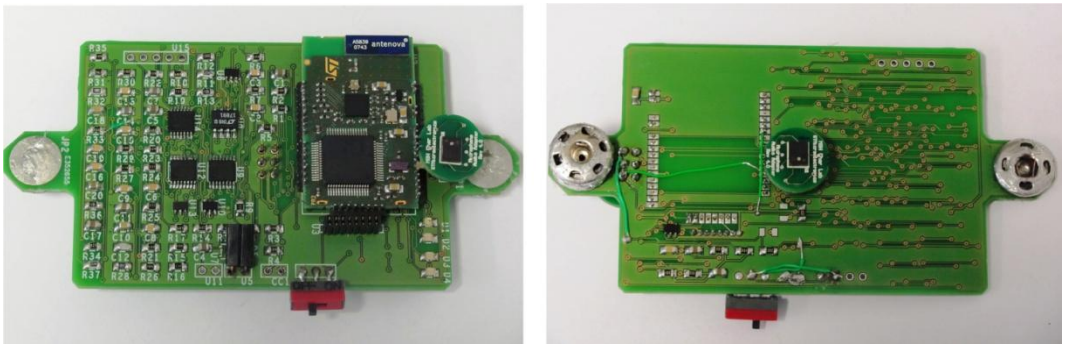

Figure 3.35. Printed Circuit Assembly

3.6.2 Case Design

The case was designed using Solid Works and was produced in ABS plastic material using a 3D printer. The case has the function of mechanical interface between the circuit and the patient's skin. Therefore, the case should be comfortable to wear, small and light.

The most important aspect about the design of the case was mechanical interface between the internal microphone and the patient's chest to acquire the heart sounds. The microphone should be as close as possible to the skin but it was also necessary to consider the fact that the sound waves attenuate in the air, and therefore, an air layer between the microphone and the skin was not convenient. It was decided to add a cone under the case which would be in touch with the skin isolating the external air and permitting the sound wave to propagate from the chest to the microphone. Silicon was added to the border of the cone with the purpose of sealing the cavity between the skin and the case, in order to avoid air leaks. Figure 3.36 show the designed case.

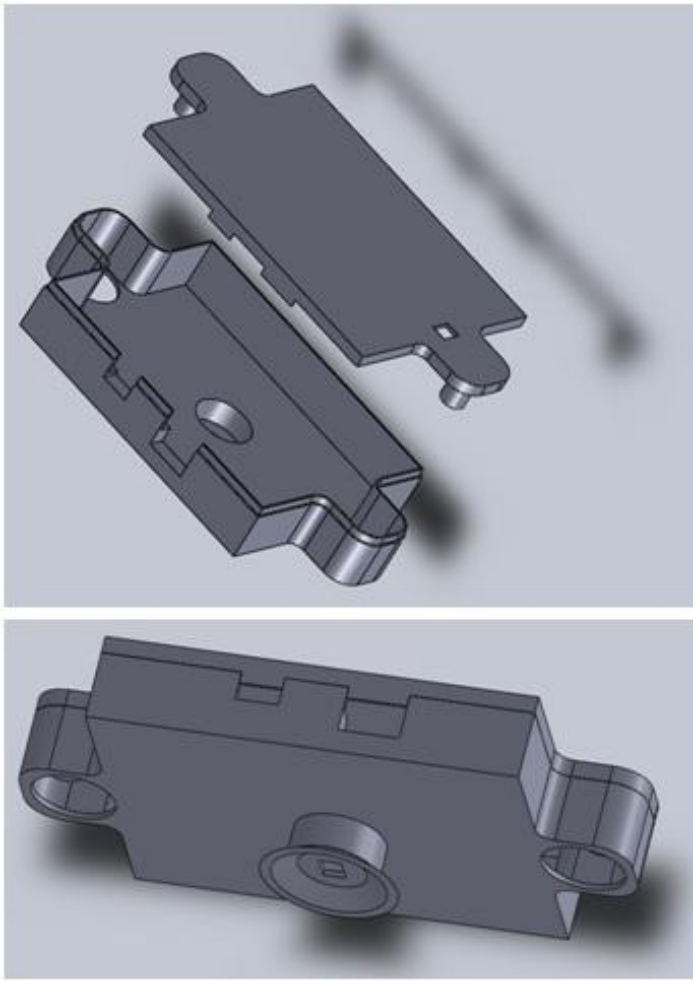

Figure 3.36. Designed Case

Figure 3.37 shows top and bottom view of the prototype and Figure 3.38 shows the interior of the case with the circuit inside.

Figure 3.37. Top and bottom view of the prototype

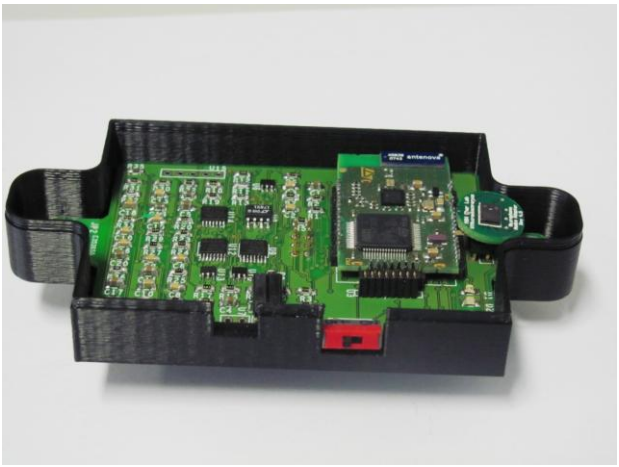

Figure 3.38. Interior of the case

Figure 3.39 shows the prototype attached to the chest, centered and left aligned.

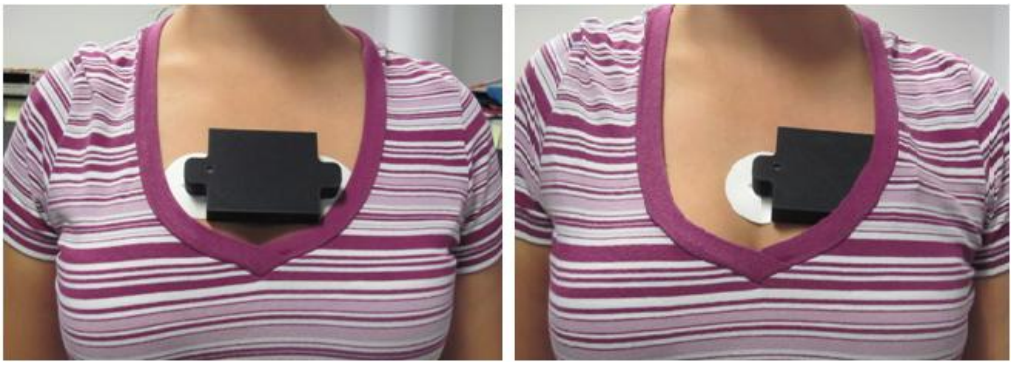

Figure 3.39. Prototype attached to the chest

Figure 3.40 shows an example of the acquired signals obtained with the prototype attached to the chest left aligned.

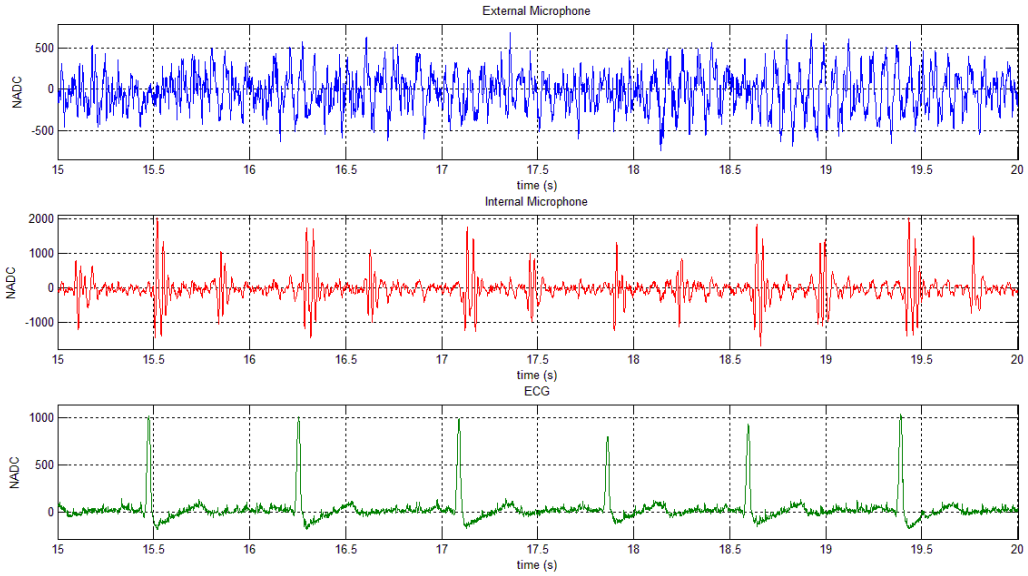

Figure 3.40. Example of the acquired signals: (a) external microphone, (b) internal microphone, and (c) ECG

Chapter 4 is focused on the analysis and elaboration of the acquired ECG and PCG signals. The implemented firmware for the STM32 microcontroller is described in the first part of the chapter. Then, some examples of the acquired signals are given, and subsequently, the analysis and elaboration of the signals is presented.

Chapter 4

FIRMWARE

Once the analog signals were acquired using the electronic device described in Chapter 3, it was necessary to convert them into digital to send them to a computer via Bluetooth for offline analysis.

This chapter covers the software design aspects of the project. The first section describes the STM32 microcontroller, used to convert the analog signals into digital and send them via Bluetooth to the PC. Section 4.2 describes the board configuration and setup. Section 4.3 provides a description of the main.c file, and the Signal_Task function is described in detail. The graphical user interface used in the PC to manage the signals that are being sent via Bluetooth is briefly described at this section. Section 4.4 provides the flow charts of the software.

4.1 STM32 MICROCONTROLLER

As it has been described in previous chapters, the microcontroller used in the implemented prototype was the STM32F103, produced by the STMicroelectronics. The STM32F103 incorporates the high performance ARM Cortex 32-bit core operating at a 72 MHz frequency, high speed embedded memories, and an extensive range of enhanced I/Os and peripherals. The device offers three 12-bit ADCs, four general purpose 16-bit timer plus two PWM timers, as well as standard and advanced communication interfaces: up to two I2Cs, three SPIs, two I2Ss, one SDIO, five USARTs, and a USB.

The STM32 operates from 2.0 to 3.6 V power supply. A comprehensive set of power saving mode allows the design of low power applications.

Figure 4.1 shows the general block diagram of the device.

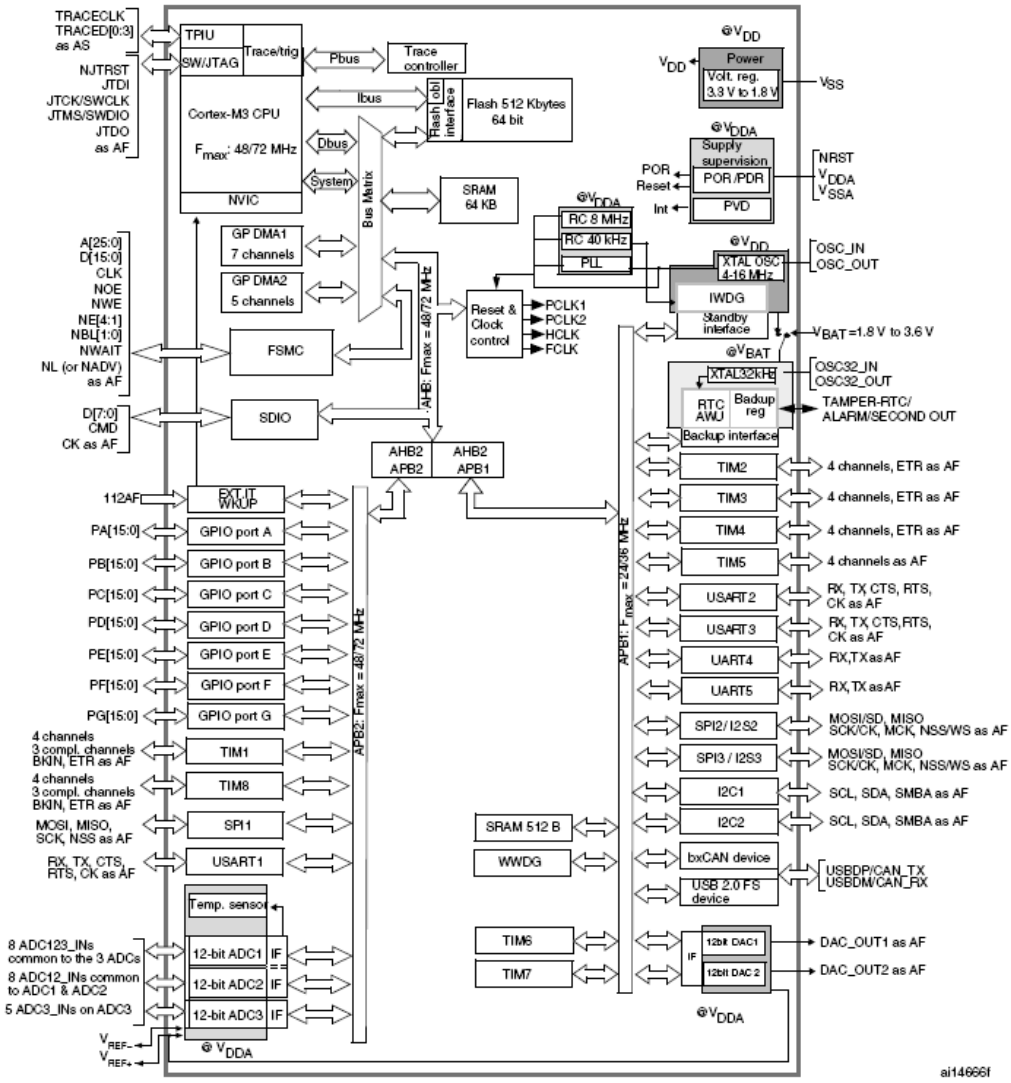

Figure 4.1. STM32F103 block diagram

As it was described in section 3.5, the SPBT2532C2A module (Figure 3.30), containing the STM32 microcontroller and the Bluetooth transmission module, was used to convert the analog signals into digital and to transmit them via Bluetooth to a PC. The complete schematic of the module is shown in Figure 3.31. As it can be seen in the schematic, the module has 40 pins, of which 5 pins correspond to the JTAG connector, and 19 pins correspond to the microcontroller I/O pins available for use. Table 3.3 shows the microcontroller I/O pins available for use and their alternate functions.

The microcontroller perform the tasks that have been programmed in the firmware. The firmware source code was developed in language C, using the µVision from Keil, which combines project management, make facilities, source code editing, program debugging, and complete simulation in one powerful environment.

Figure 4.2 shows a general schematic representation of the firmware and the peripherals used. The firmware implemented in this thesis work was a modification of a firmware previously implemented by the members of the AST Remote Monitoring Division of STMicroelectronics. The blocks shown in blue in the figure are the ones that were modified in this thesis.

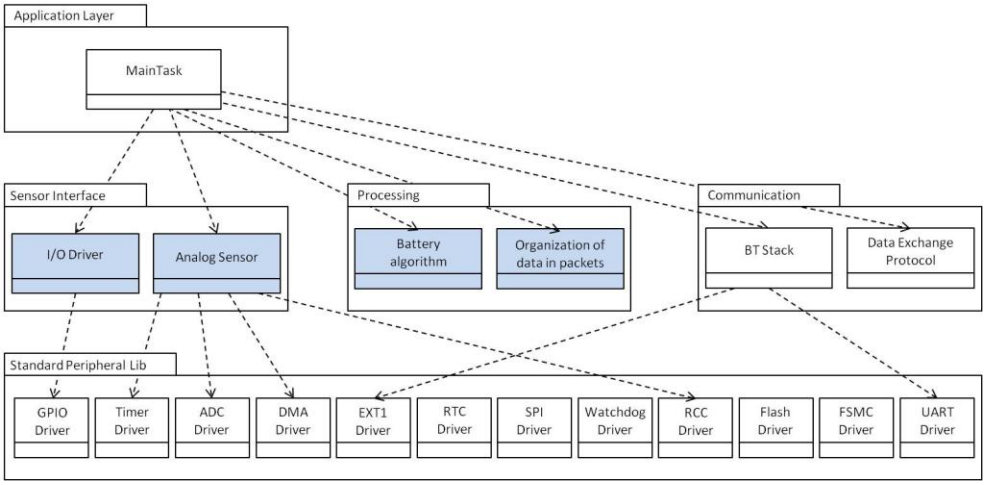

Figure 4.2. Firmware diagram

4.2 CONFIGURATION AND SETUP

A header file (BoardConfig.h) has created in order to define the board parameters. The input ADC channels, some I/O pins, global variables and constants were defined in this file. The ADC sampling frequency was also defined in this file, and it was set to 800 *Hz*.

The I/O pins, the clocks and the interrupt vector were configured in the setup.c file. Three functions were defined in this file:

- void RCC_Configuration(void): used to configure the system clock and the peripherals clocks
- void GPIO_Configuration(void): used to configure the I/O pins

- void NVIC_Configuration(void): used to configure the interrupt vector

4.2.1 Clocks Configuration

System clock selection is performed on startup. An external 13 *MHz* oscillator (HSE) was selected. An internal PLL was used to multiply the HSE clock frequency. The PLL configuration (selection of the input clock and multiplication factor) must be done before enabling the PLL. Once the PLL enabled, these parameters cannot be changed. In this case, the HSE was selected as the input clock and the multiplication factor selected was four. Therefore, the system clock had a frequency of 52 MHz ($13\,MHz * 4 = 52\,MHz$). Several prescalers allow the configuration of the different peripherals. Figure 4.3 shows the complete clock tree. As it can be seen in the figure, the ADCs are clocked by the clock of the High Speed domain (APB2) divided by 2, 4, 6 or 8. The timer clock frequencies are automatically fixed by hardware. There are two cases:

1. If the APB prescaler is 1, the timer clock frequencies are set to the same frequency as that of the APB domain to which the timers are connected.
2. Otherwise, they are set to twice (x2) the frequency of the APB to which the timers are connected.

The reset and clock control register (RCC) is used to configure and enable all the clocks. More details about the clocks configuration can be read in the STM32103 Reference Manual.

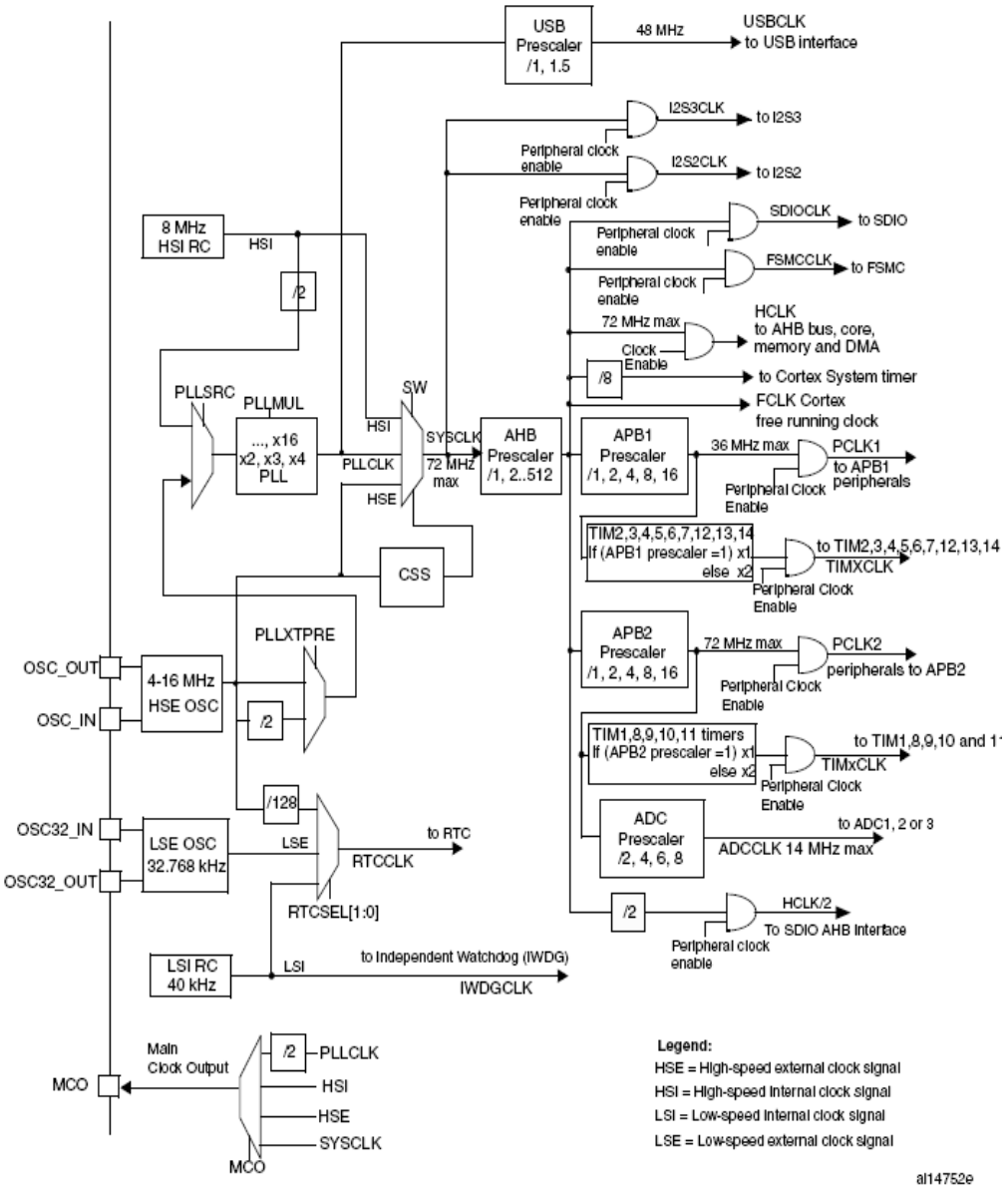

Figure 4.3. Clock Tree

4.2.2 GPIO Configuration

The STM32F103 has 64 pins. Table 4.1 shows the description of each pin. The pins in grey are not used. The selected function for each pin is evidenced in yellow highlighter. It is also indicated the connection to each pin. For more details about all the microcontroller connections, refer to Figure 3.31 and Figure 3.32.

PIN	PIN NAME	TYPE	MAIN FUNCTION	ALTERNATE FUNCTION	CONNECTED TO
1	VBAT	S	VBAT		2.8 V
2	PC13-TAMPER-RTC	I/O	PC13	TAMPER-RTC	
3	PC14-OSC32_IN	I/O	PC14	OSC32_IN	
4	PC15-OSC32_OUT	I/O	PC15	OSC32_OUT	
5	PD0	I	OSC_IN	FSMC_D2	External Oscillator (13 *MHz*)
6	PD1	O	OSC_OUT	FSMC_D3	
7	NRST	I/O	NRST		
8	PC0	I/O	PC0	ADC123_IN10	
9	PC1	I/O	PC1	ADC123_IN11	
10	PC2	I/O	PC2	ADC123_IN12	
11	PC3	I/O	PC3	ADC123_IN13	
12	VSSA	S	VSSA		0 V
13	VDDA	S	VDDA		2.8 V
14	PA0-WKUP	I/O	PA0	WKUP/USART2_CTS/ADC123_IN0 TIM2_CH1_ETR/TIM5_CH1/TIM8_ETR	VBAT/2
15	PA1	I/O	PA1	USART2_RTS/ADC123_IN1/TIM5_CH2 TIM2_CH2	MIC_INT_ADC
16	PA2	I/O	PA2	USART2_TX/TIM5_CH3/ADC123_IN2/ TIM2_CH3	MIC_EXT_ADC
17	PA3	I/O	PA3	USART2_RX/TIM5_CH4/ADC123_IN3/ TIM2_CH4	ECG_OUT
18	VSS_4	S	VSS_4		0 V
19	VDD_4	S	VDD_4		2.8 V
20	PA4	I/O	PA4	SPI1_NSS/USART2_CK/DAC_OUT1/ ADC12_IN4	
21	PA5	I/O	PA5	SPI1_SCK/DAC_OUT2/ADC12_IN5	
22	PA6	I/O	PA6	SPI1_MISO/TIM8_BKIN/ADC12_IN6/ TIM3_CH1	SWITCH_1
23	PA7	I/O	PA7	SPI1_MOSI/TIM8_CH1N/ADC12_IN7/ TIM3_CH2	SWITCH_2
24	PC4	I/O	PC4	ADC12_IN14	
25	PC5	I/O	PC5	ADC12_IN15	
26	PB0	I/O	PB0	ADC12_IN8/TIM3_CH3/TIM8_CH2N	BT_WAKEUP
27	PB1	I/O	PB1	ADC12_IN9/TIM3_CH4/TIM8_CH3N	HOST_WAKEUP
28	PB2	I/O	PB2/BOOT1		
29	PB10	I/O	PB10	I2C2_SCL/USART3_TX	BLUETOOTH: UART_RXD/SPI_DI
30	PB11	I/O	PB11	I2C2_SDA/USART3_RX	BLUETOOTH: UART_TXD/SPI_DO
31	VSS_1	S	VSS_1		0 V
32	VDD_1	S	VDD_1		2.8 V
33	PB12	I/O	PB12	SPI2_NSS/I2S2_WS/I2C2_SMBA/ USART3_CK/TIM1_BKIN	MIC_CHAN_SEL
34	PB13	I/O	PB13	SPI2_SCK/I2S2_CK/USART3_CTS/ TIM1_CH1N	BLUETOOTH: UART_RTS/SPI_CSN
35	PB14	I/O	PB14	SPI2_MISO/TIM1_CH2N/USART3_RTS	BLUETOOTH: UART_CTS/SPI_CLK
36	PB15	I/O	PB15	SPI2_MOSI/I2S2_SD/TIM1_CH3N	
37	PC6	I/O	PC6	I2S2_MCK/TIM8_CH1/SDIO_D6	

38	PC7	I/O	PC7	I2S3_MCK/TIM8_CH2/SDIO_D7	
39	PC8	I/O	PC8	TIM8_CH3/SDIO_D0	
40	PC9	I/O	PC9	TIM8_CH4/SDIO_D1	
41	PA8	I/O	PA8	USART1_CK/TIM1_CH1/MCO	Enable External Oscillator
42	PA9	I/O	PA9	USART1_TX/TIM1_CH2	MIC_CLOCK
43	PA10	I/O	PA10	USART1_RX/TIM1_CH3	
44	PA11	I/O	PA11	USART1_CTS/USBDM/CAN_RX/ TIM1_CH4	
45	PA12	I/O	PA12	USART1_RTS/USBDP/CAN_TX/ TIM1_ETR	LED_1
46	PA13	I/O	JTMS-SWDIO		JTAG
47	VSS_2	S	VSS_2		0 V
48	VDD_2	S	VDD_2		2.8 V
49	PA14	I/O	JTCK-SWCLK		JTAG
50	PA15	I/O	JTDI	SPI3_NSS/I2S3_WS	JTAG
51	PC10	I/O	PC10	UART4_TX/SDIO_D2	
52	PC11	I/O	PC11	UART4_RX/SDIO_D3	
53	PC12	I/O	PC12	UART5_TX/SDIO_CK	
54	PD2	I/O	PD2	TIM3_ETR/UART5_RX/SDIO_CMD	
55	PB3	I/O	JTDO	SPI3_SCK / I2S3_CK	JTAG
56	PB4	I/O	NJTRST	SPI3_MISO	JTAG
57	PB5	I/O	PB5	I2C1_SMBA/ SPI3_MOSI/I2S3_SD	LED_2
58	PB6	I/O	PB6	I2C1_SCL/ TIM4_CH1	LED_3
59	PB7	I/O	PB7	I2C1_SDA /FSMC_NADV /TIM4_CH2	LED_4
60	BOOT0	I	BOOT0		0 V
61	PB8	I/O	PB8	TIM4_CH3/SDIO_D4	
62	PB9	I/O	PB9	TIM4_CH4/SDIO_D5	
63	VSS_3	S	VSS_3		0 V
64	VDD_3	S	VDD_3		2.8 V

Table 4.1. Microcontroller Pin descriptions

Each of the general-purpose I/O ports has two 32-bit configuration registers (GPIOx_CRL, GPIOx_CRH), two 32-bit data registers (GPIOx_IDR, GPIOx_ODR), a 32-bit set/reset register (GPIOx_BSRR), a 16-bit reset register (GPIOx_BRR) and a 32-bit locking register (GPIOx_LCKR).

Subject to the specific hardware characteristics of each I/O port listed in the datasheet, each port bit of the General Purpose IO (GPIO) Ports, can be individually configured by software in several modes:

- **Input floating**
- **Input pull-up**

- **Input-pull-down**
- **Analog** (input or output, connected to the ADC or DAC, respectively)
- **Output open-drain** (value on register is output on the pin)
- **Output push-pull** (value on register is output on the pin)
- **Alternate function push-pull** (output signal from an on-chip peripheral)
- **Alternate function open-drain** (output signal from an on-chip peripheral)

Each I/O port bit is freely programmable, however the I/O port registers have to be accessed as 32-bit words (half-word or byte accesses are not allowed). When configured as output, the value written to the Output Data register (GPIOx_ODR) is output on the I/O pin. It is possible to use the output driver in Push-Pull mode or Open-Drain mode. When configured as input, the Input Data register (GPIOx_IDR) captures the data present on the I/O pin at every APB2 clock cycle.

For the Alternate Functions it is necessary to program the Port Bit Configuration Register before using a default alternate function.

- For alternate function inputs, the port must be configured in Input mode (floating, pullup or pull-down) and the input pin must be driven externally.
- For alternate function outputs, the port must be configured in Alternate Function Output mode (Push-Pull or Open-Drain).
- For bidirectional Alternate Functions, the port bit must be configured in Alternate Function Output mode (Push-Pull or Open-Drain). In this case the input driver is configured in input floating mode

If a port bit is configured as Alternate Function Output, this disconnects the output register and connects the pin to the output signal of an on-chip peripheral. If software configures a GPIO pin as Alternate Function Output, but peripheral is not activated, its output is not specified.

The timer used to create the clock for the microphone was the TIM1. It was configured in the PWM mode, which allows to generate a signal with a frequency determined by the value of the TIM1_ARR register and a duty cycle determined by the value of the TIM1_CCR1 register. In this case, the frequency selected was 2.4 *MHz* and the duty cycle was 50%.

The USART3 (Universal Synchronous Asynchronous Receiver Transmitter) was used for the Bluetooth interfacing. It offers a flexible means of full-duplex data exchange with the Bluetooth component. The interface is connected to the Bluetooth device by four pins: USART3_TX, USART3_RX, USART3_RTS and USART3_CTS.

- **RX:** Receive Data Input is the serial data input. Oversampling techniques are used for data recovery by discriminating between valid incoming data and noise.
- **TX:** Transmit Data Output. When the transmitter is disabled, the output pin returns to its IO port configuration. When the transmitter is enabled and nothing is to be transmitted, the TX pin is at high level. In single-wire and smartcard modes, this IO is used to transmit and receive the data.
- **nCTS:** Clear To Send blocks the data transmission at the end of the current transfer when high
- **nRTS:** Request to send indicates that the USART is ready to receive a data (when low).

The ADC1 was used for the analog to digital conversion of the signals. Four ADC channels were used, and they were defined as shown in Table 4.2.

INPUT	ADC1 CHANNEL
VBAT/2	0
MIC_INT	1
MIC_EXT	2
ECG	3

Table 4.2. ADC1 channels definition

Table 4.3 shows the used peripherals' GPIO configurations.

PERIPHERAL	PIN	CONFIGURATION	GPIO CONFIGURATION
TIM1	TIM1_CH2	Output compare channel	Alternate function push-pull
USART3	USART3_TX	Full duplex	Alternate function push-pull
	USART3_RX	Full duplex	Input floating
	USART3_RTS	Hardware flow control	Alternate function push-pull
	USART3_CTS	Hardware flow control	Input floating/ Input pull-up
ADC	ADC1_INx		Analog

Table 4.3. Peripherals' GPIO configurations

4.2.3 Interrupt Vector Configuration

The nested vectored interrupt controller (NVIC) manages all the interrupts. The NVIC has 68 maskable interrupt channels, 16 programmable priority levels, low latency exception and interrupt handling, and power management control. In the setup.c file the vector table base location was defined. Subsequently, all the interrupts used in the program were defined in other functions.

4.3 **MAIN.C**

Most of the task were defined in the main.c file. The logical sequence of events is defined as follows:

- Defines, includes and variables definition
- System clocks configuration
- GPIO configuration
- NVIC configuration
- Bluetooth configuration and initialization (USART3)
- Timer configuration and initialization (MIC_CLOCK)
- Create Signal_Task

The main part of the program is the Signal_Task, in which the ADC conversion is perform, the acquired data is organized in packets and it is send via BT to the PC. This function will be explain in detail.

Three LEDs were used to indicate the status of the board and one LED was used for debug. Table 4.4 shows the status indicated with the LEDs.

LED	STATUS	DESCRIPTION
LED_1	Battery Status	Turn on when VBAT/2 < 1.45 V
LED_2	Debug	
LED_3	Initialization complete	Turn on to indicate that the board is ON and the firmware is running
LED_4	BT Connection	Turn on when the BT connection is open

Table 4.4. Status indicated with the LEDs

4.3.1 Signal_Task

The Signal_Task is the most important function of the implemented firmware. Inside this function, the main loop of the firmware is performed. This function can be divided in the following parts:

- ADC Initialization
- Enable sampling in DMA mode
- Organization of the data in packets
- Transmission of the packets via Bluetooth

4.3.1.1 *ADC Initialization*

The first part of the function corresponds to the ADC initialization. In this part two functions have been used.

- STM32_ADC_Init_Group: This function initialize ADC. The inputs of the function are: channels to sample, sampling frequency expressed in Hz, and external trigger.
- STM32_ADC_Add_Channel_To_Group: This function add a channel to the sampling group. The inputs of the function are: channel to add and the sampling frequency

All the analog signals (ECG, MIC_INT, MIC_EXT, VBAT/2) connected to the microcontroller ADC have been sampled with a frequency of 800 *Hz*.

The 12-bit ADC is a successive approximation analog-to-digital converter. The A/D conversion of the various channels has been performed in the scan mode using a DMA request generation during the regular channel conversion. The result of the ADC was stored in a left-aligned 16-bit data register.

The ADC has been powered-on by setting the ADON bit in the ADC_CR32 register. The ADC input clock is generated from the PCLK2 clock divided by a prescaler (2, 4, 6 or 8) and should be in the range 600 *kHz* to 14 *MHz*. In this case, the prescaler equal to 8 ($ADC\_Clock = PCLK2\ /2\ = 1.625\ MHz$).

It is possible to organize the conversions in groups. A group consists of a sequence of conversions which can be done on any channel and in any order. In this case, the used sequence was Ch3, Ch0, Ch2, Ch1. The regular channels and their order in the conversion sequence must be selected in the

ADC_SQRx registers. The total number of conversions in the regular group must be written in the L[3:0] bits in the ADC_SQR1 register.

The scan mode is used to scan the group of analog channels. Scan mode can be selected by setting the SCAN bit in the ADC_CR1 register. Once this bit is set, ADC scans all the four channels selected in the ADC_SQRx registers. A single conversion is performed for each channel of the group. After each end of conversion the next channel of the group is converted automatically. If the CONT bit is set, conversion does not stop at the last selected group channel but continues again from the first selected group channel. If the DMA bit is set, the direct memory access controller is used to transfer the converted data of regular group channels to SRAM after each EOC.

Conversion can be triggered by an external event (e.g. timer capture, EXTI line). If the EXTTRIG control bit is set then external events are able to trigger a conversion. The EXTSEL[2:0] and control bits allow the application to select decide which out of 8 possible events can trigger conversion for the groups. In this case, a timer (TIM4) was used to generate the 800 *Hz* that serve as trigger for the conversion.

4.3.1.2 *Enable DMA mode*

Since the converted regular channels value are stored in a unique data register, it is necessary to use DMA for conversion of more than one regular channel. This avoids the loss of data already stored in the ADC_DR register. Only the end of conversion of a regular channel generates a DMA request, which allows the transfer of its converted data from the ADC_DR register to the destination location selected by the user.

The function implemented to enable the DMA mode was the STM32_ADC_enableSamplingDMAMode. This function initializes and starts DMA-transfer of ADC's data. The inputs needed are: destination location address, MAX_ADC_SAMPLE, data callback.

Figure 4.4 reassumes the operation of the function:

1. The ADC starts the conversion of the first channel of the group (Ch_3).
2. DMA is used to transfer the converted data to SRAM after EOC. The data is transferred to the memory address pointed by

My_Active_Sampling pointer. After the data has been transferred, the pointer is incremented by 1.

3. The steps 1 and 2 are repeated for all the channels in the group (Ch_0, Ch_2, Ch_1).
4. When all the channels have been converted, the ADC conversion continues again from the first selected group channel (step 1)
5. The above steps are repeated until the ADC has perform a number of conversions defined by the constant MAX_ADC_SAMPLE ($My\_Sampling\_Idx = a * MAX\_ADC\_SAMPLE$, where a is an integer). When this occurs, it generates a callback to the function My_App_ADC_Sample_Ready_cb .
6. When the function My_App_ADC_Sample_Ready_cb is called, it means that there is enough data to be send via Bluetooth. The function will increment the DATA_READY_COUNTER by 1. When My_Active_Sampling pointer reaches the end of the buffer ($BUFFER\_SIZE = MAX\_ADC\_SAMPLE*NR\_OF\_PACKETS$), this function will also restart the pointer to its original value.

In this case the values of the constants were:

- MAX_ADC_SAMPLE = 60
- NR_OF_PACKETS = 4
- BUFFER_SIZE = MAX_ADC_SAMPLE*NR_OF_PACKETS = 240

This means, that each time the ADC has perform 60 conversions for each channel, the callback function is called. When the pointer reaches the end of the buffer (BUFFER_SIZE) it is restarted to its original value.

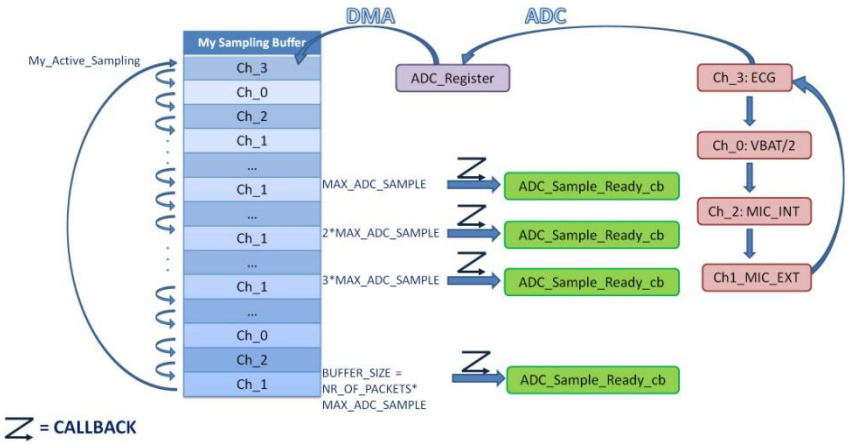

Figure 4.4. Schematic representation of the ADC and DMA

4.3.1.3 *Organization of the Data in Packets and Transmission Via Bluetooth*

If the Bluetooth connection is open and the DATA_READY_COUNTER> 0, it means that a packet can be sent via Bluetooth to the remote device (PC). The collected data is organized in a data structure. This data structure, called MY_TOTAL_DATA, has the information necessary for the Bluetooth transmission and the data of the four channels sampled by the ADC. Each packet contains the a number of TOT_DATA ($TOT\_DATA = 60$) samples of each channel of the ADC. Figure 4.5 shows an schematic representation of the Bluetooth packet.

Figure 4.6 shows an schematic representation of the organization of the collected in packets. A pointer called "My_Active_Splitting" points the position of the data in My_Sampling_Buffer. When 60 samples (MAX_ADC_SAMPLES) of each channel have been copy to MY_TOTAL_DATA, the packet is sent via BT. After it has been sent, another packet is created, starting with the data pointed by My_Active_Splitting. When My_Active_Splitting pointer reaches the end of the buffer, it is restated to its original value.

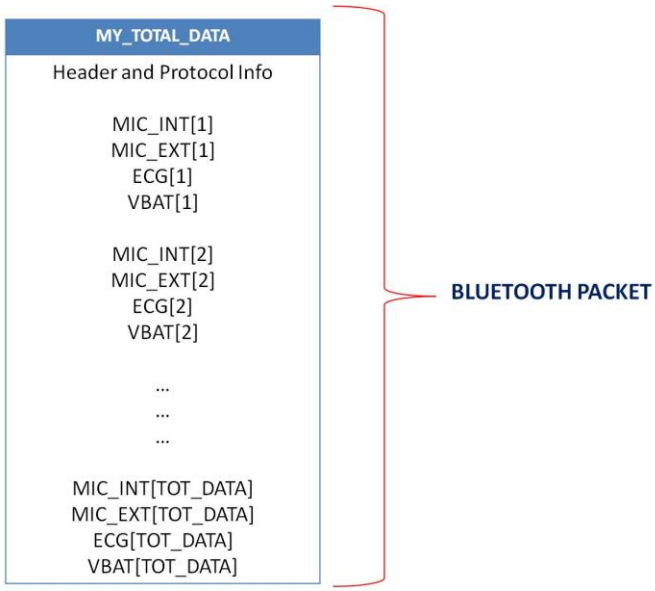

Figure 4.5. Schematic representation of the Bluetooth Packet

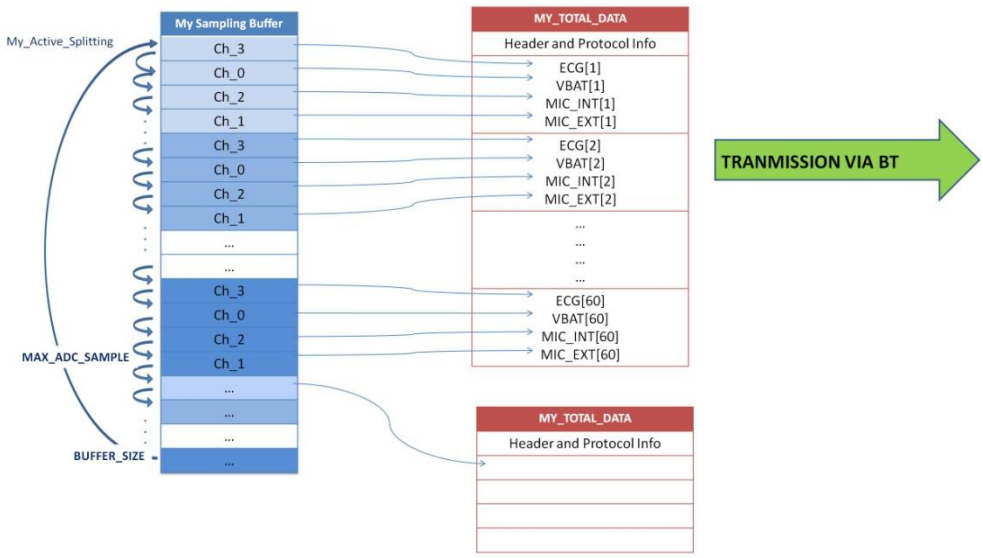

Figure 4.6. Schematic representation of the organization of the collected data in packets

When the packet is ready, the microcontroller send the collected data to a remote device via Bluetooth module installed in the board. The Bluetooth transmits at a speed of 1.2 *Mbit/s*.

A Bluetooth Viewer Software installed on the PC (Gangia HIM 6.7), knows the protocol by which the data are packed in the Bluetooth transmission and is able to extract useful information and visualize the signals. The data is displayed and saved in a file .dat, which can be elaborated using other programs (such as Matlab) for signals processing. Figure 4.7 shows the data displayed in the PC using the Bluetooth viewer.

As it can be seen in the figure, the viewer allows to visualize 6 channels (ACCX, ACCY, ACCZ, ECG1, ECG2, ECG3). For this application, only 4 channels were used, and their correspondence with the input signals is shown in Table 4.5.

SIGNAL	BT VIEWER CHANNEL
MIC_INT	ACCx
MIC_EXT	ACCy
ECG	ECG2
VBAT/2	ECG3

Table 4.5. Correspondence between the input signals and the BT viewer channels

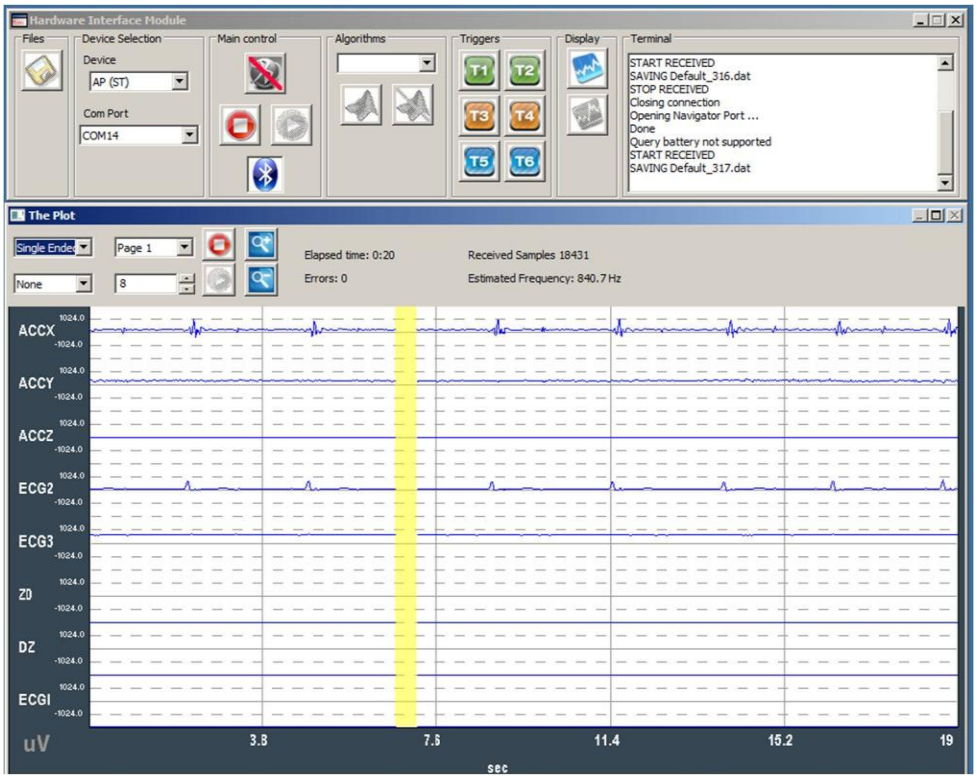

Figure 4.7. Displayed data with the Bluetooth viewer

4.4 FIRMWARE FLOWCHARTS

The flowcharts of the main processes of the firmware are shown blow.

4.4.1 Main.c Flowchart

The first part of the process is the initialization in which the clocks, the GPIO, and the NVIC are configured, the variables and the constants are defined, the defines and includes are specified, and the BT and TIM1 configuration is performed. After the initialization, a LED is turn on (LED_3) to indicate that the board is ON. Subsequently, the main loop starts: it verifies if the BT connection is open, and if it is open, it turns on the LED_4, enables the ADC and calls the SIGNAL_TASK function.

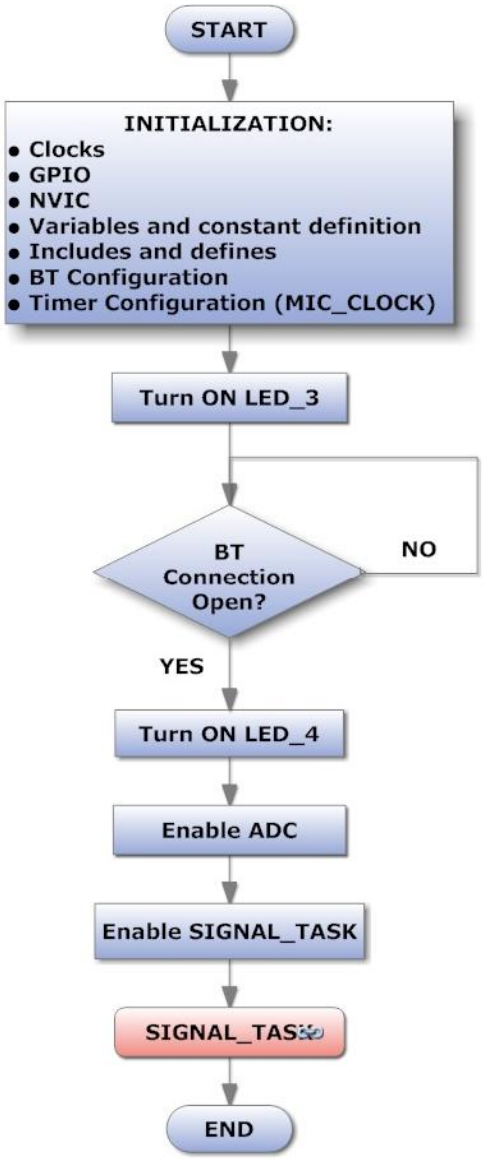

Figure 4.8. Main.c flowchart

4.4.2 Signal_Task Flowchart

The operation of the Signal_Task function was explained in section 4.3.1. It basically performs the ADC conversion of the analog signals, organize the collected data in packets and send them via BT to a PC. It uses the DMA mode, in which the converted data is transfer from the ADC_Ragister to the SRAM memory, at the specified address.

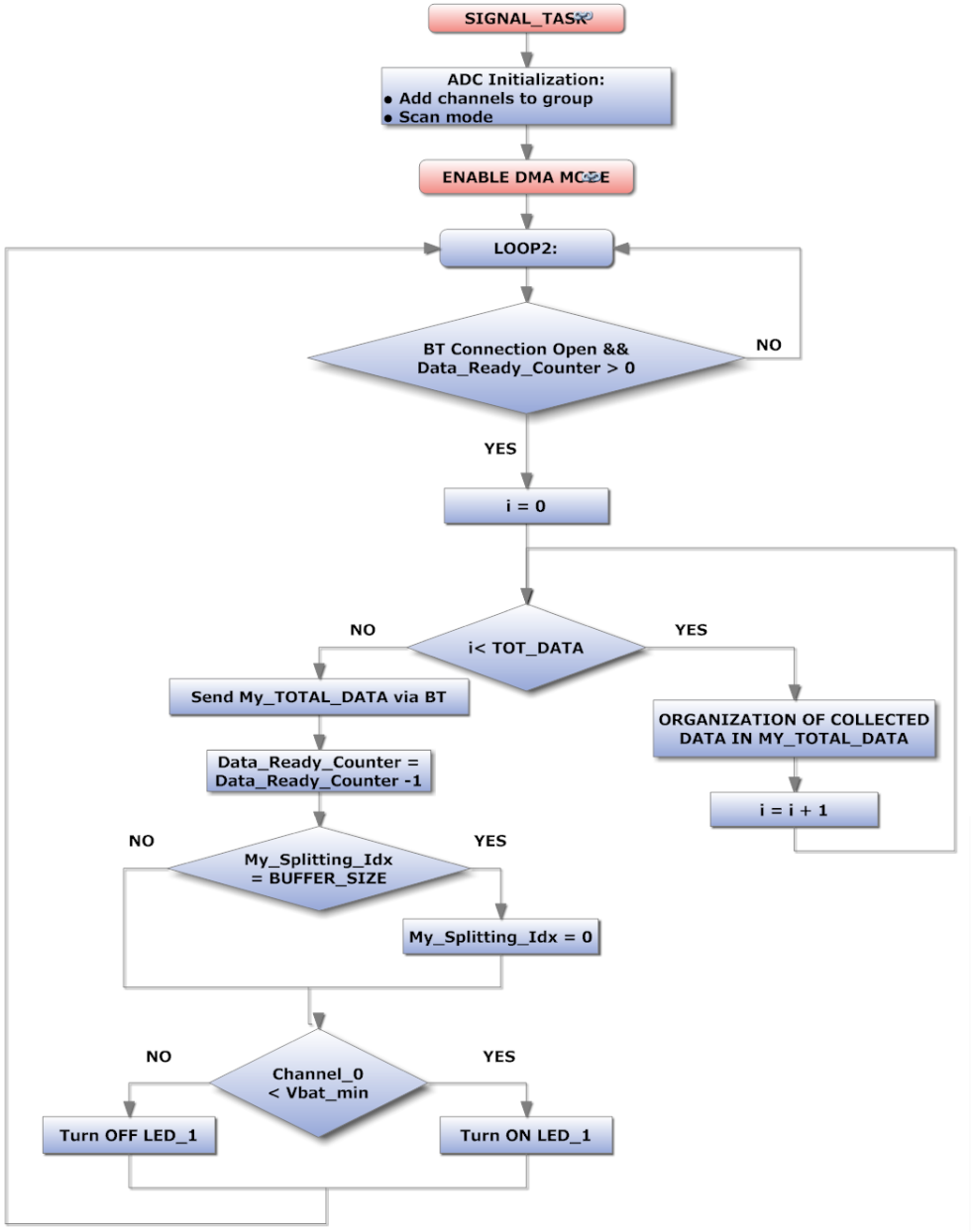

Figure 4.9. SIGNAL_TASK Flowchart

4.4.3 Enable_DMA_Mode Flowchart

This function uses as input the memory address to transfer the data from the ADC_Register (My_Active_Sampling) and the constant MAX_ADC_SAMPLE. As described in section 4.3.1.2, it performs the

sampling of the channels in the group and transfers the data to SRAM memory. When all the channels have been sampled, it starts again with the first channel of the group. When a number of MAX_ADC_SAMPLE samples have been perform for each channel, it generates the callback to the function My_App_ADC_Sample_Ready_cb, as described in section 4.31.3.

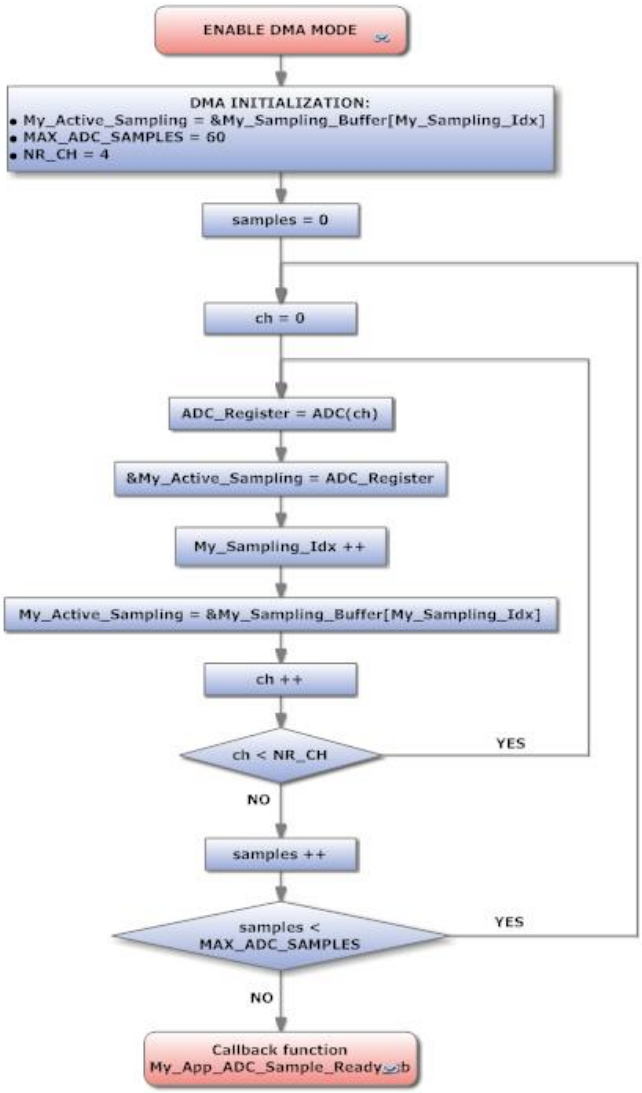

Figure 4.10. Enable_DMA_Mode Flowchart

4.4.4 Callback Function Flowchart

When the function My_App_ADC_Sample_Ready_cb is called, it basically increments the DATA_READY_COUNTER by 1, and when

My_Active_Sampling pointer reaches the end of the buffer (*BUFFER_SIZE = MAX_ADC_SAMPLE*NR_OF_PACKETS*), it restarts the pointer to its original value.

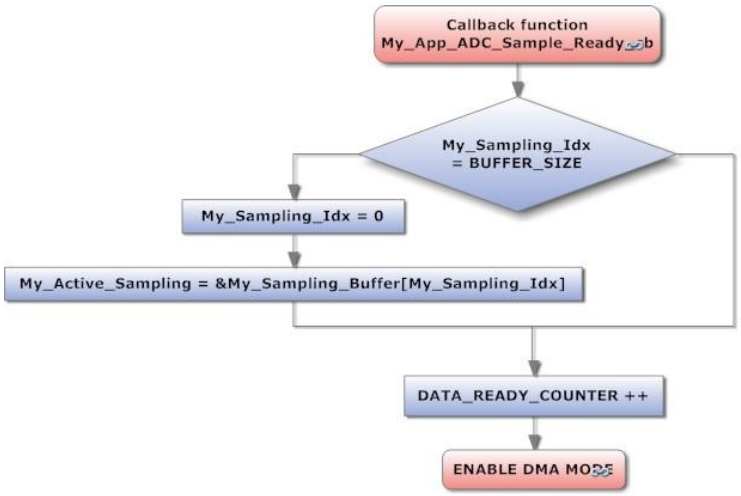

Figure 4.11. DMA Callback Function Flowchart

One the signals have sent to the PC via BT, the aim of the work moves towards the analysis and elaboration of the signals and the extraction of the vital parameters, such as the heart rate and the blood pressure. Next chapter is focused on the signal processing using Matlab, and the test results.

Chapter 5

SIGNAL PROCESSING AND TEST RESULTS

The ECG and PCG signals carry information that is useful for the estimation of blood pressure. Nevertheless, such information cannot be available directly from the raw recorded signals; it can be masked by other biologic signals contemporaneously detected or buried in some additive noise. For such reasons, some additional processing is usually required to enhance the relevant information and to extract from it parameters that quantify the behavior of the system under study.

Generally, the recorded ECG and PCG signals are often contaminated by noise and artifacts that can be within the frequency band of interest and manifest with similar characteristics as the signals itself. In order to extract useful information from the noisy ECG and PCG signals, it is necessary to process the raw signals. ECG and PCG signal processing can be roughly divided into two stages by functionality: preprocessing and feature extraction. The preprocessing stage removes or suppresses noise from the raw ECG and PCG signals and the feature extraction stage extracts diagnostic information from the signals.

Several processing techniques can be used for such purposes; time or frequency domain methods including filtering, averaging, spectral estimation, and others. The digital processing is more efficient and flexible than the analog one. Digital techniques have several advantages: Their performance is generally powerful, being able to easily implement even complex algorithms, and accuracy depends only on the truncation and round-off errors, whose effects can generally be predicted and controlled by the designer.

Moreover, design parameters can be more easily changed because they involve software rather than hardware modifications.

A review of different signal processing techniques used in this project will be given in this chapter. They include traditional filtering, peak detector, and spectral estimators. The main concepts of analysis and design of digital filters are presented in section 5.3, and a some examples are illustrated in the processing of the ECG and the PCG signals. Section 5.4 shows the test results of an experiment conducted on 5 healthy subjects to analyze the capabilities of RS2 on SBP estimation.

5.1 ECG SIGNAL PROCESSING

Electrocardiography (ECG) is the acquisition of electrical activity of the heart captured over time by an external electrode attached to the skin. Each of the cell membranes that form the outer covering of the heart cell have an associated charge which is depolarized during every heart beat. These appear as tiny electrical signals on the skin which can be detected and amplified by the ECG. The term “lead” in context to an ECG refers to the voltage difference between two of the electrodes, and it is this difference which is recorded by the equipment.

Preprocessing ECG signals helps to remove contaminants from the ECG signals. Broadly speaking, ECG contaminants can be classified into the following categories:

- power line interference
- electrode pop or contact noise
- patient–electrode motion artifacts
- electromyographic (EMG) noise
- baseline wandering (low frequency noise)

Among these noises, the power line interference and the baseline wandering are the most significant and can strongly affect ECG signal analysis. In this case, the power line interference was not considered since the device works with battery. Baseline wandering usually comes from respiration at frequencies wandering between 0.15 and 0.3 Hz, and can be suppress it by a highpass digital filter.

Extracting useful clinical information from the real (noisy) ECG requires reliable signal processing techniques. For the purpose of this project the

ECG signal was process using classical techniques in the time domain to detect the R-peaks, compute their RR interval, and the cardiac rhythm. The RR-interval is the time between successive R-peaks, the inverse of this time interval gives the instantaneous heart rate. More details about the implemented algorithm will be given in the following sections.

An example of an acquisition of the ECG signal (raw signal) is shown in Figure 5.1.

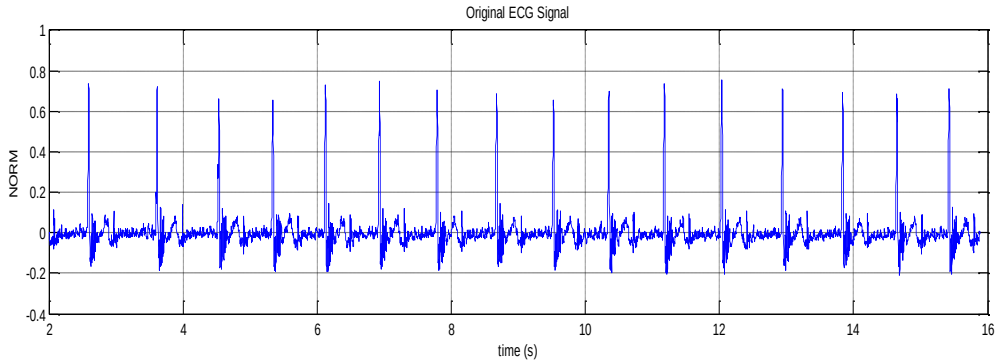

Figure 5.1. Raw ECG Signal

5.2 PCG SIGNALS PROCESSING

The PCG signal discloses information about cardiac function through vibrations caused by the working heart. Heart sounds and murmurs are of relatively low intensity and are band-limited to about 10-400 *Hz* (see Figure 2.12). In healthy subjects, the frequency spectrum of S1 contains a peak in the low frequency range (10-50 *Hz*) and in the medium frequency range (50-140 *Hz*). S2 contains peaks in low (10-80 *Hz*), medium (80-220 *Hz*) and high-frequency ranges (220-400 Hz). S2 is composed of two components, one originating from aortic valve closure and one originating from pulmonary valve closure. Normally, the aortic component (A2) is of higher frequency than the pulmonary component (P2). S3 and S4 are believed to originate from vibrations in the left ventricle and surrounding structures powered by the acceleration and deceleration of blood flow. The time and frequency properties of heart sounds are summarized in Table 5.1 and examples of two phonocardiographic (PCG) signals and their frequency spectra are illustrated in Figure 5.2 [**16**].

Sound	Location (*ms*)	Duration (*ms*)	Frequency range (*Hz*)
S1	10-50 after R-peak in ECG	100-160	10-140
S2	280-360 after R-peak in ECG	80-140	10-400
S3	440-460 after R-peak in ECG	40-80	15-60
S4	40-120 after the beginning of P-wave in ECG	30-60	15-45

Table 5.1. Time and frequency properties of the heart sounds.

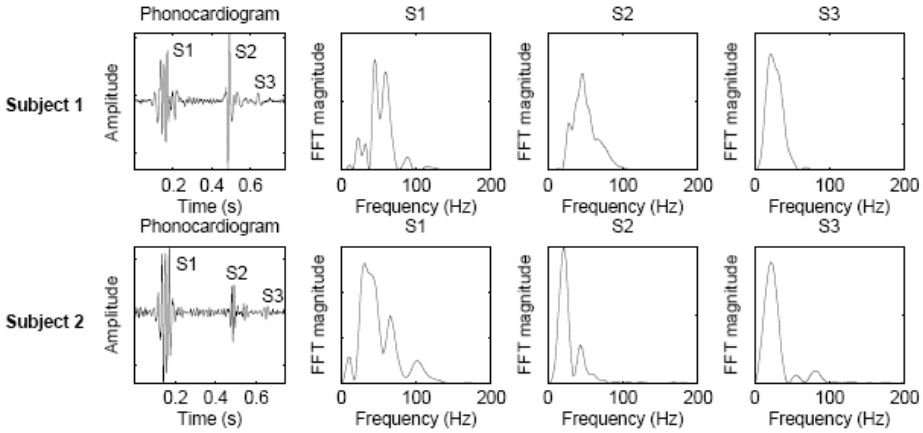

Figure 5.2. Heart sounds and their respective frequency spectra from a 13 year old girl and a 36 year old male [16**].**

Noise is a big problem in PCG recordings. The sensor, the sensor contact surface, the patient's position, the auscultation area, the respiration phase and the background noise all influence the quality of the sound. In practice this means that the recordings often contain noise such as friction rubs, rumbling sounds from the stomach, respiratory sounds from the lungs and background noise from the clinical environment.

Similarly to the ECG signal processing, the PCG signal processing can be divided into two stages, the preprocessing and the feature extraction. The preprocessing stage removes or suppresses noise from the raw signal and the feature extraction stage extracts diagnostic information. The feature extraction stage includes the heart sound location and segmentation. The ECG can provide information about where to search for heart sounds (S1 occurs subsequent to the QRS complex and S2 occurs after the T-wave). Based on the ECG signal, predefined search windows are used to locate the heart sounds. For the purpose of this thesis, accurate temporal localization of the heart sounds is necessary.

The details about the implemented algorithm for preprocessing and feature extraction are be given in the next sections. Figure 5.3 shows an example of an acquired PCG signal.

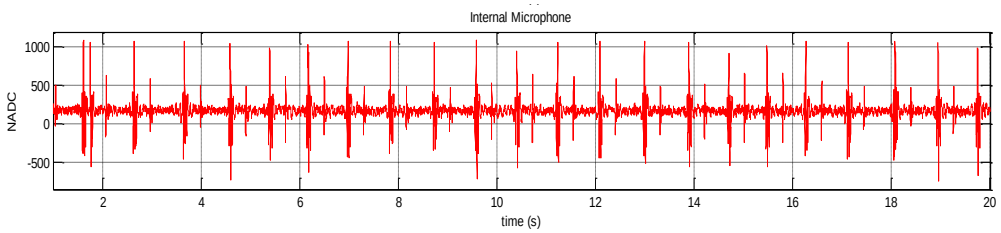

Figure 5.3. Raw PCG signal

5.3 SIGNAL PROCESSING FRAMEWORK

The implemented Matlab algorithm for signal preprocessing and feature extraction is presented in the following sections.

5.3.1 Importing the File .dat

As it was described in section 4.3.1.3, the data transmitted to the PC via BT is saved in a file .dat. This file is divided in several columns, each one representing a channel of the viewer. The microcontroller sends the data belonging to the same signal to the same channel of the viewer.

The file have been imported to Matlab using the *UIGETFILE* function, which displays a dialog box for the user to select the file that wants to open, and returns the filename and path strings of the selected filter. Subsequently, the *IMPORTDATA* function was used to load data from a file into Matlab. Using this function, the data is saved into a matrix.

The first column of the matrix corresponds to the signal acquired with the internal microphone (PCG signal), the second column corresponds to the signal acquired with the external microphone, and the fourth column to the ECG signal. For convenience, each columns have been into a different vector.

The temporal distance between the samples can be obtained by knowing the sampling rate (*Fs = 800 Hz*); the distance in time, of two successive samples of the same channel is equal to 1.3 *ms* ($1/800\ Hz\ =\ 1.3\ ms$).

An example of a plot of the imported data is shown in Figure 5.4.

Later, the signals have been normalized, and, in case it was necessary, a detrend has been performed.

An audio file .wav of the raw PCG signal (internal microphone) was created in order to make it possible to hear the acquired PCG signal.

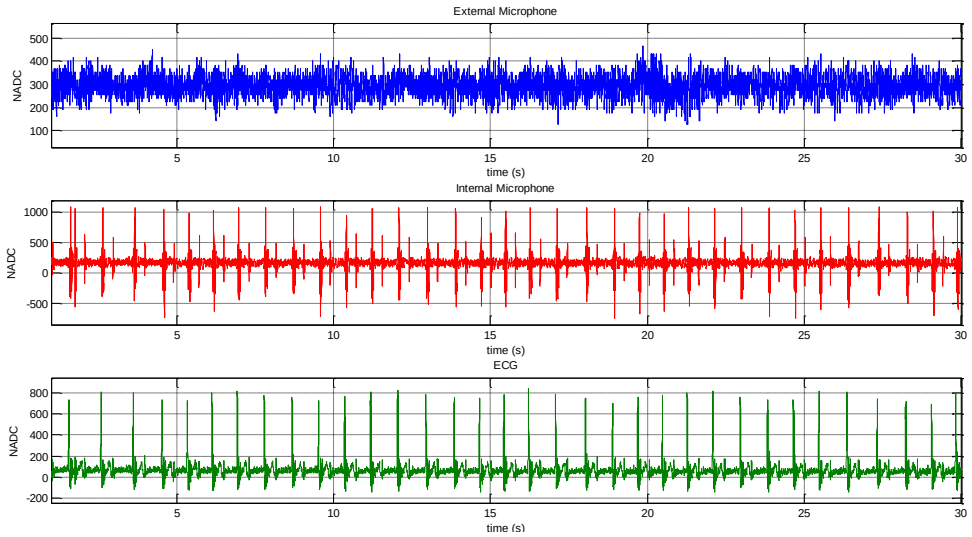

Figure 5.4. Acquired signals: (a) external microphone, (b) internal microphone (PCG), (c) ECG.

5.3.2 Spectral Density Estimation

The power spectral density (PSD) has been performed using the Welch's method, which estimates PSD of the input signal vector x using Welch's averaged modified periodogram method of spectral estimation. In this case:

- The vector x has been segmented into sections of equal length (1024 samples), each with 50% overlap.
- Any remaining (trailing) entries in x that could not be included in the segments of equal length were discarded.
- Each segment was windowed with a Hamming window that was the same length as the segment.

In general, the length *N* of the FFT and the values of the input x determine the length of Pxx and the range of the corresponding normalized frequencies. The length of the FFT can be specified (*nfft = 1024*). The window size must be greater than or equal to nfft. The sampling frequency (*fs*) can also be specified in Hz to compute the PSD vector (*Pxx*) and the corresponding vector of frequencies (*f*). In this case, the units for the frequency

vector are in Hz. The spectral density produced is calculated in units of power per Hz. Using Matlab, the syntax of the used function was:

[Pxx,f] = pwelch(x,window,noverlap,nfft,fs)

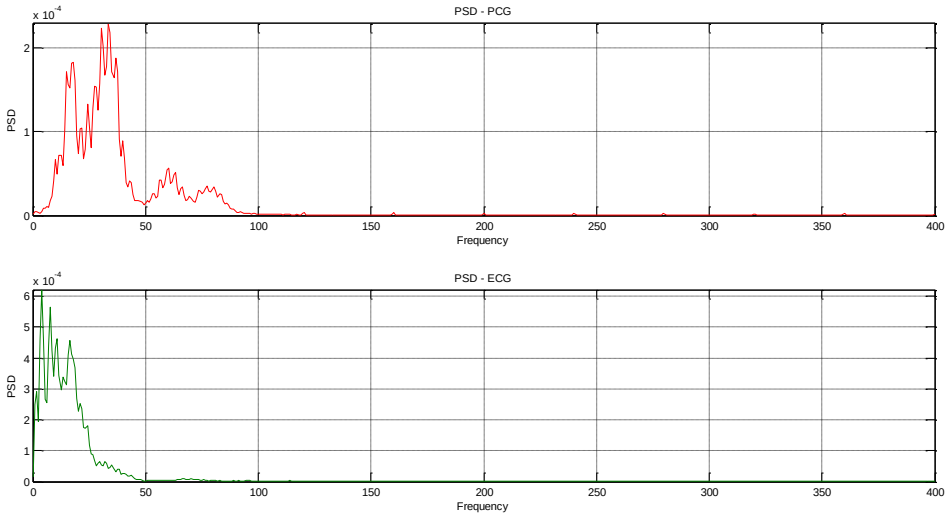

Figure 5.5. PSD of the original ECG and PCG signals

As it can be seen in the figure, the power spectral density is concentrated on the lower frequencies area. The PSD for the PCG is concentrated at frequencies below 100 *Hz* and PSD for the ECG signal is concentrated at frequencies below 50 *Hz.* For this reason, it was decided to filter the signals with low pass filters: the ECG signal with a cutoff frequency of 50 *Hz*, and the PCG signal with a cutoff frequency of 100 *Hz*.

5.3.3 Signal Filtering

A digital filter is a discrete-time system that operates some transformation on a digital input signal *x[n]* generating an output sequence *y[n]*, as schematically shown by the block diagram in Figure 5.6.

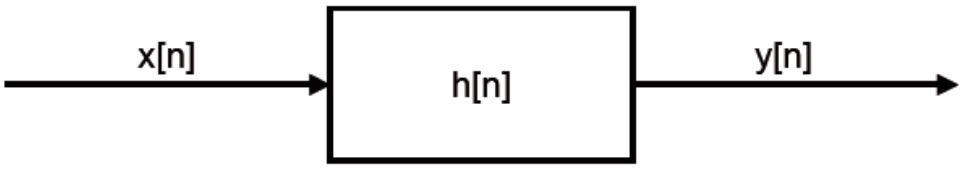

Figure 5.6. General block diagram of a digital filter.

The characteristics of transformation *h[n]* identify the filter. The behavior of a filter is usually described in terms of input-output relationships. They are usually assessed by exciting the filter with different inputs and evaluating which is the response (output) of the system. In particular, if the input is the impulse sequence $\delta(n)$, the resulting output, the impulse response, has a relevant role in describing the characteristic of the filter. Such a response can be used to determine the response to more complicated input sequences.

In the z-domain, the relationship between the input and the output can be written as a simple multiplication:

$$Y(z) = H(z) * X(z) \qquad \textbf{Eq. 5.1}$$

where $H(z)$, known as transfer function of the filter, is the z-transform of the impulse response. $H(z)$ plays a relevant role in the analysis and design of digital filters. For a large class of linear, time-invariant systems, $H(z)$ can be expressed in the following general form:

$$H(z) = \frac{\sum_{m=0}^{M} b_m z^{-m}}{1 + \sum_{k=1}^{N} a_k z^{-k}} \qquad \textbf{Eq. 5.2}$$

which describes in the z domain the following *difference equation* in this discrete time domain:

$$y(n) = \sum_{k=1}^{N} a_k y(n-k) + \sum_{m=0}^{M} b_m x(n-m) \qquad \textbf{Eq. 5.3}$$

When at least one of the a_k coefficients is different from zero, some output values contribute to the current output. The filter contains some feedback, and it is said to be implemented in a recursive form. On the other hand, when the a_k values are all zero, the filter output is obtained only from the current or previous inputs, and the filter is said to be implemented in a nonrecursive form.

A common way of classifying digital filters is based on the characteristics of their impulse response. For finite impulse response (FIR) filters, $h(n)$ is composed of a finite number of nonzero values, while for infinite response (IIR) filters, $h(n)$ oscillates up to infinity with nonzero values. It is clearly evident that in order to obtain an infinite response to an impulse in input, the IIR filter must contain some feedback that sustains the output as

the input vanishes. The presence of feedback paths requires putting particular attention to the filter stability. FIR filters are usually implemented in a nonrecursive form and IIR filters in a recursive form. Two important requirements for filters are stability and linear phase response. FIR filters can be easily designed to fulfill such requirements; they are always stable (having no poles outside the origin), and the linear phase response is obtained by constraining the impulse response coefficients to have symmetry around their midpoint.

A digital filter is described by the two vectors of coefficients a and b. Given an input sequence x(n), the output of the filter is obtained by the discrete convolution between the input sequence and the impulse response of the filter.

FIR filters have the following primary advantages:

- They can have exactly linear phase.
- They are always stable.
- The design methods are generally linear.
- They can be realized efficiently in hardware.
- The filter startup transients have finite duration.

The primary disadvantage of FIR filters is that they often require a much higher filter order than IIR filters to achieve a given level of performance. Correspondingly, the delay of these filters is often much greater than for an equal performance IIR filter.

The primary advantage of IIR filters over FIR filters is that they typically meet a given set of specifications with a much lower filter order than a corresponding FIR filter. Although IIR filters have nonlinear phase, data processing within Matlab software is commonly performed "offline," that is, the entire data sequence is available prior to filtering. This allows for a noncausal, zero-phase filtering approach (via the *filtfilt* function), which eliminates the nonlinear phase distortion of an IIR filter. Digital filters with finite-duration impulse response (all-zero, or FIR filters) have both advantages and disadvantages compared to infinite-duration impulse response (IIR) filters. The classical IIR filters are: Butterworth, Chebyshev Types I and II, elliptic, and Bessel.

For any of the two types of filters, FIR or IIR, the filter design is the process of creating the filter coefficients to meet specific filtering requirements. Filter implementation involves choosing and applying a particular

filter structure to those coefficients. Table 5.2 provides the filter method summary of the some of the functions included in the Matlab Signal Processing Toolbox [**28**].

In this thesis, the goal of the digital filter was to remove noise above a certain frequency from the ECG and PCG signals (sampled at 800 *Hz*). As it has been explained before, the ECG signals has a bandwidth from 0.05 to 100 *Hz*, and the PCG signal a bandwidth from 10 to 400 *Hz*. Since the signals have different bandwidths, it was convenient to filter each signal with a different cutoff frequency.

	FILTER METHOD	DESCRIPTION	FILTER FUNCTIONS
IIR	Analog Prototyping	Using the poles and zeros of a classical lowpass prototype filter in the continuous (Laplace) domain, obtain a digital filter through frequency transformation and filter discretization.	**Complete design functions:** besself, butter, cheby1, cheby2, ellip **Order estimation functions:** buttord, cheb1ord, cheb2ord, ellipord **Lowpass analog prototype functions:** besselap, buttap, cheb1ap, cheb2ap, ellipap **Frequency transformation functions:** lp2bp, lp2bs, lp2hp, lp2lp **Filter discretization functions:** bilinear, impinvar
	Direct Design	Design digital filter directly in the discrete time-domain by approximating a piecewise linear magnitude response.	yulewalk
FIR	Windowing	Apply window to truncated inverse Fourier transform of desired "brick wall" filter	fir1, fir2, kaiserord
	Multiband with Transition Bands	Equiripple or least squares approach over sub-bands of the frequency range	firls, firpm, firpmord

Table 5.2. Filter design methods

Both the ECG and the PCG have been filtrated using a high pass FIR filter with a cutoff frequency of 2 *Hz*, to eliminate the low frequency noise (baseline wandering). In order to eliminate the high frequency noise, it was

decided to filter the ECG signal with a low pass filter with a cutoff frequency of 50 *Hz* and to filter the PCG signal with a low pass filter with a cutoff frequency of 100 *Hz*.

Figure 5.7 shows the frequency response of the FIR low pass filter. It can be seen that the filters have linear phase in the pass band. Figure 5.8 shows the results of the digital filtering using a FIR filter. The 20^{th} order FIR filters were obtained using the *fir1* function with cutoff frequencies (*fc*) of 50 Hz and 100 Hz, for ECG and PCG, respectively.

[b2,a2] = fir1(20,fc/400);

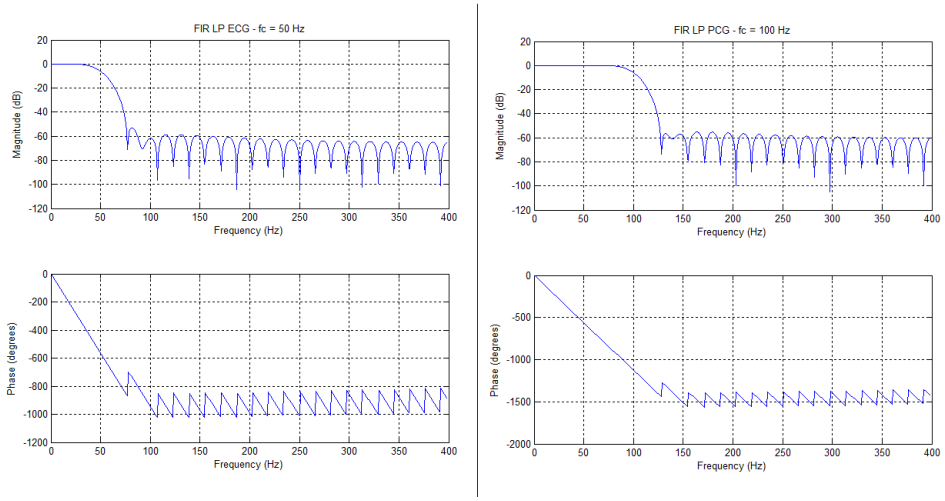

Figure 5.7. Frequency response of the FIR low-pass filters

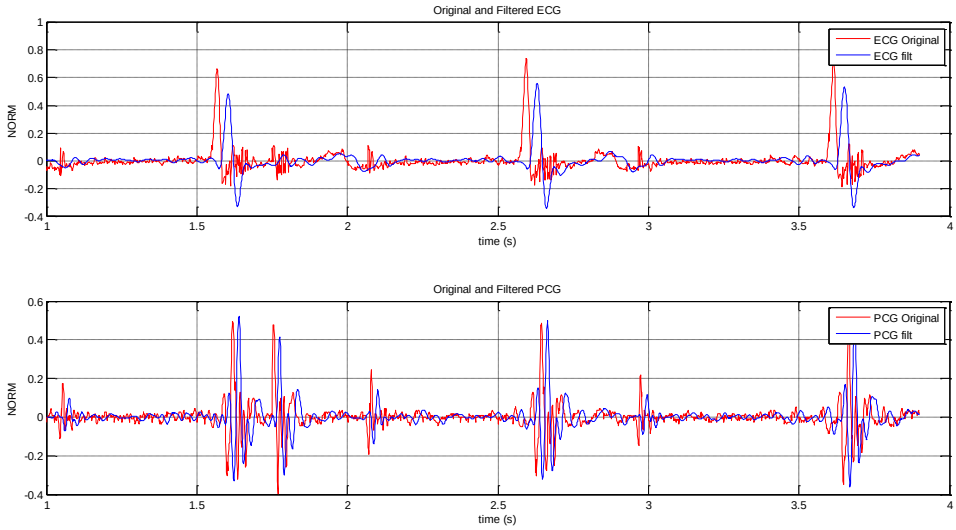

Figure 5.8. ECG and PCG original and filtered signals using a low pass FIR filter with cutoff frequencies of 50 and 100 Hz, respectively.

As it can be seen in Figure 5.8, a delay was introduced in the filtered signals. Since the filters used were not equal (they had different cutoff frequencies), the delay introduced was different for the ECG and the PCG signals. This was not convenient since the aim was to find the time interval between the signals. The delay could be calculated, but it was decided to use an IIR filter to avoid inconveniences causes by these delays.

A 10^{th} order low pass IIR filter was obtain with the *yulewalk* function and the noncausal zero-phase filtering approach (via the *filtfilt* function). The frequency response of the filters is shown in Figure 5.9, and the obtained filtered signals are shown in Figure 5.10.

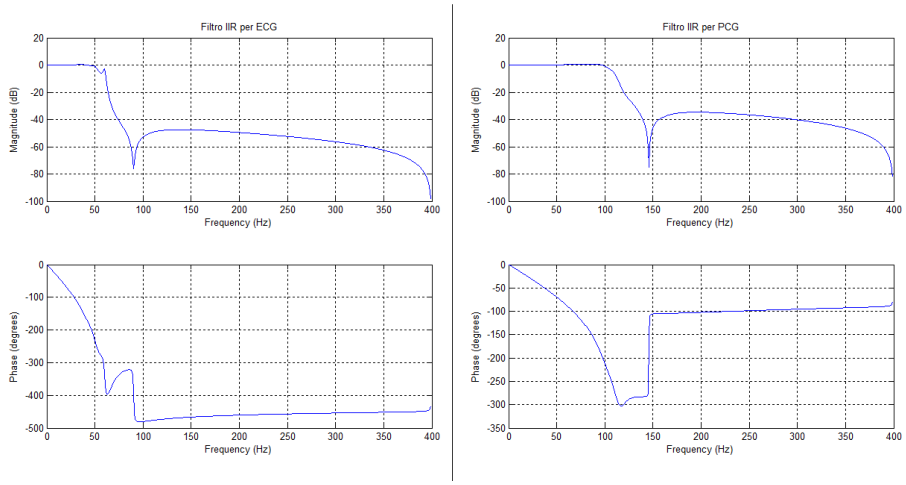

Figure 5.9. Frequency response of the IIR low-pass filters

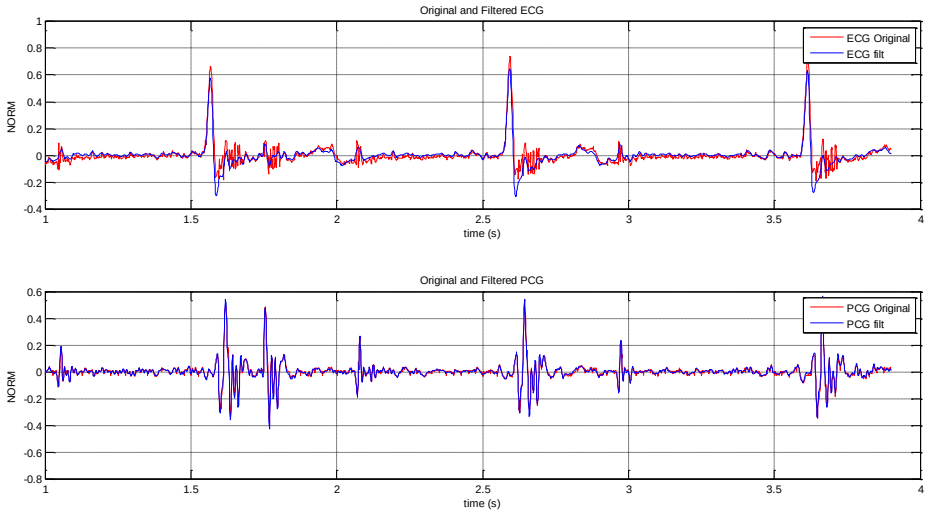

Figure 5.10. ECG and PCG original and filtered signals using a low pass IIR filter with cutoff frequencies of 50 and 100 Hz, respectively.

Figure 5.11 shows the PSD of the filtered signals.

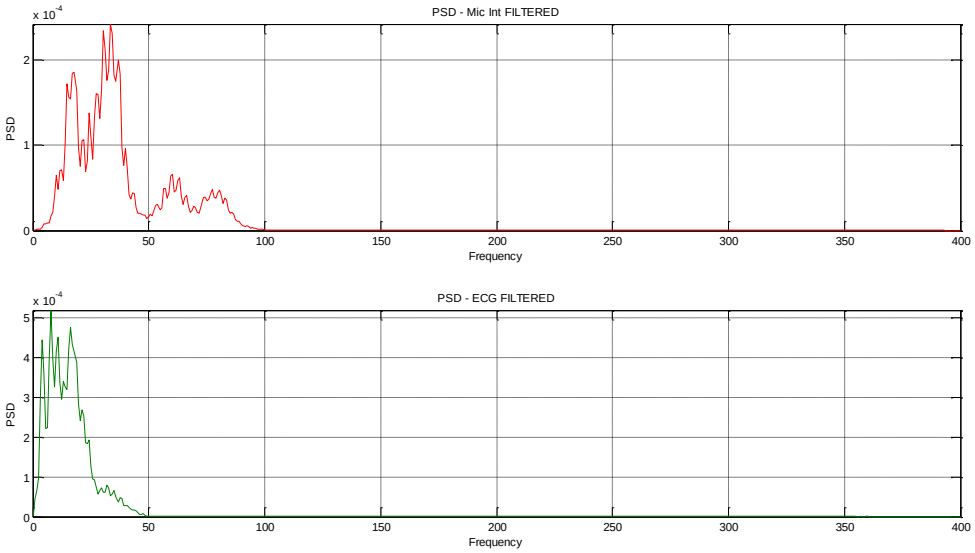

Figure 5.11. PSD of filtered ECG and PCG signals

5.3.4 R-Peaks Detection

The R-peaks from the ECG signal were detected. First, all the local maxima were found. Since the R peaks have an amplitude considerably bigger than the rest of the signal, a threshold was used to differentiate the R peaks from the rest of the local maxima. A vector was created with the position of the R peaks. The result of the detection is shown in Figure 5.12.

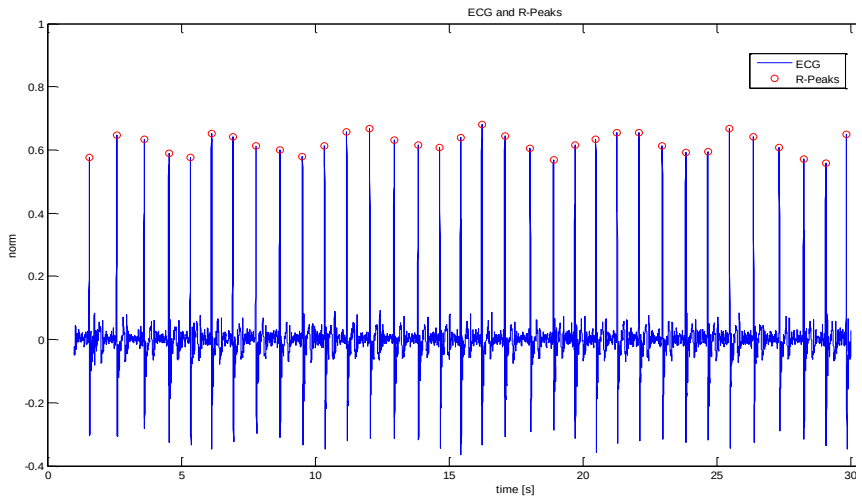

Figure 5.12. R-peaks detection

5.3.5 Heart Rate (BPM) Estimation

The heart rate estimation was perform using the vector containing the location of the R peaks. The time elapsing between two consecutive R peaks is known as R-R interval.

In clinical practice, heart rate is measured in beats per minute (bpm) and is almost always computed by extrapolation (for example, by counting the beats in a six-second interval and multiplying by ten). In studies of heart rate variability (HRV), however, heart rate is modeled as a quasi-continuous signal, and the R-R interval series is used to obtain samples of that signal at more frequent intervals. The simplest way to do this is to calculate the reciprocal of each interval in minutes. An example of the result of the instantaneous heart rate estimation (resting heart rate for a 24 year old adult) is shown in Figure 5.13.

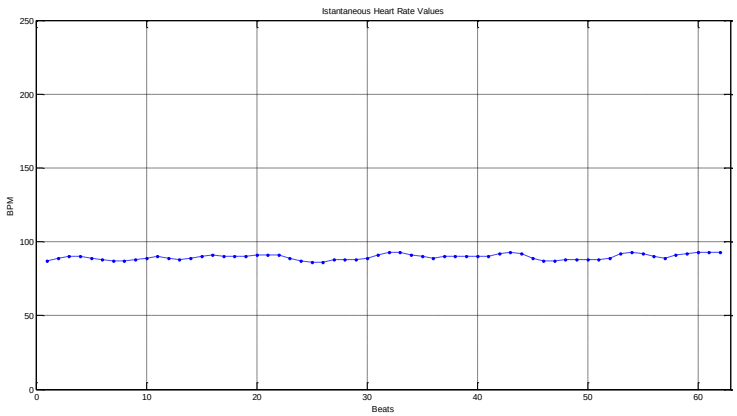

Figure 5.13. Instantaneous heart rate

The average, maximum and minimum heart rate were also calculated. For the aforementioned example, the values obtained (in bpm) were 90, 93 and 86, respectively.

5.3.6 Heart Sound Localization and Segmentation

Heart sound localization refers to the task of finding the normal heart sounds, but without distinguishing the two from each other. Heart sound segmentation partitions the PCG signal into cardiac cycles and further into S1, systole, S2 and diastole. Both heart sound localization and segmentation can be divided into direct and indirect approaches. Indirect methods exploit

the ECG information, while direct methods are operating solely on the PCG signal.

In this thesis, the indirect method was used, based on ECG-gating. ECG-gating means that temporal information from the ECG is used to segment the PCG signal into heart cycles. This is very convenient since the QRS complexes in the ECG are fairly easy to detect automatically. Since the heart sounds occur in certain time intervals after the QRS complex, the detection procedure is immensely facilitated. For example, finding S1 in a narrow search window where we know that it exists (but we do not know its exact location) is much easier than finding S1 in a larger search window where there might be multiple occurrences of S1 as well as S2 or other signal components.

A related topic to ECG-gated heart sound segmentation is accurate localization of S1. The QRS complex is here regarded as a trigger for S1, making it possible to use this information to find S1. Very accurate localization of S1 is necessary since the timing of events is important.

S1 marks the onset of systole while S2 occurs at the start of diastole. The timing of the sounds is thus related to ventricular depolarization and repolarization. Hence, the ECG provides information about where to search for heart sounds (S1 occurs subsequent to the QRS complex and S2 occurs after the T-wave). QRS detection was explain in the previous section.

Based on the ECG signal, predefined search windows were used to locate S1 (Figure 5.14). A typical window choice for S1 detection is 0.05RR - 0.2RR, where RR is the interval between two R-peaks. How to actually find the heart sounds within these windows can be accomplished in several ways. Looking for the maximum value in the selected window is one approach, and was used in this thesis.

Once the S1 peaks have been located, the S2 peaks are identified using the formula written by Braunwald [**29**], based on the temporal distance between two consecutive S1 peaks and the two constants, whose value depends on the sex of the subject.

$$[CostantA - CostantB * time\ between\ 2\ peaks\ S1]$$

The constant value for males are $KA = 413$ and $KB = 1.7$, and for females $KA = 418$ and $KB = 1.6$. For every value found using the above formula a search windows is created and used to locate S2. The maximum value in the created window is selected as the S2 peak.

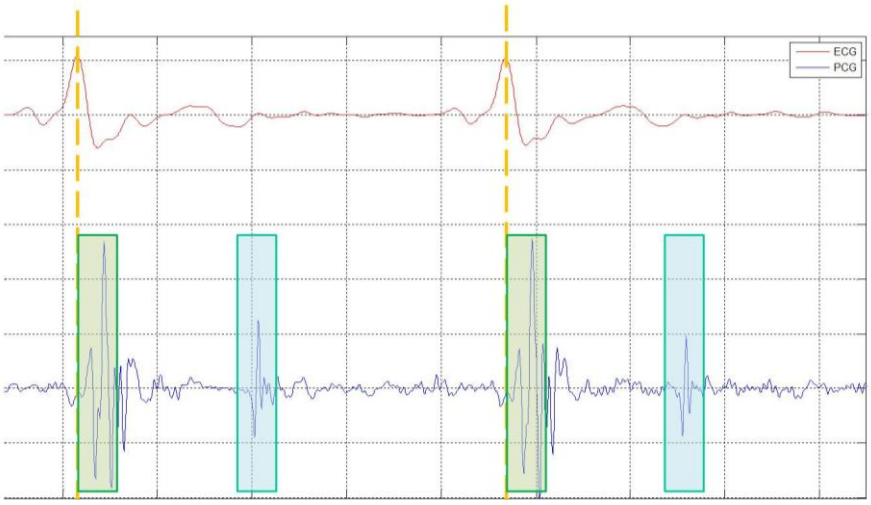

Figure 5.14. Example of ECG-gating with defined search windows for S1 and S2, respectively.

An example of the R, S1 and S2 peaks detection is shown in

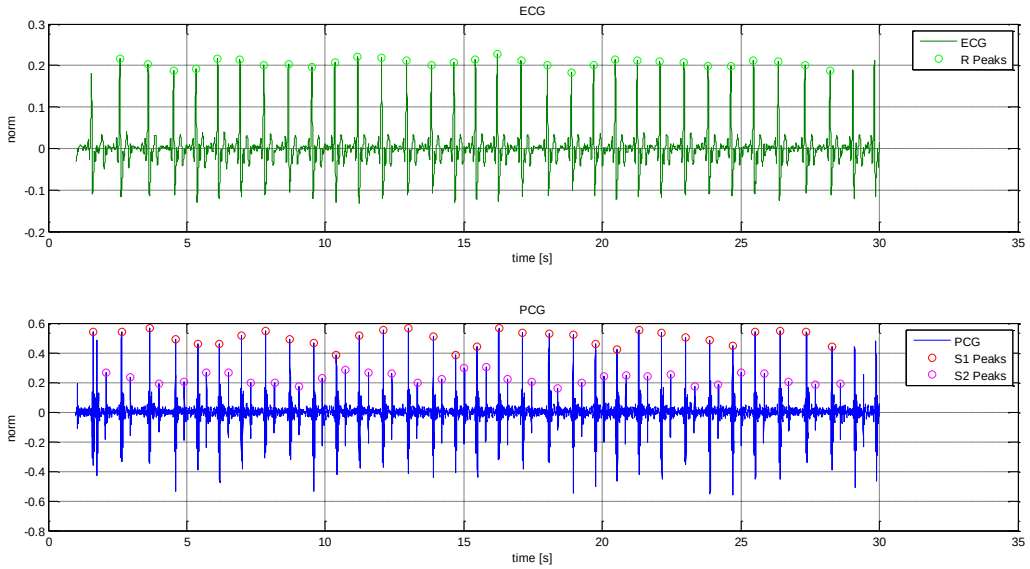

Figure 5.15. Example of the R, S1 and S2 peaks detection

5.3.7 R-S2, R-S1 and S1-S2 Time Intervals Estimation

After the peak detection, the estimation of the time intervals RS1, RS2 and S1S2 was performed.

The RS1 and the RS2 time intervals were calculated as the temporal distance between the peak R and the peak S1 and S2, respectively, in the same

cardiac cycle. The S1S2 time interval was calculated as the temporal distance between the peak S1 and the peak S2 in the same cardiac cycle ($RS2 = RS1 + S1S2$).

The number of correct S1 and S2 localizations was calculated via a trace of RS1 and RS2 intervals, respectively. For a subject in rest, these intervals are fairly constant between heart cycles. To get a quantitative measure of a correct S1 and S2 localization, detections that gave rise to RS1 and RS2 intervals locally deviating more than two standard deviations from its neighboring were considered erroneous. Figure 5.16 shows an example of the time interval estimation. The incorrect localizations are indicated with a black circle. The incorrect localizations were not considered for calculating the average values.

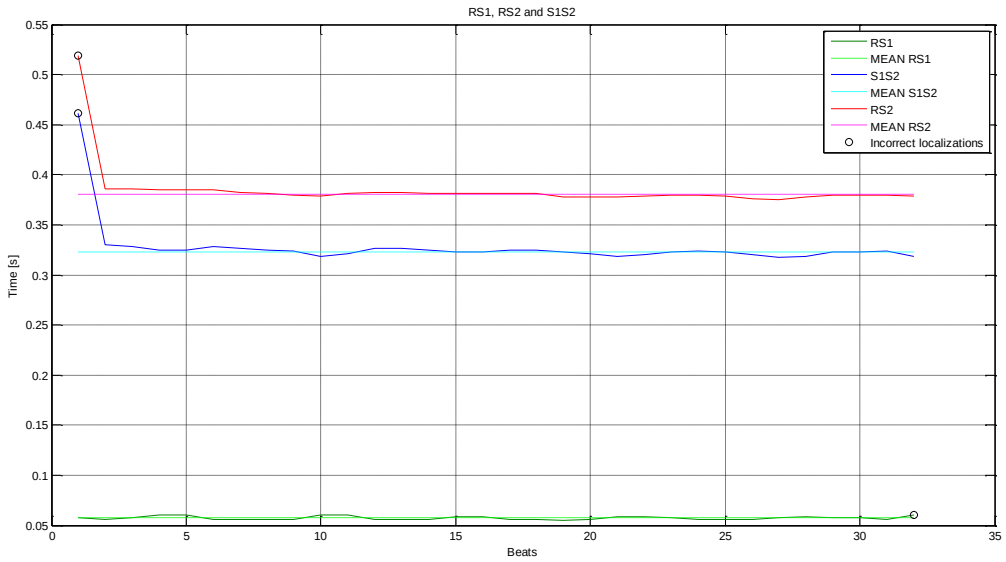

Figure 5.16. RS1, RS2 and S1S2 time intervals

5.4 TEST RESULTS

Once the algorithm necessary to estimate the RS2 interval was done, the aim of the work moved towards the relationship between the blood pressure and the RS2.

In order to compare the capabilities of RS2 on SBP estimation, the relationship between SBP and RS2 were studied in rest and after exercise. A experiment (based on the experiment performed by Zhang's research group

in [**14**]) was conducted on 2 healthy subjects, aged 25±1 years. Both subjects were not diagnosed with any chronic diseases. The electronic device developed in this thesis and described in chapter 3, was used to detect ECG and PCG signals. The signals were sampled at 800 *Hz* and recorded simultaneously for 1 minute. SBP was measured by an automatic BP machine (Ardes m250, accuracy of BP measurement: ± 3 mmHg) and exercise was carried out on a elliptical machine. Figure 5.17 shows the procedure of the experiment. At the beginning of the experiment, subjects were asked to sit down and rest for 3 minutes. BP measurements were conducted on the subject before recording the first set of signals (T1). Subjects were then directed to run on the elliptical machine at 9 *km/h* for 3 minutes. Immediately after running, BP measurements and the signal recording (T2) were carried out. After resting for 3 minutes, subjects ran on the treadmill at a lower speed, 7 *km/h*, for 3 minutes. BP measurements and signal recordings were carried out immediately (T3), 18 minutes (T4) and 43 minutes (T5) after the second running.

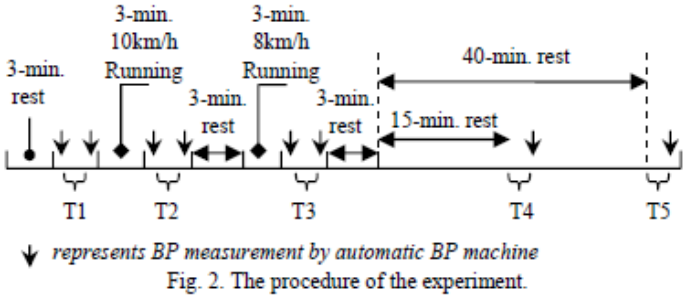

Figure 5.17. Procedure of the experiment.

Using the signal processing techniques explained previous in this chapter, the time intervals RS1, RS2 and S1S2 were calculated. Figure 5.18 shows the test results for the five subject studied.

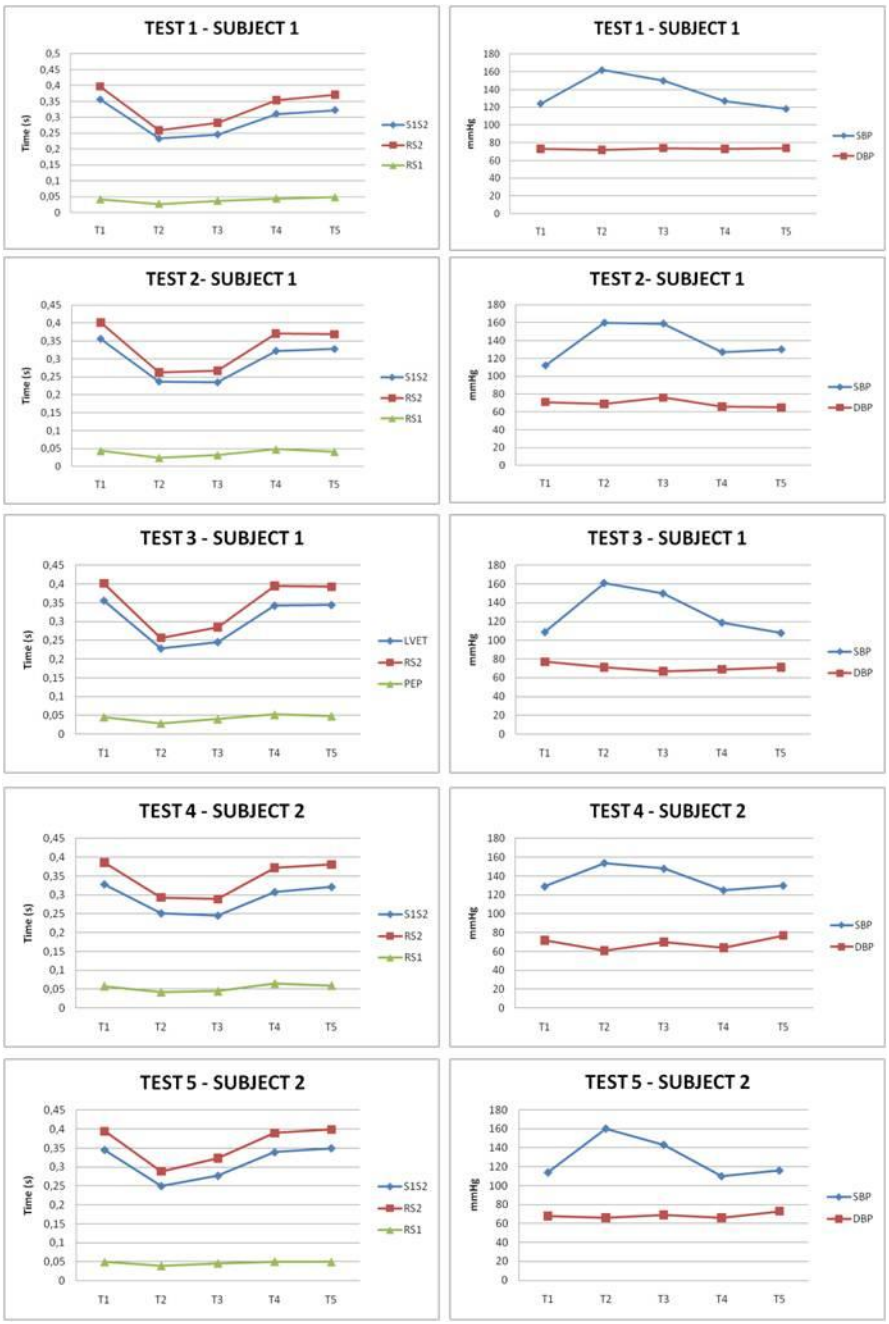

Figure 5.18. Test results:

The results showed an inverse relationship between the time intervals RS1, RS2 and S1S2 and the values of SBP. On the other hand, there is no evidence of an inverse relationship between the time intervals and the DBP.

The relationship between RS1, RS2, S1S2 and SBP was investigated. The results showed that the correlation between SBP and RS2 was higher than the correlation between RS1, S1S2 and SBP.

Figure 5.19 shows the variations of the mean RS2 and SBP. RS2 vary inversely with respect to the mean values of SBP.

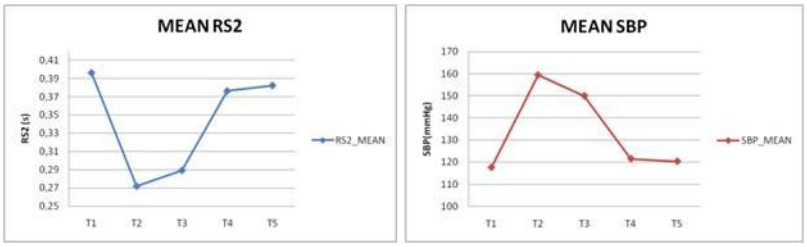

Figure 5.19. Variation of the mean RS2 and mean SBP values

Regression lines were fitted to individuals. SBP is inversely correlated with RS2, where the mean individual correlation was $r = -0.9501$.

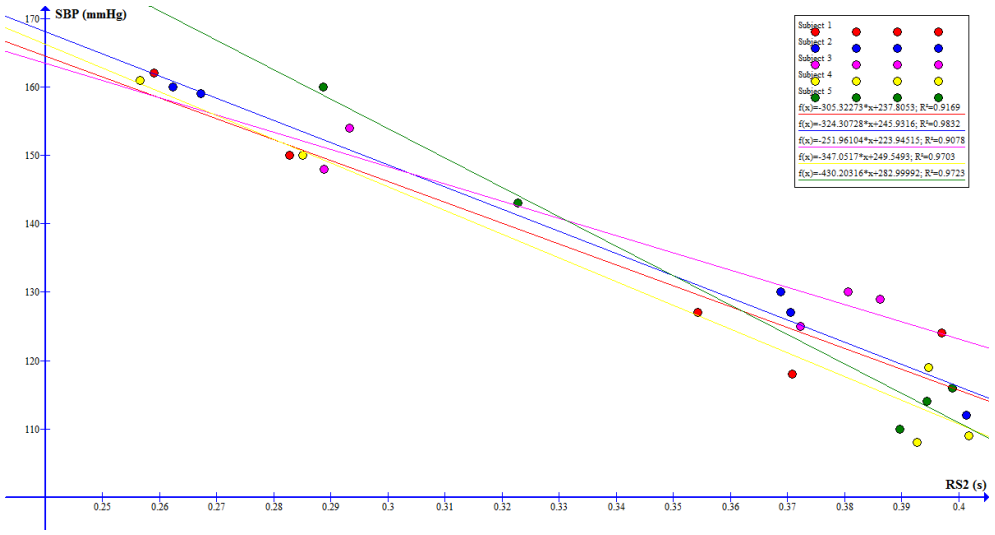

Figure 5.20. The scatter plots of SBP against RS2 and regression lines

To conclude, the study further confirms using RS2 for providing continuous monitoring of SBP is possible. In the future, it is important to investigate more robust techniques for locating characteristic points on the PCG signals.

Chapter 6

CONCLUSIONS AND FUTURE DEVELOPMENTS

This chapter presents the conclusions and results regarding this thesis work and its possible futures developments.

6.1 CONCLUSIONS

Continuous and non-invasive measurement of blood pressure (BP) is always important to critically ill patients. Existing tools are usually limited to provide continuous but invasive monitoring of BP. A noninvasive beat-to-beat measurement of BP would be extremely valuable. A number of approaches have been developed, including finger blood-volume clamping (e.g. Finapres systems) and arterial tonometry (e.g. SphygmoCor system). Although some studies have suggested that there is reasonable accuracy with these systems, the technology itself is generally expensive, cumbersome, and prone to motion artifacts (due to voluntary or involuntary movements of patient while recording the data from the sensor). An alternative technique involves measuring the transit time of the pulse pressure wave through the arterial tree... Previous literatures reported that pulse transit time (PTT) was a potential parameter to provide continuous and non-invasive BP monitoring. Several researchers revealed that PTT was inversely correlated with systolic BP (SBP) individually. PTT is usually recorded as the time delay from the R wave of electrocardiographic (ECG) signal to the upstroke of a peripheral pulse wave signal, wherein photoplethysmographic (PPG) signal is a popular choice of the pulse wave signal. Recently, a novel parameter RS2 (defined as the time interval measured from the R wave of electrocar-

diographic (ECG) signal to the peak of second heart sound of phonocardiographic (PCG) signal) was proposed as an alternative to PTT for BP measurement and the results showed that SBP was correlated with RS2. The relationship between SBP and RS2 was studied in this thesis and the results showed that RS2 is possible to be used for continuous and non-invasive monitoring of SBP.

In this thesis work, an electronic prototype was implemented in order to acquire the ECG and PCG signals. An STM32 microcontroller was used to convert the analog signals into digital and send them via Bluetooth to the PC for offline processing and analysis.

Processing techniques were used to enhance the relevant information carried in the ECG and PCG signals. ECG and PCG signal processing was divided into two stages: preprocessing and feature extraction. The preprocessing stage was used to suppress noise from the raw ECG and PCG signals and the feature extraction stage extracts diagnostic information from the signals. Different signal processing techniques were used in this thesis. They include traditional filtering, peak detector, and spectral estimators and several algorithms for segmentation, decomposition and classification of heart sounds. After the peak detection, the estimation of the time intervals RS1, RS2 and S1S2 was performed. The RS1 and the RS2 time intervals were calculated as the temporal distance between the peak R and the peak S1 and S2, respectively, in the same cardiac cycle. The S1S2 time interval was calculated as the temporal distance between the peak S1 and the peak S2 in the same cardiac cycle.

In order to compare the capabilities of RS1, RS2 and S1S2 on SBP estimation, the relationship between them were studied in rest and after exercise. An experiment was conducted on 2 healthy subjects, aged 25±1 years. The electronic device developed in this thesis was used to detect ECG and PCG signals. The results showed that the correlation between SBP and RS2 was higher than the correlation between RS1, S1S2 and SBP. The results showed that the SBP is inversely correlated with RS2, where the mean individual correlation obtained was$r = -0.9501$. The test results suggest that using RS2 for providing continuous monitoring of SBP is possible.

6.2 FUTURE DEVELOPMENTS

This section presents possible future works for this research.

6.2.1 Integration of the device within the Body Gateway

The future goal is to integrate the system implemented in this thesis to the Body Gateway device, development by Remote Health monitoring group of the Advanced System Technology division of STMicroelectronics. The Body Gateway is a remote monitoring device, currently used to compute the heart and respiratory rate and detect heart beats from the acquired ECG and bioimpedance signals. Furthermore it is able to perform an estimation of body physical activity by acquiring accelerometer signals. The goal of this device is to integrate other sensors to perform non-invasive measurements of a range of different parameters of the body, such as blood pressure. In order to integrate the device developed in this thesis within the Body Gateway, it is necessary to make some modifications to the prototype in order to optimize three main aspects: power consumption, shape and size. It is necessary to optimize the power consumption to increase battery life, which is a very important aspect in this kind of devices. The shape and size of the device can also be improve to make it more comfortable to use and to avoid noise that is added to the signals when the interface between the device and the patient is not suited.

6.2.2 Accelerometer approach to detect heart sounds

In the future the idea is to focus on the accelerometer approach to detect heart sounds and respiratory activity. The Body Gateway, in fact, already integrates an accelerometer, and exploiting it for heart sounds detection could allow using the same sensor for different purposes, thus avoiding the energy and space requirements of a microphone and the related circuitry (filter and amplifier stages). Moreover with the appropriate improvements it could allow to detect very low frequency heart sounds, as the third and the fourth heart tones that current recording systems often fail to perceive. A possible future development could be the use of an accelerometers array that could allow the use of multiple signal sources in order to estimate the contribution of the acceleration actually due to cardiac activity and the one due to rotation of gravity vector and breathing activity, emphasizing the first one and minimizing the non homogeneous information contents deriving from different body sites characterized by different acoustic, muscular and attenuation properties.

6.2.3 Pulse Wave Velocity Approach using two Microphones/Accelerometers

Pulse Wave Velocity (PWV) is a measure of the elasticity (or stiffness) of peripheral arterial blood vessels and its measurement is based on simultaneous measurement of two pulse waves at two different positions. By determining the pulse transit time (PTT) between these points and the distance measured between the two locations, PWV can be calculated

$$PWV = \frac{L}{PTT}$$

The pressure pulse detection can be done with different kind of sensors, such as microphones or accelerometers. By using two sensors at two different positions it can be possible to calculate PWV and furthermore, estimate blood pressure using the formulas described in chapter 2.

6.2.4 Using Other Sensors to Measure Pulse Transit Times

In this thesis we have explored the use of ECG and PCG sensor to estimate BP. However, there are other techniques that allow continuous measurements of pulse transit times by means of other types of sensor. The information provided by the ECG and PCG signals combined with the information provided by the impedance cardiography (ICG) and the photoplethysmography (PPG) can be use for an accurate detection of the cardiovascular time intervals. Combined ICG and PCG can be used to detect the opening of the aortic valve, from which a pre-ejection period (PEP) value can be estimated. PPG can be use to detect the distal pulse-arrival time (PAT), and finally, the PTT value can be calculated as PTT = PAT − PEP. PTT values (in millisecond) can be converted into PWV values (in meter per second) by measuring an associated arterial path length *d* (in meter) and blood pressure can be estimated using the formulas described in chapter 2

6.2.5 Intelligent Stethoscope

Phonocardiography and auscultation are noninvasive, low-cost and accurate methods for assessing heart disease. However, heart diagnosis by auscultation is highly dependent on experience and there is a considerable inter-observer variation. A future work is therefore to develop objective signal

processing tools to emphasize and extract information from the PCG signal. More specifically, it is important to investigate more robust techniques for locating characteristic points on the PCG signals. The future aim is to develop signal analysis methods for a computerized cardiac auscultation system, the intelligent stethoscope. In particular, the work can be focus on classification and interpretation of features derived from the PCG signal by using advanced signal processing techniques. The PCG signal is traditionally analyzed and characterized by morphological properties in the time domain, by spectral properties in the frequency domain or by nonstationary properties in a joint time-frequency domain. In future, nonlinear analysis techniques can be explored to extract more information from the PCG signal. Robust processing of this kind can provide an interpretation of the dynamics of the signal, whose structure can be utilized for both system characterization and classification as well as for signal processing tasks such as detection and prediction. In the emerging field of telemedicine and home care, an intelligent stethoscope with decision support abilities would be of great value, not only in the estimation of BP but also in the diagnosis and tracking the progress of many cardiovascular diseases.

BIBLIOGRAPHY

[1] H. Coni and N. Coni, *Blood Pressure: all you need to know*. USA: The Royal Society of Medice. Oxford University Press.I Edition, 2002.

[2] AtCor Medical. (2005) A Clinical Guide: Pulse Wave Analysis.

[3] H. Sorvoja and R. Myllyla, *Noninvasive Blood Pressure Measurement Methods.* Findland: University of Oulu, 2006.

[4] D.J. Sebald, D.E. Bahr, and A.R. Kahn, *Narrowband auscultyatory blood pressure measurement*. USA: IEEE Trans. Biomed. Eng. , 2002, vol. 49.

[5] A.E. Schutte, H.W. Huisman, J.M. van Rooyen, N.T. Malan, and R. Schutte, *Validation of the Finometer device for measurement of blood pressure in black women*.: Journal of Human Hypertension, 2004, vol. 18.

[6] G. Drzewiecki, J. Melbin, and A. Noordengraaf, *Arterial Tonometry: review and analysis*.: J. Biomech, 1983, vol. 16.

[7] Y. Yoon, J.H. Cho, and G. Yoon, *Non-constrained Blood Pressure Monitoring Using ECG and PPG for Personal Healthcare*.: Journal Medicine System, 2008.

[8] A. Johansson, C. Ahlstrom, T. Lanne, and P. Ask, *Pulse wave transit time for monitoring respiration rate*.: Med Bio Eng Comput, 2006, vol. 44.

[9] H.H. Asada, D.B. McCombie, A.T. Reisner, and P. Shaltis, *Wearable Pulse Wave Velocity Blood Pressure Sensor and Methods of Calibration Thereof*.: Unites States Patent, 2010.

[10] Intelesens. Extracts from Recent Publications on ST+D Ltd PWV System.

[11] W. Chen, T. Kobayashi, S. Ichikawa, Y. Takeuchi, and T. Togawa, *Continuous estimation of systolic blood pressure using the pulse arrival time and intermittent calibration*.: Med. & Bio. Eng. & Comput., 2000.

[12] E. Belardinelli and S. Cavalauti, *A New Nonlinear Two-Dimensional Model of Blood Motion in Tapered and Elastic Vessels*.: Comput. Bio

Med, 1991, vol. 21.

[13] Q. Zhang et al., *Pulse Transit Time-based Blood Pressure Estimation Using Hilbert-Huang Transform*. Minneapolis, Minnesota, USA: 31st Annual International Conference of the IEEE EMBS, 2009.

[14] M.Y.M. Wong, C.C.Y. Poon, and Y.T. Zhang, *Can the Timing-Characteristics of Phonocardiographic Signal be Used for Cuffless Systolic Blood Pressure Estimation?* New York City, USA: Proceedings of the 28th IEEE. EMBS Annual International Conference, 2006.

[15] X.Y. Zhang and Y.T. Zhang, *A Model-based Study of Relationship between Timing of Second Heart Sound and Systolic Blood Pressure*. New York City, USA: Proceedings of the 28th IEEE. EMBS Annual International Conference, 2006.

[16] Christer Ahlstrom, *Nonlinear Phonocardiographic Signal Processing*. Linkoping, Sweden: Institute of Technology, Linkoping University, 2008.

[17] T. Sakamoto, R. Kisikawa, D.M. Maccanon, and A.A. Luisada, *Hemodynamic Determinants of the Amplitude of the First Heart Sound*.: Circulation Research, 1965, vol. 16.

[18] J.L. Heckman, *Relation between the second derivative of left ventricular and aortic pressure and left ventricular and aortic phonocardiogram*.: American Heart Journal, 1982.

[19] A. Bartels and D. Harder, *Non-invasive determination of systolic blood pressure by heart sound pattern analysis*.: Clin. Phys. Physiol. Meas., 1992, vol. 13.

[20] T. Bombardini et al., *Arterial pressure changes monitoring with a new precordial noninvasive sensor*.: Cardiovascular Ultrasound, 2008.

[21] X.Y. Zhang and Y.T. Zhang, *Model-based analysis of effects of systolic blood pressure on frequency characteristics of the second heart sound*.: Proceedings of the 28th IEEE. EMBS Annual International Conference, 2006.

[22] J. Xu and P. Pibarot, *Method and Apparatus for Estimating Systolic and Mean Pulmonary Artery Pressures of a Patient*.: United States Patent, 2002.

[23] S. Mohler, *Passive/Noninvasive Systemic and Pulmonary Blood Pressure Measurement*.: United States Patent, 2000.

[24] Longhini C. et al., *A new noninasive method for estimation of pulmonary arterial pressure in mitral stenosis*.: The American Journal of Cardiology, 1991, vol. 68.

[25] Tranulis C., Durand L.G., Senhadji L., and Pibarot P., *Estimation of pulmonary arterial pressure by a neural network analysis using features based on time-frequency representations of the second heart sound*.: Med Biol Eng Comput, 2002, vol. 40.

[26] Longhini L. and Peretto L., *Noninvasive Apparatus and Method for Estimating Blood Pressure*.: Patent WO/2207/015153, 2007.

[27] E. Braunwald, *Heart Disease: A Textbook of Cardiovascular Medicine*, Fifth Edition ed. Philadelphia: W.B. Saunders Co., 1997.

[28] MathWorks. (2011) MATLAB R2001a Product Documentation: Signal Processing Toolbox. [Online]. http://www.mathworks.com/help/toolbox/signal/f4-1046.html

[29] Robert Bonow, Douglas Mann, Douglas Zipes, and Peter Libby, *Braunwald's Heart Disease: A Textbook of Cardiovascular Medicine*, Seventh Edition ed. USA: Elsevier Saunders, 2004.